OXIDATION KINETICS OF LEAD SULFIDE

by

JEAN PIERRE CONSTANTINEAU

B.Ing., École Polytechnique de Montréal, 1996

A THESIS SUBMITTED IN PARTIAL FULFILMENT

OF THE REQUIREMENTS FOR THE DEGREE OF

MASTER OF APPLIED SCIENCE

in

THE FACULTY OF GRADUATE STUDIES

(Department of Metals and Materials Engineering)

We accept this thesis as conforming

~~to the~~ required standard

THE UNIVERSITY OF BRITISH COLUMBIA

April, 1999

In presenting this thesis in partial fulfilment of the requirements for an advanced degree at the University of British Columbia, I agree that the Library shall make it freely available for reference and study. I further agree that permission for extensive copying of this thesis for scholarly purposes may be granted by the head of my department or by his or her representatives. It is understood that copying or publication of this thesis for financial gain shall not be allowed without my written permission.

Department of Metals and Materials Engineering

The University of British Columbia
Vancouver, Canada

Date April 19, 1999

DE-6 (2/88)

Abstract

This project is a theoretical and experimental study of the oxidation kinetics of lead sulfide. Experimental intrinsic kinetic data applicable to the pre-ignition oxidation of lead sulfide particles has been undertaken to enable a better understanding of flash smelting processes through modelling.

A thorough literature review has shown that the knowledge needed for modelling the oxidation of lead sulfide is limited even though numerous studies have already been done on the subject. The main objectives of this project were to obtain the activation energy of the oxidation of lead sulfide in the presence of sulfur dioxide as well as the reaction order with respect to the oxygen and sulfur dioxide concentrations.

Experiments were performed to verify the effect of temperature, oxygen and sulfur dioxide concentrations on the reaction rates of lead sulfide oxidation. Between 250 and 450°C, under an atmosphere of 20.4% O_2 and 2.7% SO_2, the observed activation energy is 36.8 +/- 5.6 kJ/mol. The reaction order with respect to the oxygen concentration is fractional. Sulfur dioxide does not seem to have an effect on the initial oxidation rates. In all cases, lead sulfate was the oxidation product. The observations can be explained by a reaction mechanism that includes adsorption and ionic diffusion through the sulfate layer.

A new type of diagram describing gas-solid reactions has been created. These diagrams unite thermodynamics and kinetics into a new tool that should be useful for many metallurgical and chemical systems. These diagrams are created from predominance diagrams by applying a mathematical transformation derived from kinetic equations. The diagrams, called modified predominance diagrams, predict the reaction product for given kinetics conditions and atmospheric compositions.

The approach presented to modify the predominance diagrams can also be used for hydrometallurgical systems to modify Eh-pH diagrams. Their applicability for this purpose, has, however, not been verified.

Table of Contents

List of Figures

List of Tables

Glossary

Anglesite	Lead sulfate	$PbSO_4$	
Galena	Lead sulfide	PbS	
Lanarkite	Mono basic lead sulfate	$PbO*PbSO_4$	
Litharge	Lead oxide	PbO	Low temperature form
Massicot	Lead oxide	PbO	High temperature form
	Ammonium carbonate	$(NH_4)_2CO_3$	Decomposes into H_2O, CO_2 and NH_3
	Dibasic lead sulfate	$2PbO*PbSO_4$	Stable at high temperature
	Tetra basic lead sulfate	$4PbO*PbSO_4$	

Nomenclature

a_i	Activity of compound i (-)
A	Surface area (m^2)
B	Pre-exponential constant (mol m^{-2} s^{-1})
D_{III}	Third Damköhler number (-)
Ea	Activation energy (J mol^{-1})
k	Mass transfer coefficient (cm s^{-1})
K	Equilibrium constant (-)
m,n	Stoichiometric coefficients (-)
P_i	Partial pressure of i (atm)
r_i	Molar rate of i (mol s^{-1})
R	Ideal gas constant (8.3144 J $mol^{-1}K^{-1}$)
T	Temperature (K)
T_{mPbS}	Melting point of PbS (°C)
ε_p	Porosity of pellet
ρ_P	Density of pellet (g cm^{-3})
ρ_{PbS}	Density of PbS (g cm^{-3})

Acknowledgments

The author is grateful to the late J. Keith Brimacombe. It was an honour to know him and study under his supervision. Many thanks are also expressed to Indira V. Samarasekera and John R. Grace for their supervision. Their input has been invaluable throughout this project.

Discussions with the other members of the UBC flash smelting group including Grant Caffery, Grant Morgan and Anabel Thomas have been very helpful in many stages of this work.

Many thanks are expressed to Sylvie Bouffard for her support and her help in the statistical analysis and the verification of the mathematical developments as well as for proof reading this thesis.

Many people must also be acknowledged for their help in the preparation of the experimental apparatus: Ross McLeod and Carl Ng from the MMAT machine shop as well as Serge Milaire from the MMAT electronics shop. Pat Wenman has also been very helpful for his assistance on various technical issues. The BET surface area analysis could not have been done without the help of Jim Sawada in the Department of Chemistry.

1. INTRODUCTION

1.1 Smelting of lead sulfide

Extractive metallurgy of lead has a long history. Before the twentieth century, lead smelting was carried out in reverberatory and ore-hearth furnaces which required high grade ore and large quantities of fuel. As high purity ores became scarce, other processes had to be devised. By the turn of the century, the lead blast furnace became the favoured process to produce lead, and it is still widely used. The Imperial Smelting Process (ISP) is a very similar process, but suitable for lead-zinc smelters. The layout of a typical lead blast furnace smelter is shown in Figure 1.1.

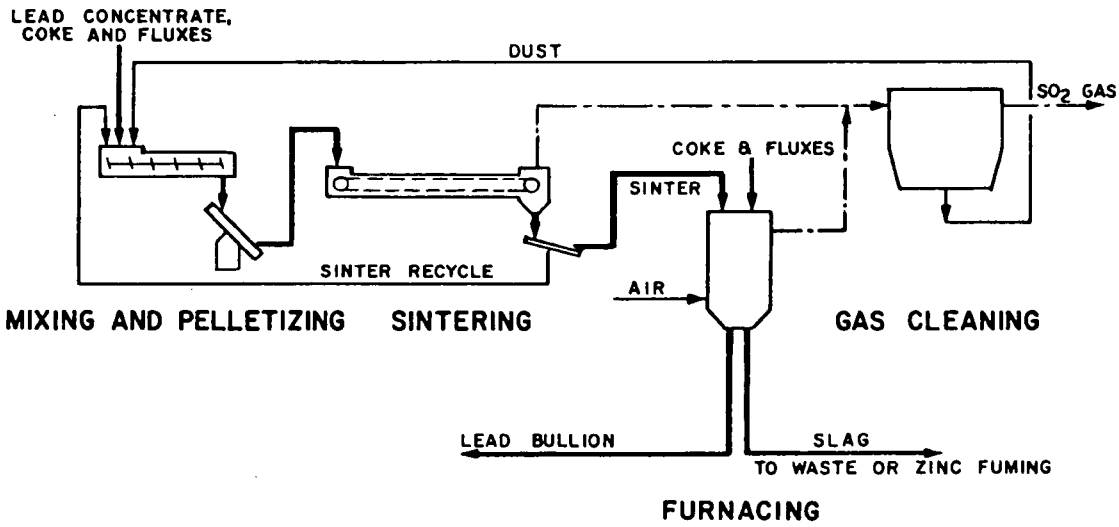

Figure 1.1: Layout of a typical blast furnace lead smelter [1].

In these processes, the concentrate is first sinter-roasted to produce an oxide-rich sinter, then crushed and finally introduced into a blast-furnace with metallurgical coke and flux additions. These two processes have produced a very large proportion of the world's lead production. However, environmental and economic considerations have led to the development of new processes. The sinter machine produces a low-concentration sulfur dioxide (SO_2) gas and is very difficult to keep gas-tight. Complete sulfur removal in the sinter is very difficult to

achieve. The remaining sulfur is introduced into the blast furnace where it produces a very dilute sulfur dioxide gas. Capture of this sulfur by a sulfuric acid plant is not economic due to the very high gas volume generated. Workers may also be exposed to high lead levels. These problems could be solved by designing new processes.

The design goals for a new process are lower capital and operating costs, better energy efficiency, higher sulfur capture, lower worker exposure and lower environmental emissions. Elimination of the sinter-roast step, reduction of coke utilization or its replacement by coal, production of low volume gases with a high SO_2 concentration and use of the heat of oxidation of lead sulfide (PbS) are key steps by which a new process could achieve the design goals.

A number of processes have been developed in efforts to replace the blast furnace. The Cominco, Kivcet, Outokumpu, Boliden, QSL, Kaldo, Ausmelt, Sirosmelt and Isasmelt processes are examples of new processes developed over the last thirty years. Descriptions and the current status of these processes have been the subject of several reviews [1,2,3,4,5]. Many of these processes use the basic principle of flash smelting, an autogeneous process in which the heat of reaction melts and desulfurizes a concentrate. In flash smelting, a concentrate is introduced with air, oxygen-enriched air or oxygen into a furnace through a burner or a lance. Before being incorporated into the bath, the particles fall through a gas zone. During their fall, they react with the surrounding gas to produce oxides, sulfates and metal. Flash smelting has the advantage of using the heat content of the concentrate to melt it, thereby reducing the energy consumption. Some designs are continuous and have a gas effluent consistently high in sulfur dioxide concentrations that is suitable for acid plants. The heat can also be recovered by using waste heat boilers. Flash smelting is then a favourable option when considering the environment and operating costs.

1.2 New lead smelting processes

Flash smelting is a relatively new process in the extraction of lead. Research on lead flash smelting began during the 1960's. Many companies have designed their own reactor from the bottom up or from existing facilities. Boliden has a smelter consisting of an electric arc

furnace where the charge is introduced by a burner. Figure 1.2 presents the layout of the Boliden electric arc furnace process.

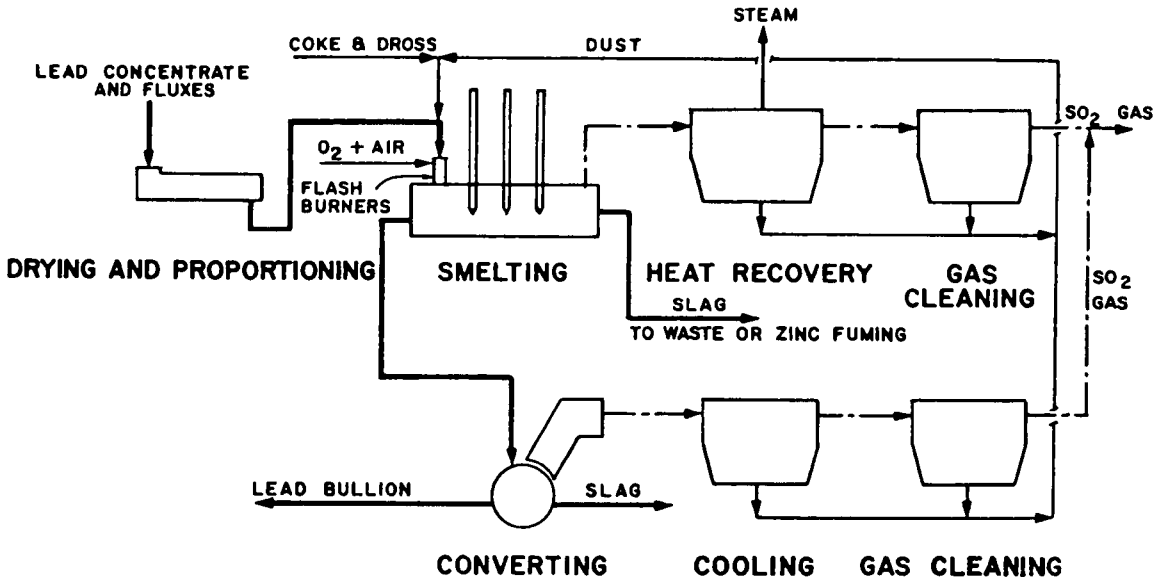

Figure 1.2: The Boliden electric arc furnace process [1].

Boliden also developed the KALDO process, presented in Figure 1.3, which is a top-blown rotary converter (TBRC) where the concentrate is introduced by a lance. The conditions in the reactor can be oxidizing or reducing, depending on the gas and fuel mixture injected by the lance. This is very similar to the Ausmelt, Sirosmelt and Isasmelt processes. The Kaldo, Ausmelt, Sirosmelt and Isasmelt processes can all be considered to be bath processes because of the penetration of the gases and particles into the melt. These processes are advantageous for small smelters due to the reduced capital cost and the use of a single furnace for smelting and reduction.

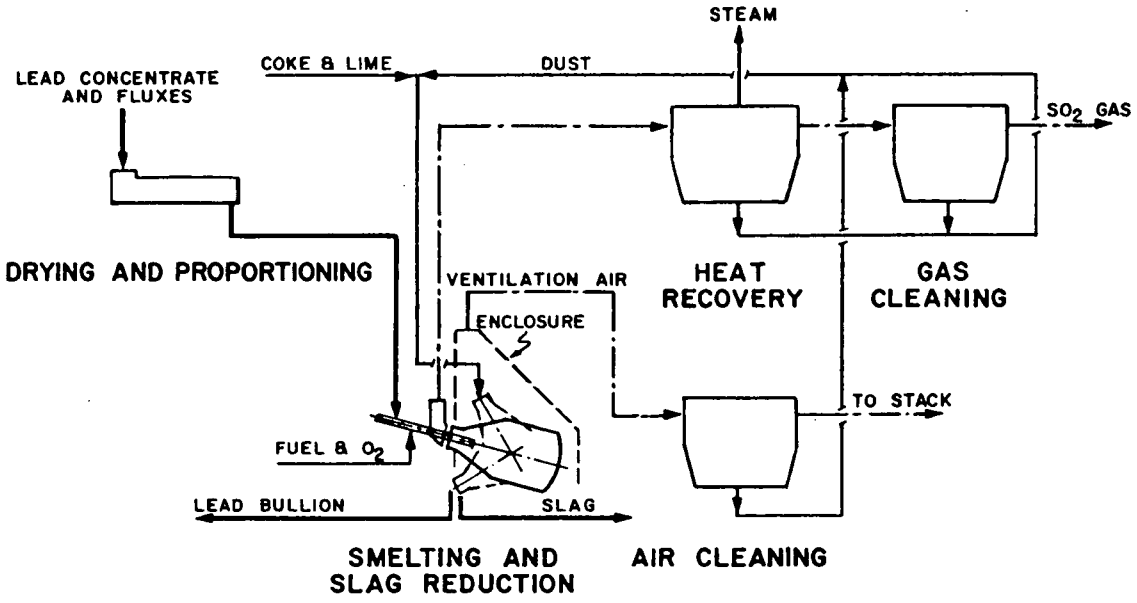

Figure 1.3: The KALDO process [1].

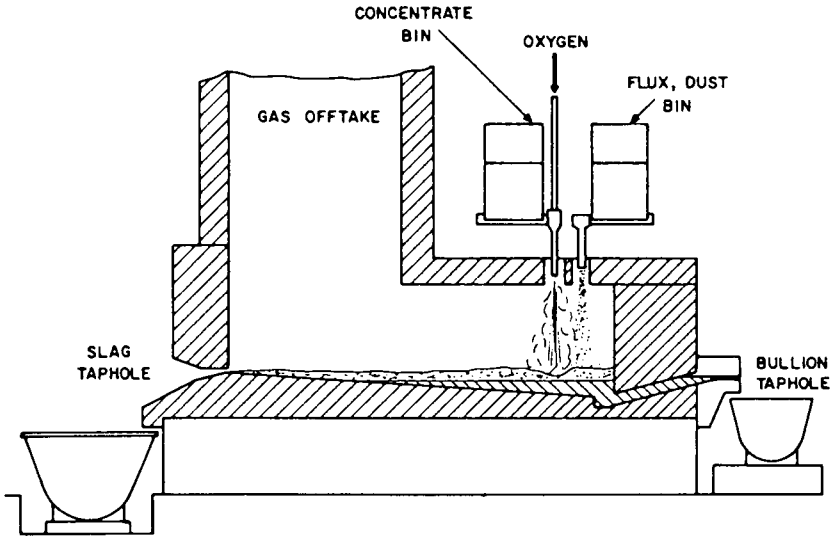

Figure 1.4: The Cominco process [3].

Cominco conducted pilot plant studies on a flash smelter of their own design in the early 1970's [3]. The Cominco process, presented in Figure 1.4, relied mainly on the roast

reactions occurring between the unreacted sulfide particles and the lead oxide present in the slag to produce the bullion. Outokumpu, a leader in flash smelting technology for copper and nickel concentrates, also built a pilot plant for the extraction of lead [6]. As seen in Figure 1.5, this uses a typical Outokumpu flash furnace design coupled with an electric furnace.

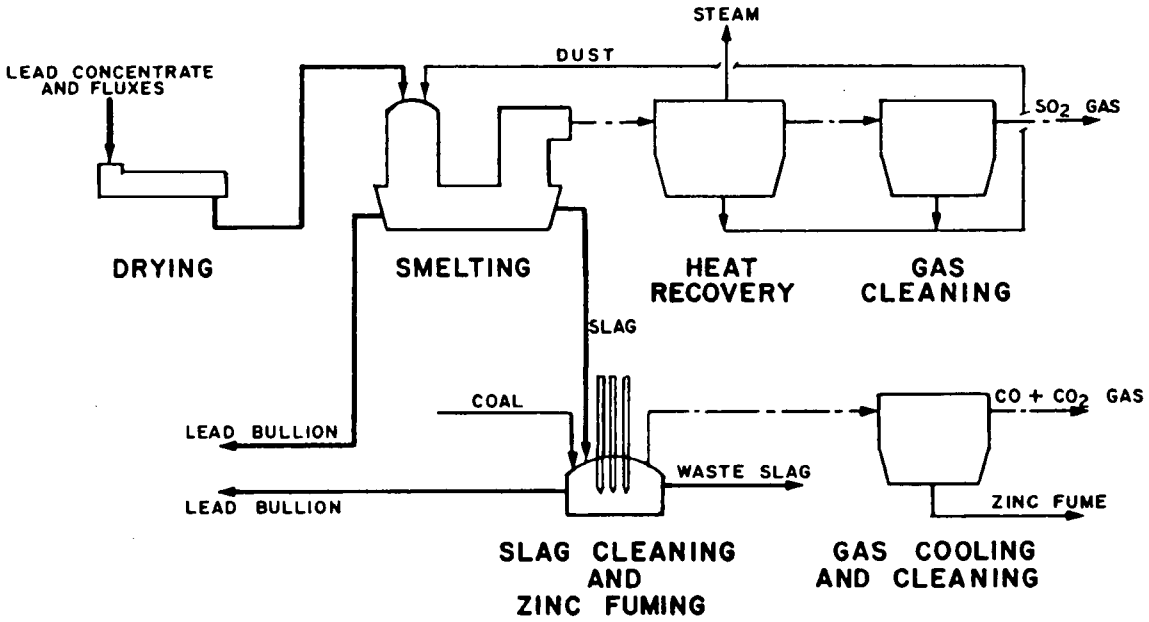

Figure 1.5: The Outokumpu pilot plant [1].

The ideas behind the Kivcet process were developed in 1967 in Kazakhstan. Kivcet stands for oxygen vortex cyclone and electrothermic, in Russian. The Kivcet furnace, presented in Figure 1.6, consists of a smelting shaft coupled to an electric furnace, all in a single vessel. The process also uses a coke checker, i.e. a coke layer floating on the surface of the slag where some reduction occurs. A good physical and chemical description of the Kivcet lead flash smelting process has been recently published by Sannikov et al [7]. Currently, there are three plants plus a pilot plant based on the Kivcet design [8], the most recent one commissioned in the spring of 1997 at Cominco in Trail, B.C. [9].

1.3 Understanding the flame region in flash smelting

When considering the residence times spent by the particles in contact with the gas, the smelters described in the last section can be classified into two categories: long and short

particle residence times. The residence times in the gas phase influence the type of reactions that are of greatest importance in the process. For the Outokumpu and Kivcet processes, a high shaft gives a longer time for gas-particle and gas-droplet reactions to occur than the Kaldo, Isasmelt, Sirosmelt, Ausmelt and Cominco processes where the flame impinges directly onto and into the bath. For short particle residence times in the gas, the importance of the combustion in the overall process is small. The bath reactions are much more important. The impinging gas and particle flow can affect mixing as well as the separation of the bullion and the slag. For long particle residence times in the gas, the combustion of the concentrate constitutes a major part of the process. In these processes, the droplets rain down onto the bath. Being a crucial part in the long residence time processes, the reactions occurring in the flame have to be understood. Modelling of these processes requires study of the phenomena occurring in the flame.

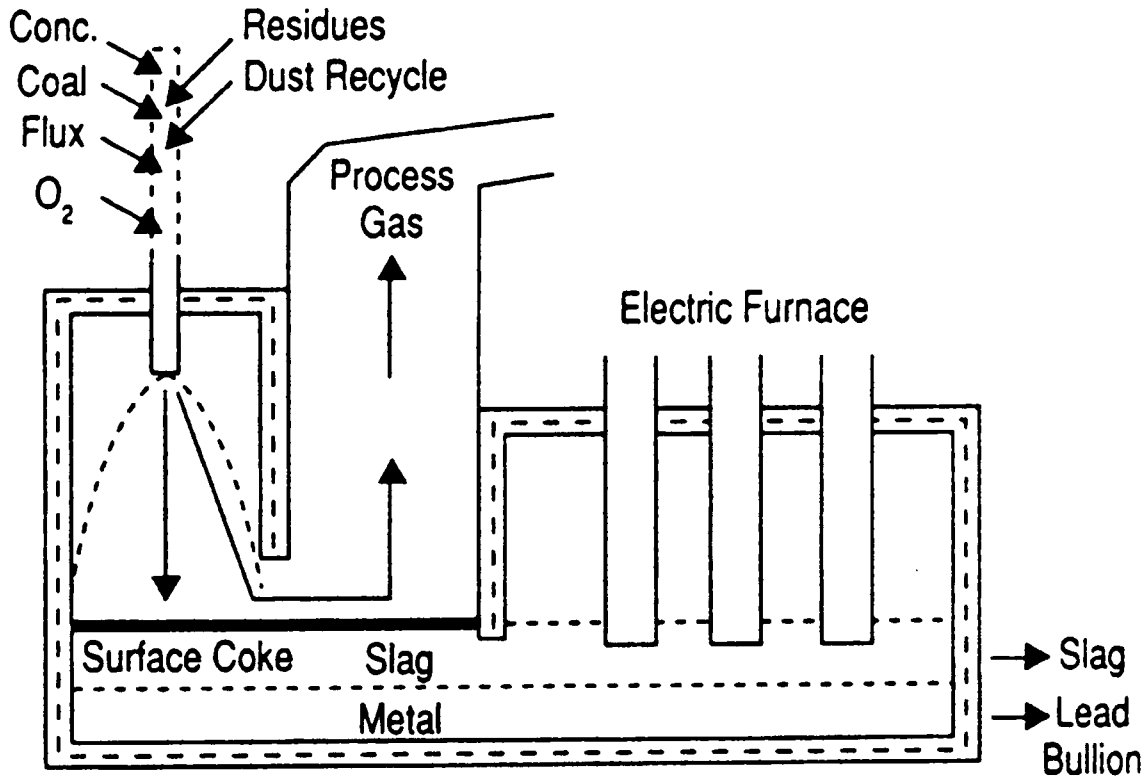

Figure 1.6: The Kivcet furnace [5].

A few studies have tried to understand the flame in lead flash smelting. Jorgenson [10] studied the combustion behaviour of galena under simulated suspension smelting conditions. He used a laminar flow furnace combined with an isokinetic particle collector. Particles were collected at different residence times and at different furnace temperatures. It was observed that monobasic lead sulfate was the major oxidation component. Depending on the experimental temperature, dibasic lead sulfate and lead sulfate were two minor reaction products. The dust collected consisted of lead sulfate and some basic lead sulfate. Salomon de Friedberg [11,12] made drop tube measurements and modelled the combustion behaviour of lead sulfide and of two concentrates. The reaction product and the dust collected were lead sulfate, while the ignition temperature obtained was 700°C in air and 610°C in oxygen. The concentrates were igniting at lower temperatures. Jokilaakso [13] also obtained an ignition temperature of approximately 700°C. High lead losses were observed.

The study of Condina et al [14] can also be used to try to understand the ignition behaviour of lead concentrates. However, the goal of their study was to set the conditions of flash drying of Elura lead concentrate. They used DTA/TGA, a laminar flow furnace, a fluidized bed and a boat-in-furnace technique. In their laminar flow studies, they obtained lead sulfate and basic lead sulfate. Their ignition temperatures varied between 330 and 550°C, depending on the method used. The fluidized bed tests gave the lowest ignition temperatures.

None of these studies proposed a mechanism for single particle combustion. However, Tuffrey et al [15] studied the combustion behaviour of galena and lead concentrate with a two-colour pyrometer. They proposed the following combustion mechanism for galena:

- Upon introduction into the furnace, the particles rapidly heat up and surface oxidation begins.
- The particles heat to ignition. During melting, the sulfate and oxides are incorporated into the droplet.
- Roast reactions occur and metallic lead is formed.

- PbS vaporizes. Depending on oxygen content, droplet disintegration may occur.

A similar mechanism was proposed for the concentrates. All the studies mentioned above have studied the combustion behaviour in air or oxygen. No sulfur dioxide was added. Its presence would simply have been a result of the combustion of the particles. However, in flash smelters, internal recirculation of gases adds sulfur dioxide and dilute the oxygen in the stream of combusting particles. The effect of sulfur dioxide has not been studied. It is doubtful that the results from combustion studies where sulfur dioxide was not considered can be directly translated to flash smelting conditions. Sulfur dioxide has to be used in order to properly relate experimental results to flash smelting conditions.

A mathematical model describing the behaviour of a combusting particle needs to include the mechanism stated above and every important reaction that occurs. One of the reactions is the initial oxidation of lead sulfide or lead concentrate. This is the first step in the combustion where the preheating and initial oxidation of the particles play an important role. The importance of the roast reactions which occur when the particle melts depend upon the availability and nature of the initial oxidation products. The ignition temperature depends on the initial oxidation kinetics as well as heat and mass transfer. Mathematically, ignition occurs when the rate of heat input due to the heat of reaction exceeds the heat losses by convection and radiation. Heat and mass transfer can be expressed using correlations. However, the chemical kinetics must be measured experimentally and cannot be determined using correlations. A thorough understanding of the initial oxidation as well as its kinetics is necessary.

This project is the first step in obtaining fundamental knowledge needed to model the flame region in flash smelting processes. This thesis begins with a literature review of the oxidation of lead sulfide as well as an overview of the chemistry of the lead-sulfur-oxygen system. Mass transfer effects are discussed and incorporated in modified predominance diagrams. After the experimental objectives are stated, the experimental procedures and apparatus are described. Results and analysis follow. Conclusions and recommendations appear in the final chapter.

2. Literature Review

2.1 Phases in the Lead-Sulfur-Oxygen system

The lead-sulfur-oxygen system is a complex system where many compounds exist. In this system, the oxides exist in the forms of PbO, Pb_3O_4 and PbO_2. Pb_3O_4 is a spinel, a mixed oxide consisting of PbO and PbO_2. Thermodynamic calculations [17] show that at one atmosphere and at temperatures above 425°C, the only stable oxide is PbO. The oxygen partial pressure in the flash smelting processes is usually below or very close to one atmosphere. Also, the sulfur dioxide partial pressure where Pb_3O_4 and PbO_2 are stable is lower than 10^{-17} atm. In smelting, the presence of sulfur usually creates partial pressures much higher than this sulfur dioxide partial pressure. The oxides Pb_3O_4 and PbO_2 can therefore be neglected.

Lead sulfate can form many intermediate compounds with lead oxide. In this category are the basic lead sulfates $PbO*PbSO_4$, $2PbO*PbSO_4$ and $4PbO*PbSO_4$. $3PbO*PbSO_4$ is a basic lead sulfate that can only be synthesized by wet methods. It is a hydrated form (i.e. $3PbO*PbSO_4*H_2O$) which decomposes into tetra and monobasic lead sulfates at temperatures above 210°C[16]. This phase is found in aqueous systems and is commonly used as a polymer stabilizer; it can be neglected in pyrometallurgical studies.

A summary of the phases is presented in Table 2.1. It can be seen that massicot and α-$2PbO*PbSO_4$ are stable at high temperatures and metastable at lower temperatures. Identification of some of the compounds can be made by their colour. However, more complex techniques must be used to identify the sulfate and the basic sulfates and to quantify the compounds present in the sample. The melting points of the compounds are also given in the table. The lowest melting point compound is metallic lead. The table does not show the behaviour of mixtures or the stability of these phases as a function of the gas composition. Phase stability diagrams or predominance diagrams must be used to present the thermodynamic behaviour of the system.

Table 2.1: Compounds found in the Lead-Sulfur-Oxygen system.

Chemical name	Chemical formula	Mineral name	Color	Melting point	Notes
Lead sulfate	$PbSO_4$	Anglesite	White	1170°C	
Lead oxide	PbO	Litharge	Red	880°C	Stable < 540°C
		Massicot	Yellow		Stable > 540°C Metastable < 540°C
Lead sulfide	PbS	Galena	Metallic gray	1113°C	
Monobasic lead sulfate	$PbO*PbSO_4$	Lanarkite	White	975°C	
Dibasic lead sulfate	α-$2PbO*PbSO_4$	None	White	960°C	Stable > 640°C Metastable 450°C < T < 640°C
	β-$2PbO*PbSO_4$	None			Metastable < 450°C
Tetrabasic lead sulfate	$4PbO*PbSO_4$	None		895°C	Incongruent transformation
Lead	Pb	Lead	Silvery gray	327°C	

Figure 2.1, Figure 2.2 and Figure 2.3 are predominance diagrams at 400°C, 600°C and 800°C created with HSC Thermodynamic software [17]. These figures present the stable phases in equilibrium with a gas whose partial pressures of sulfur dioxide and oxygen are specified.

These figures are a thermodynamic representation of the system at predetermined temperatures. In general, an increase in sulfur dioxide partial pressure favours phases closer to $PbSO_4$ than to PbO. By comparing figures 2.1, 2.2 and 2.3 one can note that the stability region of the sulfates is shifted to higher SO_2 partial pressures when the temperature is increased. To clearly see the variation of the stability with temperature, one axis must be replaced by a temperature axis. Figure 2.4 is a diagram of the same system with the oxygen partial pressure set at 0.21 atm. This figure is again created from data contained in the HSC thermodynamic database [17].

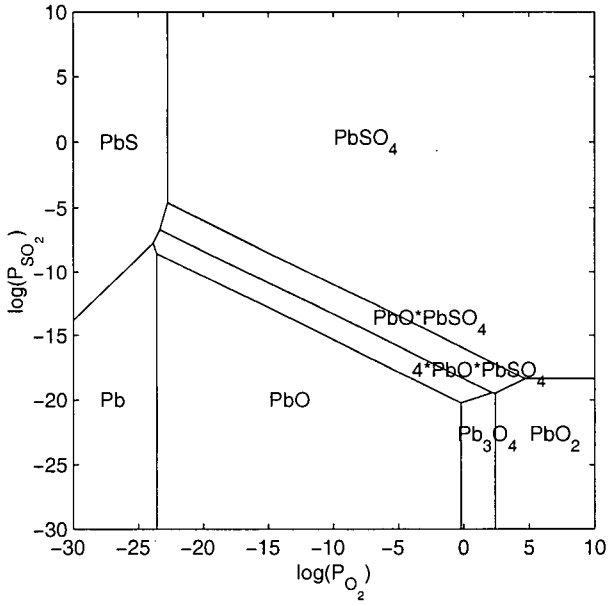

Figure 2.1: Predominance diagram of the Pb-SO_2-O_2 system at 400°C.

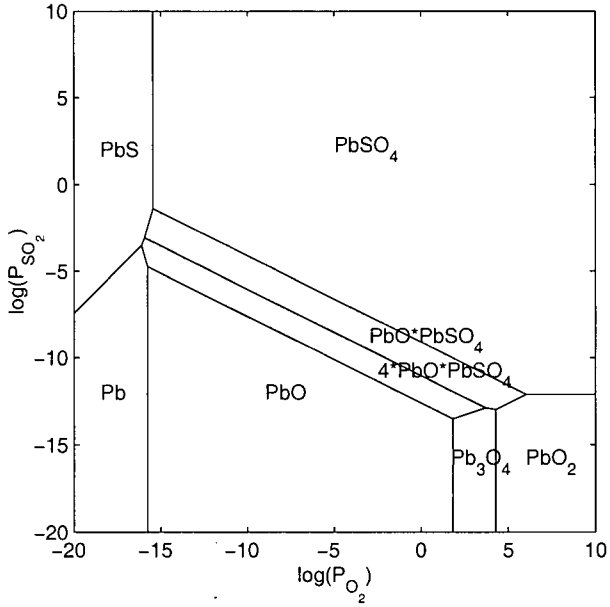

Figure 2.2: Predominance diagram of the Pb-SO_2-O_2 system at 600°C.

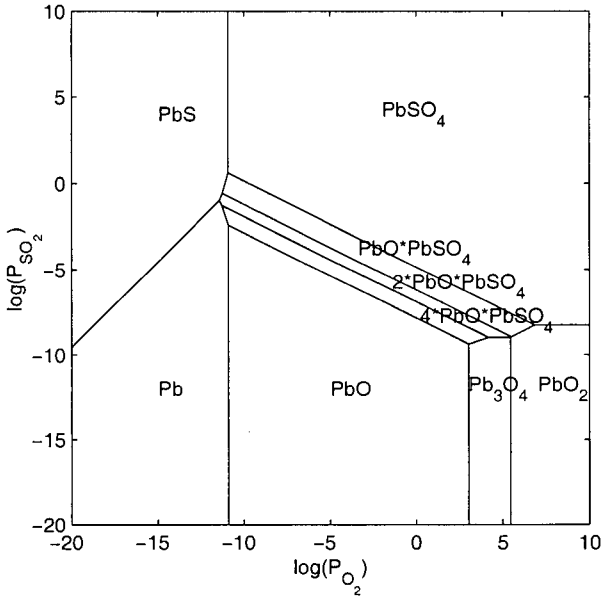

Figure 2.3: Predominance diagram of the Pb-SO_2-O_2 system at 800°C.

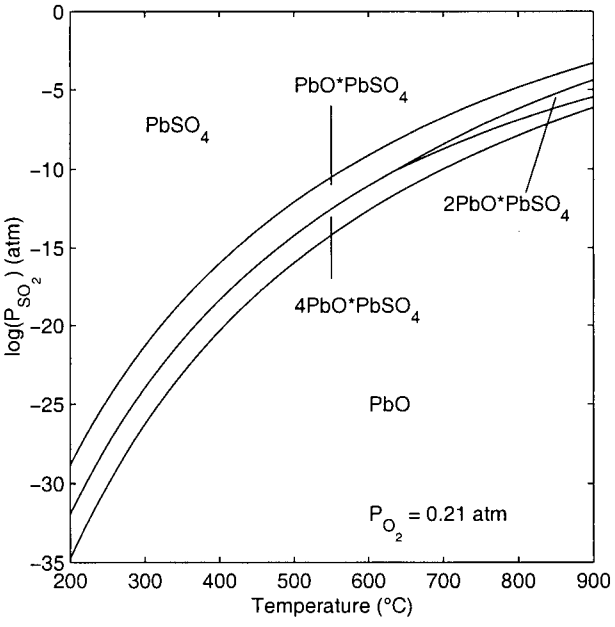

Figure 2.4: SO_2-Temperature predominance diagram in air.

A similar graph was prepared for an oxygen pressure of 1 atm, but only one graph is shown as there is very little difference between the diagrams for air and oxygen. We conclude that the presence of sulfur dioxide has a stabilizing effect on lead sulfate, and this effect decreases with increasing temperature. Also, the presence of dibasic lead sulfate is predicted only at temperatures above 600°C for a very small range of sulfur dioxide concentrations. These diagrams do not show the equilibrium between the different sulfates and the oxide. Figure 2.5 is the PbO-$PbSO_4$ phase diagram refined by Billhardt [18].

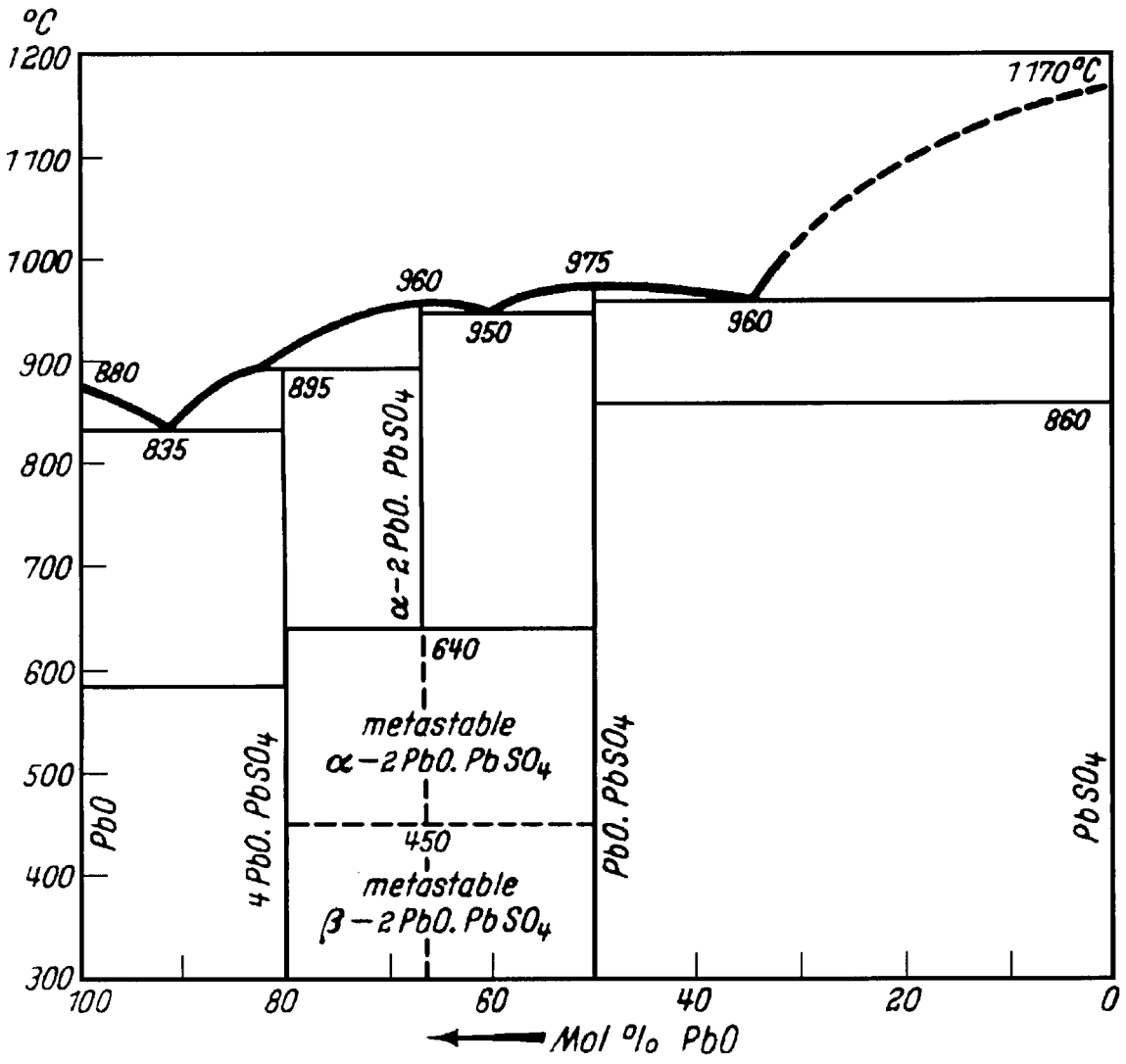

Figure 2.5: PbO-PbSO4 phase diagram.

As seen on the diagram, no solid solutions exist in this system. The lowest temperature at which a liquid phase can exist is at the PbO-4PbO*$PbSO_4$ eutectic, corresponding to 835°C. All the phases melt congruently except tetrabasic lead sulfate which melts incongruently at 895°C. 2PbO*$PbSO_4$ is metastable below 640°C. Depending on the temperature, the two forms of dibasic lead sulfate are stable or metastable. The α phase has a monoclinic crystalline structure, while the beta phase has an orthorhombic structure. Metastable below 640°C, the decomposition of α-2PbO*$PbSO_4$ is slow, while even under slow cooling (10°C/hour), it transforms rapidly into metastable β-2PbO*$PbSO_4$ below 450°C [18]. Upon heating, the metastable β-2PbO*$PbSO_4$ does not decomposes until 450°C above which, monobasic and tetrabasic lead sulfates are formed [18], indicating that 2PbO*$PbSO_4$ can be observed at room temperature. The crystalline structures of lead oxide are orthorhombic at high temperatures and tetragonal at low temperatures.

2.2 Reactions involving the reaction products

A number of reactions between the reaction products and lead sulfide have to be considered. These are known as roast reactions. Lead sulfide is volatile even at temperatures well below its melting point. It has been shown [19] that reduction of solid lead oxide by gaseous lead sulfide is possible. The high vapour pressure of solid lead sulfide then enhances the reactions where lead sulfide can interact. Gas-solid reactions are usually much faster than solid-solid reactions. The partial pressure of lead sulfide has to be taken into account when analyzing the system. Figure 2.9 presents the results of thermodynamic calculations of the vapour pressure of lead sulfide. The higher the temperature, the greater the importance of considering gaseous lead sulfide reactions.

Tuffley et al [33] present SO_2-PbS predominance diagrams where the pressure of lead sulfide is taken into account. These are called reduction diagrams and are presented in figures 2.6, 2.7 and 2.8. The dashed vertical lines represent the lead sulfide partial pressure at equilibrium with solid and liquid lead sulfide. They show that metallic lead can be produced by gaseous lead sulfide reduction of the oxidation products. Very high sulfur dioxide partial pressures are needed for the sulfate or basic sulfates phases to remain stable. Reduction of

the oxidation products is a phenomenon that should not be neglected. However, the kinetics of these reactions must be known to estimate their practical implications. It might be safe to assume that at relatively low temperatures, gaseous lead sulfide interactions are negligible. However, at 600°C and higher, gaseous lead sulfide must be considered.

Lead sulfide vaporization kinetics have been discussed by El-Rahaiby and Rao [20]. From their studies, the chemical kinetics of lead sulfide vaporization is an important parameter in the modeling of PbS vaporization.

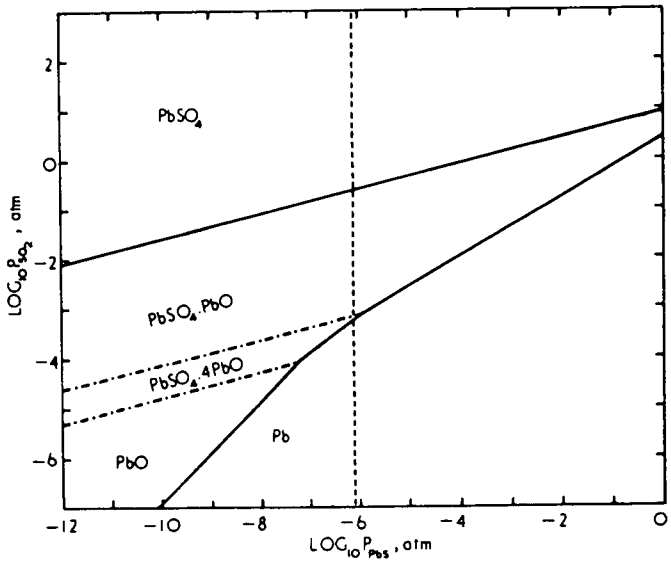

Figure 2.6: Reduction diagram at 600°C.

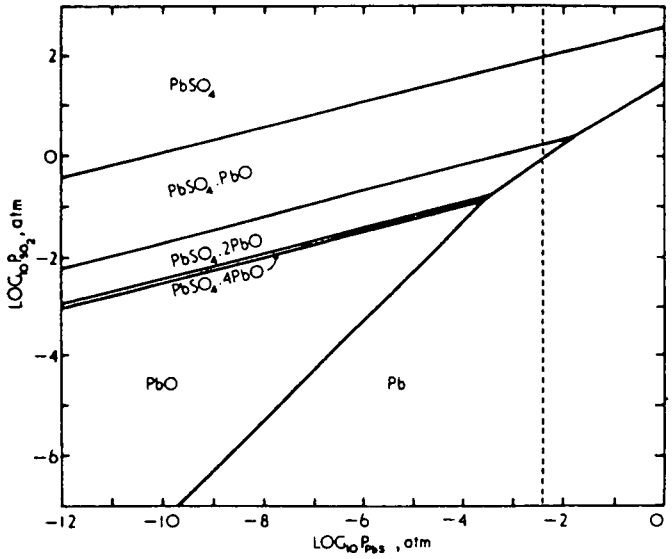

Figure 2.7: Reduction diagram at 900°C.

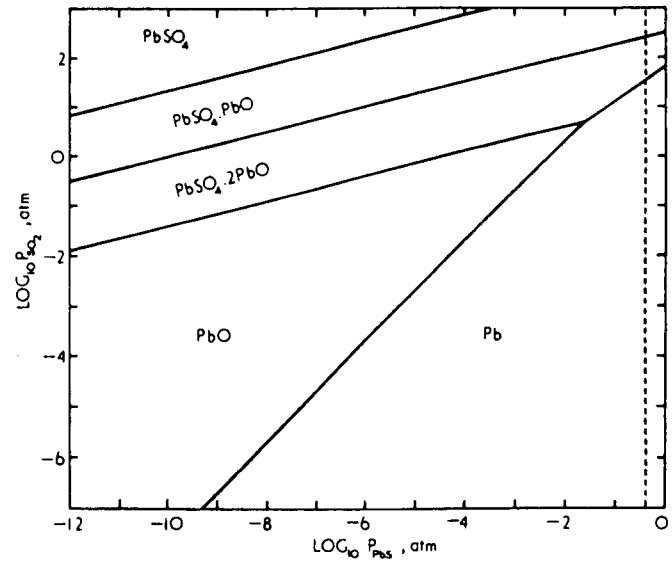

Figure 2.8: Reduction diagram at 1200°C.

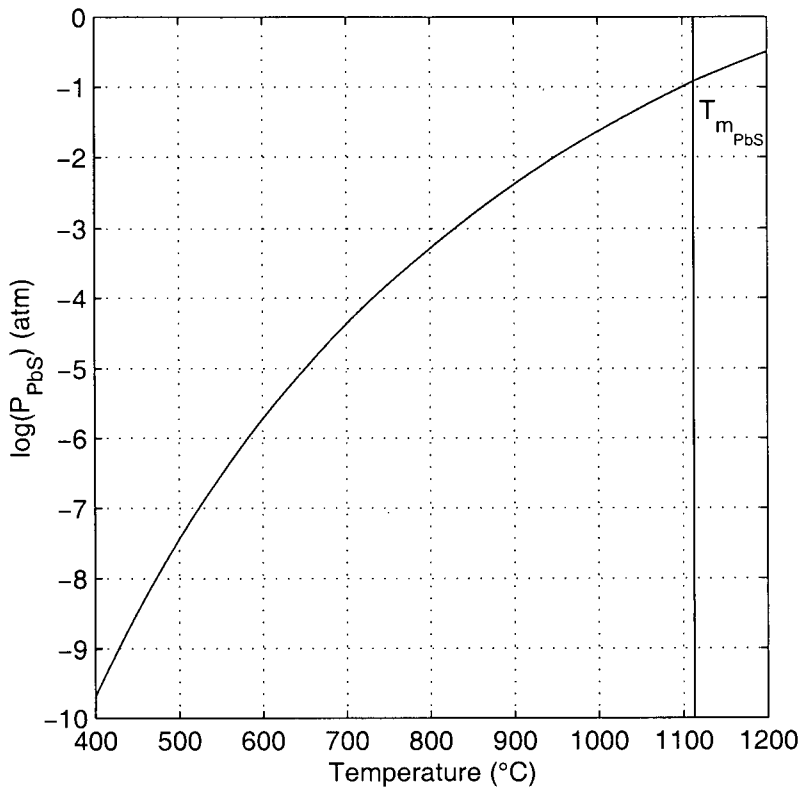

Figure 2.9: PbS vapor pressure. The melting point of PbS (1113°C) is indicated as a vertical line.

The interaction of lead sulfide with lead sulfate, lead oxide and basic lead sulfates has been studied by many authors [21,22,23,24,34]. Some consider that the reduction process occurs in stages [22,24] where lead sulfate is successively reduced to monobasic lead sulfate, dibasic lead sulfate, tetrabasic lead sulfate and finally lead oxide. Malinowski [22] proposed that only lead oxide can be reduced directly to metallic lead. However, Kiuchi et al [24] observed the formation of lead from dibasic and tetrabasic lead sulfide. To completely understand the roast reactions, a thorough review of the available literature, as well as an exhaustive experimental program, are necessary. These are beyond the scope of this project.

Another reaction that can occur is the oxidation of metallic lead to produce an oxide. This has been observed in some experimental studies [25,47]. It has been suggested by Vander Poorten et al [25,34] that oxidation of metallic lead is not possible when lead sulfide is

present in the system. Lead oxidation is possible only when the reducing action of PbS disappears due to the exhaustion of PbS.

2.3 Oxidation studies in the literature

Numerous studies have been carried out on the oxidation of lead sulfide. Some studies were done for safety reasons, such as ignition in mines [30] and in drying operations [27]. Others studied the oxidation for its effect on thin films or its influence on semiconductor properties, but these are not reviewed here. Many studied the oxidation of lead sulfide for roasting [25,34] or sintering [32,33] applications. As these studies were motivated by different applications, the experimental conditions varied extensively. Mass transfer conditions, chemical compositions and temperature all affect the oxidation of lead sulfide. Each is reviewed here based on data available in the literature.

2.3.1 Mass transfer effects

In any chemical or metallurgical process, mass transfer transports the different species thereby reducing concentration gradients. Mass transfer is often neglected in metallurgical studies. In many pyrometallurgical processes this assumption can be accepted as long as the mass transfer resistance is too small to influence the overall rates. However, in many processes such as in gas-solid systems, mass transport is important and has to be considered in any analysis.

In a gas-solid system, there are two major types of mass transfer: transport through the gas phase (boundary layer and pore diffusion) and transport of the species through the non porous product layer. Mass transport through the gas phase is influenced by the hydrodynamics surrounding the sample and the porosity of the sample. Mass transport through the reaction product layer is influenced by the amount and the nature of the solid products, as well as the nature of the diffusing species. The solid products accumulate at the surface of the sample, so that their influence varies with time. Many parameters influence mass transfer such as the total mass or depth of a loosely packed bed, the gas flow rate, the particle size, the reaction products and the density of particles in a cloud. Some of these factors have been previously studied and are reviewed here.

2.3.1.1 Total mass, bed thickness and crucible shape

Gas transport through the thickness of a loosely packed bed is subject to resistance, thus influencing the reaction rate. The mass of powdered sample in a crucible affects the gas transport to the reacting surfaces. The higher the mass, the larger the bed depth. Diffusion of the reactive gases through a thick bed is more difficult than through a shallow bed [25]. In this study, the rate and extent of the reaction were reduced by increasing the mass of the sample. The diffusion through the interstices of the sample was a non-negligible resistance that caused different bed thicknesses to give different results. Another possible problem with a crucible is the blocking of the surface interstices with reaction products. With a slow reaction, diffusion of oxygen through the crucible is possible and all surfaces initially react. Over time, the interstices are blocking progressively and evenly. With a fast reaction, only the top layer of the sample mass reacts. The interstices at the top surface are quickly blocked, and little oxygen is able to diffuse into the bulk of the sample. The diffusion along the length of the crucible can also be an important resistance. The crucible shape or aspect ratio is important in this respect. Ajersch and Benlyamani [26] used thin long crucibles to ensure that mass transport was rate-limiting. They used this technique to identify the reaction occurring between sulfides and gas.

2.3.1.2 Particle cloud density

In experiments where the sample is in a suspended state such as in fluidized beds or in laminar flow furnaces, the ignition temperature measured can vary widely depending on the measurement method. This can be viewed as an interaction between the different particles. This interaction can consist of heat and mass transfer interactions, as well as competition of the different particles for the gas and the combined generation of gases. Condina et al [27] studied the ignition of Elura lead concentrate using two suspension techniques. The laminar flow furnace ignition temperatures were much higher than those from a fluidized bed. This clearly shows the influence of the particle number density on the ignition of the particles. This is an important result in the study of flash reactions. The highest available density would be obtained by using a crucible. However, the thermal analysis data did not give ignition at the lowest temperature, probably due to the slower heating rates used in the

thermal analysis experiment. An oxidation product layer forms before ignition, thus passifying the sample.

2.3.1.3 Effect of gas flow rate

The effect of gas flow rate should not be neglected. Increasing the gas flow rate increases the mass transfer coefficient between the gas and the sample. Under gas phase mass transport controlled conditions, the mass transfer coefficient influences the reaction rate. By increasing the gas flow rate, the resistance to mass transport decreases and its importance in the overall reaction rate also decreases. However, as discussed in the next chapter, it is not sufficient to ensure that the mass transport rate of oxygen is high enough to neglect its effect on the rates. It is also necessary to ensure a high mass transport rate of sulfur dioxide away from the vicinity of the sample. Without clearing the surface of sulfur dioxide, the surface atmosphere could drift into the stability region of another phase.

Most authors who have studied lead sulfide oxidation did not verify their hydrodynamic conditions or assumed that the atmosphere surrounding the sample is exactly what is introduced into the furnace.

Vander Poorten and Meunier [25] compared two different flow rates. The higher flow rate gave a higher initial reaction rate. In both cases, the first part of the experiment showed a linear behaviour in the mass increase over time. The extent of reaction also increased with flow rate. After the diffusion of the gases through the reaction products became controlling, no effect of the flow rate was observed. They also found that under conditions where the reactive gas is not renewed, lead sulfide reacts to lead sulfate. This has also been observed by Kurian and Tamhankar [28] where static air was used in differential thermal analysis (DTA) experiments. Jayaweera and Sleeman [41] observed that the low temperature reactions were slightly different when static air or flowing air was used in DTA/TGA (thermogravimetric analysis) experiments at a very slow heating rate (5°C per minute). When flowing air was used, the sample was more reactive.

Combustion experiments by Nakamura et al [29] have shown that the flow rate influences the ignition temperature of the sulfide. The ignition temperature decreased with increasing flowrate.

2.3.1.4 Effect of particle size and mechanical activation

The particle size has an important influence on the reactivity of a sample. For a constant sample mass, decreasing the particle size increases the available surface area by the inverse of the diameter (as shown in Appendix 1, part 1). Under similar mass transfer conditions, particles of very small size will then be more reactive. Vander Poorten and Meunier [25] observed that the initial reaction rates and the extent of the reaction were higher with smaller particles. However, the difference in rates disappeared when the diffusion of the gases through the product layer became controlling. Reimers and Hjelmstad [30] also observed that finer samples were more reactive. Balaz et al [31] studied the influence of mechanical activation on the oxidation of lead sulfide. They describe mechanical activation as a method of generating defects in sulfides, thus controlling its reactivity. Milling the samples in a planetary mill reduced the temperature of maximum exothermicity in DTA experiments. It is, however, not clear if the mechanical activation simply caused a reduction of particle size, an increase in the number of defects or the removal of pre-existant surface oxidation products.

2.3.1.5 Effect of time and growth of reaction products

In non-isothermal experiments, the effect of time is coupled with the effect of temperature through the heating rate. The effect of the reaction time or accumulation of the reaction products is then not measured accurately in non-isothermal experiments. These results are presented in section 2.3.3 when temperature effects are discussed. However, in isothermal experiments, the thickness of the reaction product increases over time, reducing the possible mass transfer rates obtainable due to its resistance to the transport of the different species. The product layer then has a variable effect on the rates. With a proper model, information on the chemical kinetics and mass transport through the reacted product can be estimated. Also, having a variable effect on the mass transfer characteristics, the conditions experienced by the sample change with time, possibly changing the reaction path. Reaction between the

reaction products and the unreacted lead sulfide can also occur. Both of these phenomena are seen in the results of Tuffley and Russel [32,33], as well as those of Vander Poorten and Meunier [25]. Table 2.2 shows the presence of different compounds at different times during experiments.

Table 2.2: Results showing the effect of the product layer growth on the reaction products (N.A:. Not available, N.D. None detected).

Authors	Temperature	Product	Early	Mid	End
Tuffley and Russell [32,33]	600°C	$PbO*PbSO_4$	X	N.A.	X
	600°C	$4PbO*PbSO_4$	X	N.A.	X
	600°C	PbO	X	N.A.	N.D.
	700°C	$PbO*PbSO_4$	X	N.A.	X
	700°C	$4PbO*PbSO_4$	X	N.A.	N.D.
	800°C	$PbO*PbSO_4$	X	X	X
	800°C	$4PbO*PbSO_4$	X	X	N.D.
Vander Poorten and Meunier [25]	700°C and 750°C	$PbSO_4$	N.D.	X	X
		$PbO*PbSO_4$	X	X	X

In all cases, low sulfur dioxide products are formed initially. The product layer grows, and, after some time, the products are those stable at higher SO_2 concentrations. This suggested to Tuffley and Russell [33] that lead oxide is initially produced and then sulfated.

Vander Poorten and Meunier [34] analysed the external and internal surface of the product layer. They observed that after 4 hours at 780°C, the inner surface of the product layer consisted mainly of lead sulfate, while the outer surface was mainly PbO*PbSO4. However, an X-Ray microanalysis performed by Bugajska and Karwan [35,36] did not clearly show any transition from one product to another. They analyzed a transverse section of the product layer resulting from 150 minutes of exposure to an air atmosphere at 750°C. Their results showed a mixture of the three basic lead sulfates and gaps. A 60 μm gap was formed between the product layer and the galena.

Culver et al [43,53] also observed the formation of a gap between lead sulfide and lead sulfate. After prolonged oxidation, the adherent lead sulfate layer detached from the lead sulfide creating a spherical envelope. The volume ratio of lead sulfate to lead sulfide was greater than one, creating stresses that caused the envelope to expand. The growth of lead sulfate appeared to be controlled by an ionic diffusion process. Vaporization and dissociation produce Pb and S ions that diffuse through the sulfate layer to then react with oxygen at the surface. The ions leave vacancies that coalesce forming cavities. This discussion is valid only for longer times. In the early stages, there are deviations from the parabolic law indicating that the mechanism does not directly apply. Cracking of the sulfate envelope creates a path by which oxygen diffuses directly to the lead sulfide surface where lead sulfate is again produced.

Gold marker experiments by Gray et al [46] demonstrated that the sulfate layer grows outwards. The proposed mechanism is very similar to the previous one, except that the sulfur is left behind creating a pressure buildup that assists the expansion of the envelope until cracks develop and lead sulfate again forms on the surface. They also proposed that adsorbed sulfur trioxide creates a potential gradient causing outward diffusion of lead ions. For times between 10 and 120 minutes and temperatures between 696°C and 800°C, diffusion of lead through the sulfate layer was found to be rate controlling.

2.3.2 Composition effects

The composition of the sample and the gas affect the rates and the reactions occurring during the oxidation of lead sulfide. This section reviews the effect of the composition on the system.

2.3.2.1 Effect of material

The composition of the sulfide material has an effect on the oxidation kinetics. Impurities such as gangue material can influence the rates by acting as physical barriers to the diffusion of the species.

Vander Poorten and Meunier [25] compared the oxidation of synthetic lead sulfide with the oxidation of natural galena. They observed that lead sulfide was more reactive than galena. In order to obtain similar results, they had to increase the galena oxidation temperature by 50 to 70°C. Rao et al [37,38] looked at the oxidation behaviour of mixed sulfides by DTA and TGA analysis and showed that the mixture behaves differently than the sulfides acting separately. The mixture appeared to have a reaction sequence, with one sulfide reacting before another. This is due to the different activation energies of the different sulfides. The most reactive sulfide will react at a lower temperature than the other ones. However, due to the presence of several sulfides in a single sample, interactions can occur. Two sulfides reacting simultaneously could be competing for the oxygen. Also, chemical interactions could occur.

Kolobrodova et al [39] looked at the effect of having single crystals of lead sulfide saturated in lead or sulfur. At 400°C, the lead sulfide saturated in lead reacted at a rate 1.5 to 3 times higher than lead sulfide saturated in sulfur. At higher temperatures (500,600°C), the difference disappeared. They explained this behaviour by the higher diffusivity of lead ions compared to sulfur ions. At higher temperatures, the diffusivities of lead and sulfur ions are similar leading to a smaller effect of a deviation in the stoichiometry of PbS. Electrophysical measurements [39] indirectly support the fact that the diffusivities of the ions differs. Regardless of the composition, the authors obtained lanarkite, while at 400°C, some lead sulfate was present. Kirkwood and Nutting [40] observed that impurities on the lead sulfide surface prevented the formation of a continuous film that seals the surface. With a continuous film, lead oxide forms on the surface of the lead sulfate layer. The lead ions diffusing preferentially through the sulfate layer reacted on the surface to produce lead oxide. The sulfur remained trapped in the kernel. When the sulfur reached a sufficient pressure, cracks form in the product layer causing sulfur to erupt and become available for reaction to produce basic lead sulfates. The experiments were done at temperatures of 200° to 350°C where diffusion is quite slow. This could explain the formation of lead oxide on the outer surface of the product layer

2.3.2.2 *Effect of gas composition*

The gas composition can influence the reaction rate and path, two fundamental characteristics of the system. Its influence is seen on the kinetics and the thermodynamics.

Some authors have studied the effect of oxygen partial pressure on oxidation rates. The presence of sulfur dioxide in the system has been studied by some authors. The effect of sulfur dioxide on the oxidation of lead sulfide is very important. With respect to the predominance diagrams, the reaction path in the presence of sulfur dioxide would change from an oxidation reaction to a sulfation reaction. However, many authors have not considered the effect of SO_2 on their system.

Reimers and Hjelmstad [30] found no measurable effect when air was substituted for oxygen. Jayaweera and Sleeman [41] observed higher reactivities when flowing oxygen was used in their isothermal TGA experiments. Nakamura et al [29] also observed a higher reactivity with higher oxygen content, varying the oxygen partial pressure from 10^{-6} atm to 0.21 atm (air) in DTA experiments. In combustion experiments, the ignition temperatures were also reduced when oxygen was used instead of air, indicating a higher reactivity with higher oxygen concentrations.

Vander Poorten and Meunier [25] compared the oxidation of lead sulfide in air and in oxygen. They observed an increase in the rate and extent of reaction by using oxygen instead of air. They concluded that the order of reaction with respect to oxygen is higher than zero. They also observed an increase in the amount of lead sulfate in their products when oxygen was used, probably due to a higher sulfur dioxide concentration at the surface caused by the higher reaction rates. Another observation not mentioned in their discussion is the mass variation obtained over time under an oxygen atmosphere is non-linear. Before the reaction products have a rate-limiting effect, the reaction rate seems to increase. This non-linear shape could be caused by self-heating of the sample, but in the absence of temperature measurements, no conclusion can be drawn.

Culver et al [53] studied the oxidation of galena under different conditions. Using sulfating conditions, the reaction order with respect to oxygen was -0.15, while the reaction order with respect to SO_2 was 0.2. These values were obtained from experiments of approximately 2 hours duration and using a parabolic growth law for the data obtained after 40 minutes. Such a reaction order means that the rate is lower for higher oxygen contents. Under conditions where monobasic lead sulfate is produced, they obtained an oxygen reaction order of approximately -1.0. Both of these results can be an artifact of using a crucible in their experiments. A sample heap in a crucible is similar to a pellet: both have an internal surface and pores or void space. The Thiele modulus (mL), a dimensionless number which is the ratio of the surface reaction rate over the internal diffusion rate, can be used in the analysis of these results. It can be shown that the reactant concentration within a pellet varies according to the Thiele modulus. Figure 2.10 presents the distribution of reactant within a catalyst pellet at different Thiele modulus for a first order reaction [42]. With other reaction orders, the distribution of reactant within the pores would have a similar behaviour to the one shown in the figure. For a reaction which is not first order, the Thiele modulus changes when the oxygen partial pressure is varied. Neglecting spherical effects, the effective volume used for the reaction is the average reactant concentration. The figure shows that with increasing Thiele modulus, the effective volume used for the reaction decreases. With a smaller reaction volume, the amount of reaction products needed to slow the reaction due to pore blockage is dramatically less. Combining the effect of the oxygen concentration and the effective volume on the overall reaction rates, one can observe a reduction in the reaction rates with higher oxygen contents. The localized pore blockage will amplify the overall effect that the rates are decreasing with increasing oxygen content. This can be easily mistaken for a negative reaction order. However, it is clearly a positive reaction order coupled with diffusion and pore blockage.

Culver et al [43] stated that the reaction rate depends on the sulfur dioxide concentration, but not on the oxygen content. In some studies [44,45], sulfur dioxide concentrations above 8 or 10% caused a reduction in the reaction rates. It is thought that the adsorption of sulfur dioxide on the lead sulfide surface slowed the process.

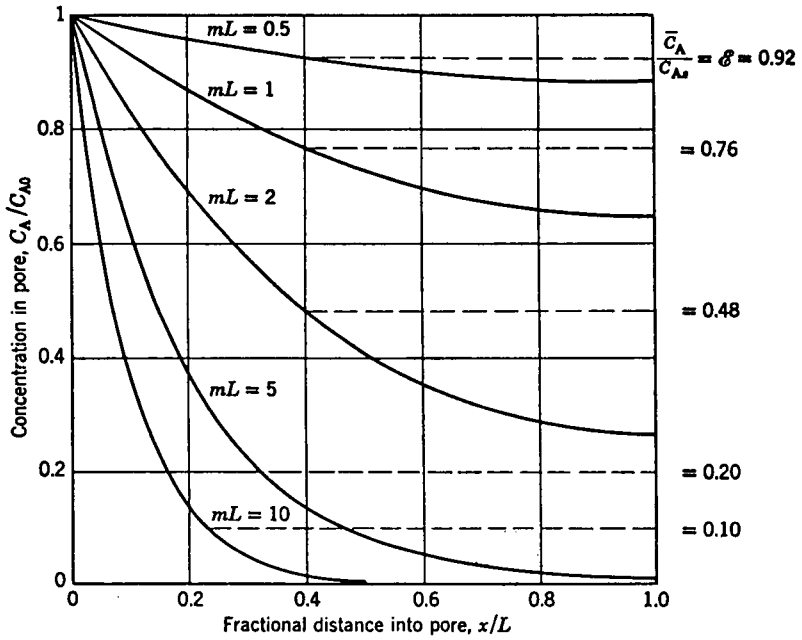

Figure 2.10: Distribution and average value of reactant concentration within a pore as a function of the Thiele modulus (mL)

However, no one has considered the effect of the concentration of sulfur dioxide on transport properties. The effect of the change of viscosity due to a higher sulfur dioxide content on the mass transfer coefficient is negligible. However, the diffusivity of oxygen in nitrogen and in sulfur dioxide and the gas densities are very different. Calculations show that the diffusivity of oxygen in sulfur dioxide is about 64% lower than in nitrogen, while the density of sulfur dioxide is more than twice the density of air. At high Sherwood numbers, the net effect of higher sulfur dioxide concentrations is a reduction in the mass transfer coefficient. At low Sherwood number, only the diffusivity affects the mass transfer coefficient and the effect is larger than at higher Sherwood numbers. However, at any Sherwood numbers, an increase in sulfur dioxide concentration reduces the mass transfer coefficient. In experiments where the mass transfer resistance through the gas phase is important, the sulfur dioxide concentration will affect the reaction rates.

In summary, the results available vary widely. Experimental reaction orders for oxygen have been reported as zero, negative and positive. The effect of an increase in sulfur dioxide

concentration seems to decrease the reaction rates, either by an adsorption mechanism or by modifying the diffusivity.

There is an equilibrium between oxygen, sulfur dioxide and sulfur trioxide. Sulfur trioxide is stable at low temperatures. Gray et al [46] observed that the rate of sulfation of lead sulfide is higher when using higher sulfur trioxide concentrations in the gas. They found a logarithmic dependence of the rates on the sulfur trioxide concentrations. However, their rates were determined for long reaction times. The scatter in the data and the number of data points do not warrant the conclusion that the rates are logarithmically related to the sulfur trioxide.

In the literature, only two studies have mentioned the effect of moisture on the reaction. The presence of moisture in the sample could catalyze the oxidation [47]. It has also been observed that a moist atmosphere (40% H_2O) promoted weight gain in a sulfation reaction [30]. Moisture has an effect similar to sulfur dioxide except that it increases the diffusivity of oxygen. It is not clear, however, if this is a mass transfer effect due to higher diffusivities in moist atmospheres, a catalytic effect or a chemical influence on the reaction.

The oxidation of lead sulfide has been described as autocatalytic by Ponomarev and Polyvyannyi [48], but Sofekun and Doraiswamy [55] showed that lag times in reaching the full oxygen concentrations when the gas is switched from an inert gas to a reactive gas can lead investigators to diagnose the reaction as autocatalytic. This lag time, created by long residence times and important axial dispersion has to be taken into account in analyzing experimental data. Important axial dispersion will cause the step change in the gas to be very gradual. Assuming that the step change from an inert to a reactive atmosphere is very sharp at the sample can be erroneous. Also, if the reaction rates are dependent on the detection of the gaseous reaction products, the axial dispersion from the sample to the detector and the detector response both have to be considered.

2.3.3 Effect of temperature

Thermodynamics, chemical kinetics and mass transport are all influenced by the temperature of the system. With respect to temperature, experiments can be isothermal or non-isothermal.

During isothermal experiments, the temperature is kept constant. The effect of the temperature is then seen when analyzing different experiments by comparing the reaction rates, reaction products and their morphology. The rates at different temperatures give information on the activation energy. The resistance due to chemical kinetics usually decreases with increasing temperature. The controlling resistance may shift from chemical kinetics to mass transfer.

Many studies have been conducted on the oxidation of lead sulfide in air. Table 2.3 summarizes the results obtained in isothermal experiments by many authors, with the numbers being reference numbers. The font size indicates if the compound was a major or minor component. If there is no mention of the relative proportions, all the components are listed as major ones.

Only one study observed $2PbO*PbSO_4$, probably due to the very limited conditions where 2PbO*PbSO4 is formed compared to other products. Also, this compound is metastable at room temperature. It is probable that it was present in other studies but decomposed into $PbO*PbSO_4$ and $4PbO*PbSO_4$ upon cooling.

The table shows a significant scatter in the observed compounds. At one temperature, different authors observed different phases. From the data, no clear boundaries can be set for the stability of one phase compared to another. This can be explained by the different experimental conditions used. According to Figure 2.4, the minimum sulfur dioxide concentration needed to produce lead sulfate varies between $10^{-28.5}$ atm at 200°C to $10^{-3.1}$ atm at 900°C. Having produced both lead sulfate and basic lead sulfate between 400°C and 850°C, one can assume that the average partial pressure was close to the boundary between the two phases. The sulfur dioxide partial pressure experienced by the lead sulfide during the experiments can be estimated by mapping the phases on Figure 2.4. Table 2.4 presents the

calculated sulfur dioxide partial pressures for the experimental results summarized in Table 2.3. When only one phase was detected, the partial pressure is given as the range of partial pressures in equilibrium with the produced phase. When two adjacent phases were detected, the partial pressure is given as the pressure in equilibrium with the two phases. When two non-adjacent or more than two phases were detected, the partial pressure is given as the two outer limits where these phases are in equilibrium. Metallic lead has been neglected in creating this table.

Table 2.3: Reaction products found at different temperatures by different authors (Minor components are indicated by smaller font).

Temperature (°C)	$PbSO_4$	$PbO*PbSO_4$	$2PbO*PbSO_4$	$4PbO*PbSO_4$	PbO	Pb
200	41					
400	$41_{,39}$	39				
500	35,41	$39_{,41}$				
550	35,41	$25_{,35,41}$				
600	35,41	$25,32,39_{,35,41}$	35	32	32	
650,660		25,35	35			
700	25,41	25,32,41			32	
750	25,41	$25,41_{,35}$	35	35		
767-796	34	34,53				
800	34,41	32,34,53		32	41	34
815-830		$53_{,25}$		$53_{,25}$	53,25	34
850,860	41	25		$53_{,25}$	25,41,53	
900,912		32		32,41	41,53	32,53
950				41	41	34
1000		32		32		32
1100		32		32		32

Table 2.4: Calculated sulfur dioxide partial pressure for experimental results found in the literature.

Temp.	SO_2 partial pressure corresponding to experimental results in literature (+ Highest SO2 partial pressure)						
°C	Ref. [25]	Ref. [32]	Ref. [34]	Ref. [35]	Ref. [39]	Ref. [41]	Ref. [53]
200						$> 10^{-28.5}_{+}$	
400					$=10^{-15.8}$	$>10^{-15.8}_{+}$	
500				$>10^{-11.9}_{+}$	10^{-14} - $10^{-11.9}$	$=10^{-11.9}$	
550	$10^{-12.3}$ - $10^{-10.2}$			$=10^{-10.2}_{+}$		$=10^{-10.2}_{+}$	
600	$10^{-10.8}$ - $10^{-8.8}$	$10^{-12.5}$ - $10^{-10.8}$		$10^{-10.8}$ - $10^{-8.8}$	$10^{-10.8}$ - $10^{-8.8}$	$=10^{-8.8}_{+}$	
650,660	$10^{-9.4}$ - $10^{-7.7}$			$10^{-9.4}$			
700	$=10^{-6.5}_{+}$	$10^{-9.8}$ - $10^{-8.1}$				$=10^{-6.5}_{+}$	
750	$=10^{-5.6}_{+}$			$10^{-7.7}$ - $10^{-7.3}$		$=10^{-5.6}_{+}$	
767-796			$=10^{-5.2}$				$10^{-6.5}$ - $10^{-5.2}$
800		$10^{-6.9}$ - $10^{-4.8}$	$=10^{-4.8}$			$10^{-7.7}$ - $10^{-4.8}$	10^{-6} - $10^{-4.8}$
815-830	$10^{-7.3}$ - $10^{-5.6}$						$10^{-7.3}$ - $10^{-5.6}$
850,860	$10^{-6.7}$ - 10^{-5}					$10^{-6.7}$ - $10^{-3.8}_{+}$	$=10^{-6.7}$
900,912		$10^{-5.2}$ - $10^{-4.2}_{+}$				$=10^{-6}$	$<10^{-6}$

The sulfur dioxide partial pressure for a single experiment can vary by a few orders of magnitude. For example at 600°C, reference 32, the partial pressure varies by about two orders of magnitude. Also, comparing the different columns in the table, we find significant differences between the studies. Again at 600°C, the partial pressure for reference 41 is at least two orders of magnitude higher than for reference 32. This very wide range in sulfur dioxide concentrations and the scatter in Table 2.3 indicate that the mass transfer conditions varied considerably from one study to another. The experimental conditions where the partial pressures of sulfur dioxide are highest are those of reference 41. This is not unexpected as this study used static atmospheres. Generally, the partial pressure of sulfur dioxide increases with temperature. This increase is probably due to the higher reaction rates generating more sulfur dioxide. The mass transfer coefficients being relatively constant from one temperature to another, the higher rates caused a higher SO_2 surface concentration.

The production of lead in air is not predicted by Figure 2.4. Predominance diagrams show that very low oxygen potentials are needed to reduce lead sulfide directly to lead. Therefore another reaction must exist to allow the production of lead. Initial formation of basic lead sulfate and lead oxide followed by the formation of lead has been observed [25,33]. These results suggest that roast reactions are occurring. In these reactions, lead sulfide reacts with the oxide and basic lead sulfates to produce metallic lead.

The reducing diagrams of Tuffley and Russel [33] suggest that the presence of gaseous lead sulfide prevents the oxidation of metallic lead due to its reducing action. However, when lead sulfide is completely consumed, metallic lead can be oxidized to lead oxide. This is confirmed by the experimental results of Vander Poorten and Meunier [25] and Terem et al [47].

Another means of summarizing the data in Table 2.3 is presented in Table 2.5. This table shows the temperature range at which the compounds were observed.

Table 2.5: Temperature range of the compounds.

Compound	Temperature Range Observed (°C)
$PbSO_4$	200 - 600
$PbO*PbSO_4$	400 - 1100
$2PbO*PbSO_4$	600 - 750 Minor only
$4PbO*PbSO_4$	600 - 1100
PbO	600 - 950
Pb	800 - 1100

Generally, as temperature increases, the components gradually changes from lead sulfate to basic lead sulfates and from lead oxide to metallic lead. Further oxidation of the metallic lead is possible when no lead sulfide is available to the oxygen. This is similar to the observations made in non-isothermal experiments discussed below.

In non-isothermal experiments, the temperature is usually scanned linearly from room temperature to a predetermined high temperature. The heating rate is a variable, unique to this type of experiment. DTA and TGA are two types of thermal analysis usually conducted in non-isothermal conditions. An advantage of non-isothermal experiments is their simplicity and rapidity. Very few experiments are needed to characterize a sample. The main disadvantage in the analysis of gas-solid reactions is the history of the sample. Reaction products obtained at lower temperature can influence the results at higher temperature. Also, in the case of a complete reaction at an intermediate temperature, the analysis at higher temperatures describes only the behavior of the reaction products. Some authors [49,50] have compared different sulfides and have determined characteristic temperatures under which certain reactions occur. These experiments are mainly qualitative in nature, and due to heat and mass transfer effects, cannot be used reliably to determine valuable kinetic data useful for modeling.

Results presented in the literature where chemical analyses were available are shown in Table 2.6.

Table 2.6: Reaction products obtained in non-isothermal experiments.

Authors	Temperature range (°C)	Gas flow rate	Reaction products or reactions observed during non-isothermal experiments
Reimers and Hjelmstad [30]	100-500 25°C/min	40 cc/min	$PbSO_4$
Hattori et al [51]	360-725 10°C/min	n.a.	$PbSO_4$
Balaz et al [31]	300-1000 10°C/min	8.33 cc/min	$PbSO_4 \rightarrow PbSO_4 + PbO*PbSO_4$ $\rightarrow PbSO_4 + PbO*PbSO_4 + PbO$
Terem and Arslan [47]	160-1075 3.5°C/min	n.a.	$PbSO_4 \rightarrow PbSO_4 + PbO*PbSO_4 \rightarrow PbSO_4 +$ $PbO*PbSO_4 + Pb \rightarrow PbSO_4 + PbO*PbSO_4 + Pb + PbO$
Nakamura et al [29]	700-1000 10°C/min	200 cc/min	$2PbO*PbSO_4 \rightarrow 2PbO*PbSO_4 + PbO*PbSO_4$ $\rightarrow PbO*PbSO_4 + PbSO_4 \rightarrow PbO*PbSO_4 + 2PbO*PbSO_4$

The reaction products are usually lead sulfate at low temperature. However, at higher temperature, the reaction products depend on the experimental conditions. In the experiments of Hattori et al [51], the sulfate is still present at high temperature indicating that their atmosphere was not renewed. This is due to the stabilizing action of sulfur dioxide on lead sulfate. Terem and Arslan [47] probably used a small flow rate, but due to their slow heating rate, they obtained an adequate oxygen supply and sulfur dioxide removal. Even with small flow rates, the reaction products evolve from lead sulfate to basic lead sulfate and then to lead or lead oxide. This is very similar to the above observations for isothermal experiments.

In non-isothermal experiments, the heating rate is chosen by the experimenter for all experiments. Nakamura et al [29] studied the effect of the heating rate on the DTA behavior of lead sulfide and lead concentrates. An increase in heating rate from 10°C/min to 200°C/min resulted in a shift of the exothermic peaks to higher temperatures. The multiple peaks also joined to form only one at the highest heating rate.

Care must be taken when analyzing data at various rates. Lags between the thermocouple and the sample could cause shifts in the position of the peaks. Such lags could be caused by a heat transfer resistance between the sample and the thermocouple. Also, with different heating rates, the amount of reaction products produced at lower temperature depends on the heating rate. The faster the rate, the lesser the amount of reaction products available to react with the sulfide in roast reactions.

2.3.3.1 Activation energy

The activation energy is a measure of the dependence of a process on the temperature as described by the Arrhenius equation. The activation energy of the oxidation of lead sulfide has been determined by many authors. Table 2.7 shows the results available in the literature.

The activation energies available in the literature were obtained by using non-isothermal methods or long term isothermal data. In both these cases, the product layer can influence greatly the measured effective activation energy. Generally, the values obtained in non-

isothermal experiments were much lower than those derived from isothermal experiments. This can be explained by the history of the sample. In non-isothermal experiments, the reaction product from previous temperatures influences further reaction. Heat transfer to the sample could also influence the results. Isothermal experiments are generally better due to reduced heat transfer effects. Also, the history of the sample is generally better known. The sample is free of reaction products before the experiment, which can be helpful when measuring the chemical kinetics. Measurements taken after the formation of the reaction product layer are affected by mass transfer through this layer. Modelling of the layer is, however, much simpler than in non-isothermal experiments. All the experiments used to determine the above values are for long experiments (minutes, hours). The isothermal values for the sulfation reaction are then lower as a result of the mass transfer resistance through the product layer.

Table 2.7: Activation energies measured in different studies.

Authors	E_a for $PbSO_4$ (kcal/.mol)	E_a for $PbO*PbSO_4$ (kcal/.mol)	E_a for Pb (kcal/.mol)	Notes
Kurian and Tamhankar [28]	12			DTA in static air Non Isothermal
Paunova et al [52]	7-9 (400-600°C)			Non Isothermal
Culver et al [53]	50 (673-787°C parabolic rate after 40 minutes)	200 (763-796°C parabolic rate)	9 (818-912°C linear)	Isothermal
Gray et al [46]	40 +/- 5 (666-800°C)			Isothermal 10 minutes intervals fitted to model
Spasov et al[54]		44.920 (700-850°C)		Isothermal Probably $PbOPbSO_4$

2.4 Reaction Path

The chemical reaction path can depend on the type of experiment and the experimental conditions. This is often neglected when comparing various studies. Non-isothermal experiments do not have the same conditions as isothermal experiments. For example, in DTA experiments, where the mass transfer coefficients are usually low, the products obtained can be lead sulfate at low temperatures. When the temperature increases, the products formed are the basic lead sulfates. At even higher temperatures, the reaction products tends towards lead oxide. This differs dramatically from the second situation where in isothermal experiments lead oxide is formed initially. The growth of the oxide layer increases the difficulty of removing sulfur dioxide from the reaction interface. This causes other products to form, e.g. basic lead sulfates. We can see quite clearly that these two reaction paths are directly opposed. One forms the sulfate, while the other forms the oxide initially. Both mechanisms correctly describe reactions occurring in their respective experiments. However, mass transfer conditions have to be considered. Most authors who have conducted DTA/TGA experiments neglected the effect of mass transfer on their experiments. Some studies have been undertaken in static atmosphere, i.e. with no gas renewal. Under these conditions, the sulfur dioxide concentrations and the oxygen concentrations can change dramatically during an experiment.

Some authors have considered the effect of mass transfer in their experiments. They increased the gas flow rates until no change in the rates was observed. This ensures that the rate is not mass-transfer-controlled by transport through the external boundary layer. However, other mass transfer resistances could be important. For example, solid reaction products or the porosity of a sample could add appreciable resistances.

Under some conditions, increasing the flow rate not only ensures chemical rate control but also changes the reaction path. This is seen in the oxidation of zinc sulfide. It has been shown by Sofekun et al [55] that a reduction in the gas flow rate changes the kinetic control to mass transport control, while the reaction path would produce basic zinc sulfates instead of zinc oxide. This shows that mass transport not only affects the rate-limiting step but also the

reaction path. In this case, both the reaction path and the rate-limiting step were changed by reducing the flow rate. However, it is not sufficient to ensure chemical control of the reaction rates to ensure a proper reaction path.

Assuming that the reaction proceeds according to the thermodynamics, the reaction path would change when the composition of the atmosphere at the surface moves from one stability region to another. The atmosphere at the surface of the sample is influenced by the mass transfer regime. Using very high mass transfer conditions, the concentration of sulfur dioxide at the surface would be much lower than if low mass transfer conditions were used. This is discussed further in the next chapter.

3. Mass transfer effects and modified predominance diagrams

Many metallurgical processes are heterogeneous. Mass transfer can have a significant effect on a process such as flash smelting especially if heterogeneous reactions are taking place. In flash smelting, gas-particle mass transfer occurs in many ways: by oxygen transfer from the gas to the particle, by transfer of SO_2 from the particle to the gas, and by metal/oxide/sulfide vaporization. Mass transfer resistances can affect the rate of reaction processes. For mass transfer control, the resistance due to mass transfer is significantly greater than any other resistance. However, mass transfer may have a significant influence on the reaction even when it is not rate-limiting. In this chapter the effect of mass transfer on the reaction path is considered.

3.1 Effect of mass transfer on the reaction rate

A brief discussion of the effect of mass transfer on the reaction rate is necessary before looking its effect on the reaction path. This section briefly presents the development of the overall reaction rate equation considering only two resistances: chemical kinetics and mass transport through the gas phase. Other resistances are left out for simplicity.

The equations can be applied to any heterogeneous system where a solid reacts with a gas. In the present case, we consider the general reaction:

$$1\ MS + m\ O_2 \rightarrow Products + n\ SO_2 \qquad (3.1)$$

where the products can be a metal (M), oxide (M_xO_y), sulfate (MSO_4) or any basic sulfate ($(MO)_xMSO_4$). The solid reaction product composition is not important in this discussion. Considering a pseudo-steady state, the rates of reaction, transport of oxygen and transport of sulfur dioxide are related by the stoichiometric coefficients:

$$r_{MS} = -\frac{r_{O_2}}{m} = \frac{r_{SO_2}}{n} \tag{3.2}$$

The rate of MS consumption is considered to be first order with respect to oxygen so that:

$$r_{MS} = A \cdot B \cdot e^{-E_a/RT} \cdot P_{O_{2S}} \tag{3.3}$$

where A is the surface area, B is the pre-exponential constant in the Arrhenius equation, E_a is the activation energy, R is the gas constant, T is the temperature and $P_{O_{2S}}$ is the oxygen partial pressure at the surface. This equation assumes that the chemical kinetics are the same for any product. While this assumption is usually not strictly valid, it is very useful for the discussion and simplifies the analysis later. The SO_2 mass transport rate from the surface to the bulk gas is:

$$r_{SO_2} = k \cdot A \cdot \left(P_{SO_{2S}} - P_{SO_{2\infty}} \right) \tag{3.4}$$

where k is the mass transfer coefficient. Similarly the O_2 mass transport rate is:

$$r_{O_2} = k \cdot A \cdot \left(P_{O_{2S}} - P_{O_{2\infty}} \right) \tag{3.5}$$

where the mass transfer coefficient is assumed to be the same for SO_2 and O_2. These equations do not take into account any bulk flow and assume low mass transfer rates [56]. To obtain the reaction rate, we must eliminate the unknown $P_{O_{2S}}$ from equation (3.5). This is accomplished with the aid of equation (3.3) leading to:

$$P_{O_{2S}} = \frac{r_{MS}}{A \cdot B \cdot e^{-E_a/RT}} \tag{3.6}$$

By substituting $P_{O_{2S}}$ from equation (3.6) into equation (3.5) we obtain:

$$r_{MS} = -\frac{k \cdot A}{m} \cdot \left(\frac{r_{MS}}{A \cdot B \cdot e^{-E_a/RT}} - P_{O_{2\infty}} \right) \tag{3.7}$$

The reaction rate being equal to the MS consumption rate (3.2), we can isolate the reaction rate to obtain :

$$r_{MS} = \frac{A \cdot P_{O_{2\infty}}}{\frac{m}{k} + \frac{1}{B \cdot e^{-E_a/RT}}} \tag{3.8}$$

This equation is a variant of the reaction rate equation used in many models. The numerator is the driving force, while the denominator is the sum of the resistances in the system. Any resistance due to the presence of a product layer is neglected. If there is a significant resistance to mass transfer through a solid product layer, another term must be added. However, equation (3.8) is sufficient for the present discussion.

Next, let us consider the two limiting cases: mass transfer control and chemical kinetics control. Assume that one resistance is 1% of the other as a threshold between the resistances for considering the controlling regime. (While some authors use a threshold of 5 or 10%, a value of 1% is more conservative in determining the rate-limiting step.) We then obtain for mass transfer control:

$$0.01\frac{m}{k} > \frac{1}{B \cdot e^{-E_a/RT}} \tag{3.9}$$

or

$$\frac{B \cdot e^{-E_a/RT}}{k} > \frac{100}{m} \tag{3.10}$$

Similarly for chemical control we obtain:

$$\frac{B \cdot e^{-E_a/RT}}{k} < \frac{0.01}{m} \tag{3.11}$$

The group on the left hand side of equations (3.10) and (3.11) is a dimensionless number called the third Damköhler number:

$$D_{III} = \frac{B \cdot e^{-E_a/RT}}{k} \tag{3.12}$$

This dimensionless number is simply the ratio of the chemical kinetic rate constant, expressed on a per-unit external area basis, over the mass transfer coefficient. When considering resistances, it is the mass transport resistance divided by the chemical reaction resistance. Using the Damköhler number, we obtain the simple relation for mass transfer control:

$$D_{III} > \frac{100}{m} \tag{3.13}$$

and for chemical control:

$$D_{III} < \frac{0.01}{m} \tag{3.14}$$

Recall that m is the stoichiometric coefficient for oxygen. In our case, m varies between 1.5 and 2 depending on the reaction products. For Damköhler numbers between 0.01/m and 100/m, the controlling mechanism can be described as mixed. Using a higher threshold for determining the type of control would simply narrow the range of mixed control. If the threshold was to be equality of the two resistances, the criterion would become D_{III} higher or lower than 1/m. If other resistances exist, for example due to diffusion through the reaction products, it can be added to the mass transfer resistance in defining the Damköhler number.

We now have a simple dimensionless number and a criterion describing the type of control the reaction is experiencing. This criterion is useful for determining the controlling regime of a reacting system, but does not give any information on the reaction path.

3.2 Effect of mass transfer on the reaction path

To show the effect of mass transfer on the reaction path, we consider the same system and the same equations as in the previous section. From equations (3.2), (3.3) and (3.4) we can show that:

$$A \cdot B \cdot e^{-E_a/RT} \cdot P_{O_{2S}} = \frac{k \cdot A}{n} \cdot \left(P_{SO_{2S}} - P_{SO_{2\infty}} \right) \tag{3.15}$$

The areas cancel, and dividing both sides by the mass transfer coefficient, we can rewrite the above equation as:

$$\frac{B \cdot e^{-E_a/RT}}{k} \cdot P_{O_{2S}} = \frac{\left(P_{SO_{2S}} - P_{SO_{2\infty}} \right)}{n} \tag{3.16}$$

Using the Damköhler number and rearranging, we obtain:

$$\left(P_{SO_{2S}} - P_{SO_{2\infty}} \right) = D_{III} \cdot P_{O_{2S}} \cdot n \tag{3.17}$$

Similarly for oxygen, we can show that:

$$\left(P_{O_{2\infty}} - P_{O_{2S}} \right) = D_{III} \cdot P_{O_{2S}} \cdot m \tag{3.18}$$

(Note the sign reversal in the oxygen partial pressure difference.) From equations (3.17) and (3.18), the difference between the surface and bulk concentrations are directly related to the Damköhler number and the oxygen partial pressure at the surface. When the Damköhler number approaches zero, the difference in partial pressures also approaches zero. A very small Damköhler number is found in systems where the chemical kinetics is slow relative to

the mass transfer. As the Damköhler number increases, the differences between the partial pressures at the surface and in the bulk also increase.

Explicit expressions for the surface partial pressures can be derived from equations (3.17) and (3.18) to give :

$$P_{O_2 S} = P_{O_2 \infty}\left(\frac{1}{1 + D_{III} m}\right) \tag{3.19}$$

$$P_{SO_2 S} = P_{SO_2 \infty} + P_{O_2 \infty}\left(\frac{D_{III} n}{1 + D_{III} m}\right) \tag{3.20}$$

To illustrate the effect of mass transfer on the reaction path, consider the following example: A Damköhler number of 0.001, an oxygen partial pressure of 1 atm and a simple oxidation reaction where the sulfide (MS) reacts with the oxygen to produce the oxide (MO) and sulfur dioxide. In this case, m and n in equation (3.1) are 1.5 and 1, respectively. The Damköhler number is about 10 times below the threshold defined for chemical control, so that the rate-limiting step is clearly the chemical reaction. The bulk partial pressure of sulfur dioxide is very small (for example 10^{-7} atm). Assuming a negligible oxygen partial pressure difference between the bulk and the surface, the difference in sulfur dioxide partial pressure between the surface and the bulk is 0.001 atm. With a difference of 0.0015 atm, our assumption of a very small oxygen partial pressure difference between the bulk (1 atm) and the surface (0.9985 atm) is valid. However, for the sulfur dioxide, the partial pressure of sulfur dioxide at the surface (10^{-3} atm) is several orders of magnitude higher than in the bulk (10^{-7} atm). Depending on the temperature, this higher surface concentration could very well influence the reaction path to yield MO, MO*MSO_4 or MSO_4. Care must be taken when the reaction product changes. For example, under oxide producing conditions, the atmosphere would shift to a sulfate producing region of the predominance diagram where no sulfur dioxide is produced. In the system considered, the predominance diagram could predict one phase, while experimentally we could be producing another. Kinetics must then be considered to

understand any deviations between thermodynamics and experiments. Mass transfer still affects the reaction path even if the Damköhler number shows that the reaction is chemically controlled.

Usually for given experimental dimensions, e.g. sample size and tube diameter, an experimenter increases the reactive gas flow rate until there is no measurable increase in the rate of disappearance of the reactant. This ensures that the reaction rate is not limited by mass transfer. However, it may not ensure that there is no effect on the reaction path. Differences between mass transfer resistances of 1%, 0.1% and 0.01% are not experimentally distinguishable. In all such cases, the reaction rate would be virtually the same. However, after dramatically increasing the flow rate, one could observe a change in the reaction product. The experimental conditions under which mass transfer no longer affects the reaction path depend on mass transfer, chemical kinetics and the thermodynamics of the system.

A tool is needed to interpret the effect of mass transfer on the reaction path. It is conceivable that with equations (3.17) and (3.18), the predominance diagram could be modified to include kinetic data. This new diagram will predict which phase is produced for a given set of conditions. This approach is introduced in the next section.

3.3 Modified predominance diagrams

The equations developed previously can be very helpful to determine if there is a significant partial pressure difference between the reacting surface and the bulk of the gas. They do not, however, indicate how a system would behave if the mass transfer resistance is not negligible. They also do not indicate the conditions under which mass transfer can be neglected. However, these equations can be used to create diagrams which extend well-known predominance diagrams to include considerations of kinetic and mass transfer rates.

The starting point for the creation of the modified diagrams is very simple: the reactions occurring are those predicted by the predominance diagram for a sample at equilibrium in

contact with its atmosphere. The gas composition used for the prediction with the predominance diagram is the composition at the surface of the sample. This approach differs from the usual approach where the surface concentrations are assumed to be equal to the bulk concentrations.

Observing equations (3.17) and (3.18), one can note that the bulk partial pressures can be calculated by defining the Damköhler number and using a predominance diagram for the surface concentrations. Lines on the predominance diagram have their counterparts on the modified diagram. The modified predominance diagram is then a bulk gas phase diagram for given kinetic conditions and is related to the predominance diagram valid at the surface.

For simplicity, we consider a hypothetical M-O_2-SO_2 system where the metal is a metal, sulfide, oxide or sulfate. The following reactions describe the lines in the hypothetical predominance diagram:

$$MS + 2O_2 \rightarrow MSO_4 \qquad K = \frac{a_{MSO_4}}{a_{MS} P_{O_2}^2} \qquad slope = \infty \qquad (3.21)$$

$$MS + O_2 \rightarrow M + SO_2 \qquad K = \frac{a_M P_{SO_2}}{a_{MS} P_{O_2}} \qquad slope = 1 \qquad (3.22)$$

$$MS + \frac{3}{2}O_2 \rightarrow MO + SO_2 \qquad K = \frac{a_{MO} P_{SO_2}}{a_{MS} P_{O_2}^{3/2}} \qquad slope = 3/2 \qquad (3.23)$$

$$MO + SO_2 + \frac{1}{2}O_2 \rightarrow MSO_4 \qquad K = \frac{a_{MSO_4}}{a_{MO} P_{O_2}^{1/2} P_{SO_2}} \qquad slope = -1/2 \qquad (3.24)$$

$$M + \frac{1}{2}O_2 \rightarrow MO \qquad K = \frac{a_{MO}}{a_M P_{O_2}^{1/2}} \qquad slope = \infty \qquad (3.25)$$

With these reactions, only two triple points exist and are arbitrarily set at (-9,-6) and (-5,0) for the M-MO-MS and MO-MS-MSO_4 triple points, respectively, leading to the predominance diagram presented in Figure 3.1.

The surface partial pressures are used in the predominance diagram. The stability region of each phase is delineated by the equilibrium between two phases. If the partial pressure lies

directly on one line, the activity of two solid phases is one, and two solids are at equilibrium with the gas. If the composition of the gas is on either side, the activity of only one solid is unity, so that only one solid is at equilibrium with the gas.

To modify the diagram, the initial reactants and the possible reaction products must all be known. The four reactions considered and their stoichiometric constants, n and m, are defined in Table 3.1.

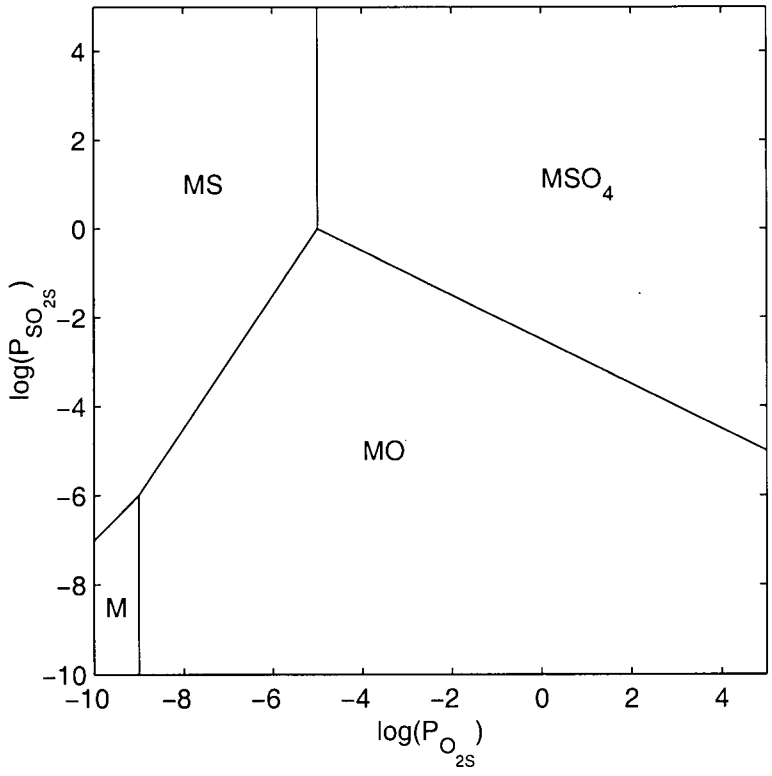

Figure 3.1: Hypothetical predominance diagram.

The new diagram is created by considering each of these reactions. Knowing the stability region of each phase and considering that only one product is produced at a composition infinitesimally close to the equilibrium line, the stability region of one phase can be modified

using equations (3.17) and (3.18). Since each reaction product corresponds to its own stoichiometric coefficients, each line on the predominance diagram has the potential to create two lines on the modified predominance diagram. The regions between these lines is discussed below.

Table 3.1: Reactions used to modify the predominance diagram.

	m	n	
$MS \rightarrow MS$	0	0	(3.26)
$MS + 2O_2 \rightarrow MSO_4$	2	0	(3.27)
$MS + O_2 \rightarrow M + SO_2$	1	1	(3.28)
$MS + \frac{3}{2}O_2 \rightarrow MO + SO_2$	3/2	1	(3.29)

3.3.1 Stable MS phase

No reaction occurs when the surface partial pressures are in the MS stability region. When considering the equations and the stoichiometric coefficients for oxygen and sulfur dioxide, we find that there is no partial pressure difference between the surface and the bulk gas phase, irrespective of the mass transfer conditions. This is not unexpected, because without any reaction, no mass transfer occurs and there is no concentration difference between the surface and bulk. As shown in Figure 3.2, the lines defining the stability region of MS in the modified diagram are then the same as those for the predominance diagram and are valid for any Damköhler number.

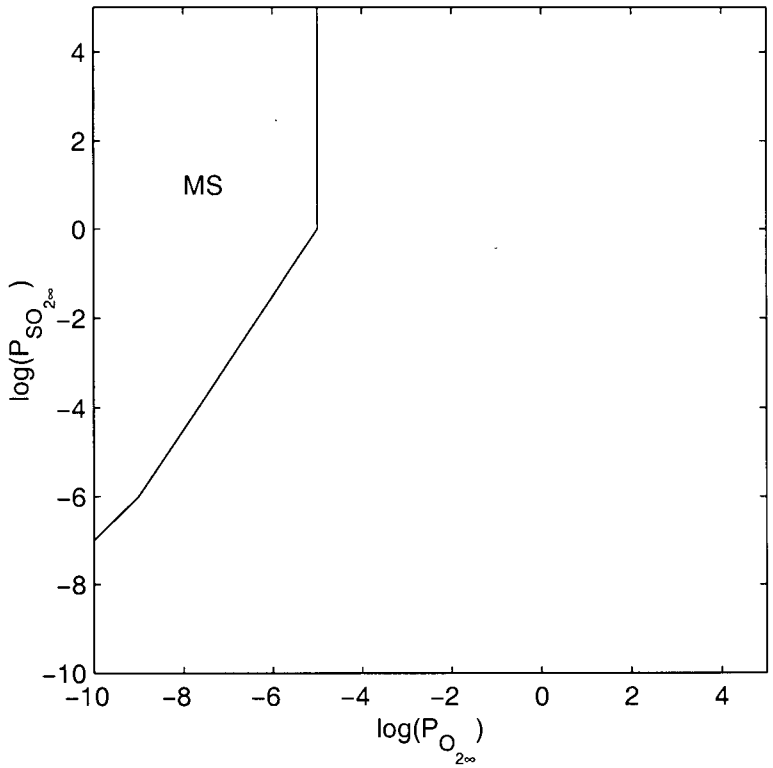

Figure 3.2: Modified predominance diagram construction. MS phase, for any Damköhler number.

3.3.2 MS to MSO_4

Reaction (3.25) represents the sulfation of the sulfide. The stoichiometric coefficient for SO_2, n, being zero (n=0), there is no sulfur dioxide partial pressure difference. However, the stoichiometric coefficient for O_2, m, is two, so that oxygen partial pressure differences can exist between the surface and the bulk of the gas. As equation (3.18) shows, this difference is proportional to the Damköhler number and the surface oxygen partial pressure. Figure 3.3 presents a family of MSO_4 stability regions drawn on the modified predominance diagram, with Damköhler numbers of 0.01, 0.1, 1, 10 and 100 chosen to illustrate the transition from chemical kinetics control to mass transfer control. Increasing the Damköhler number shifts the stability to higher oxygen partial pressures. Damköhler numbers smaller than those used in the figure create virtually identical lines to that for D_{III} equal to 0.01.

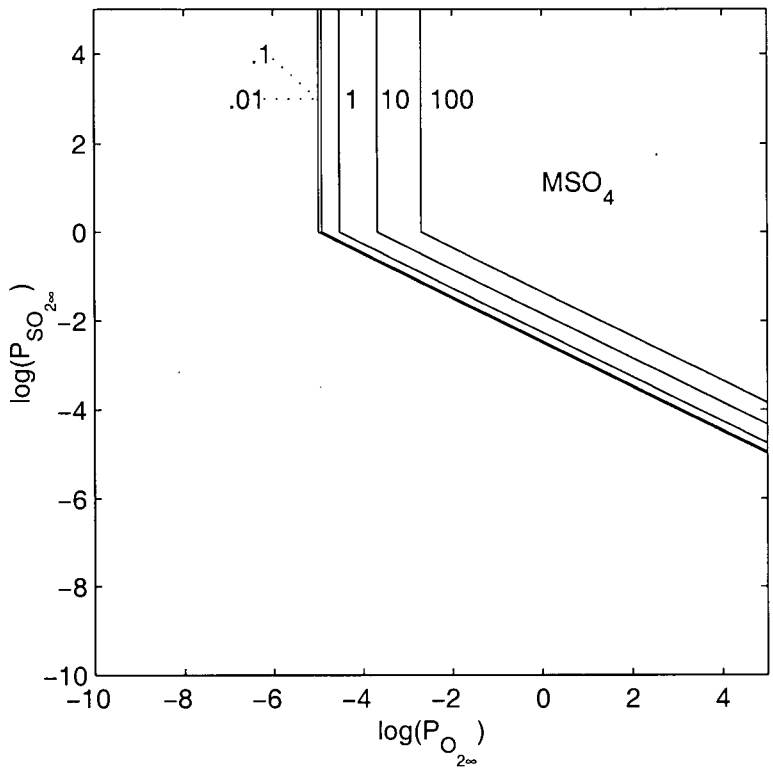

Figure 3.3: Modified predominance diagram construction. MSO_4 phase. Left to right: D_{III} = 0.01, 0.1, 1, 10 and 100.

3.3.3 MS to M

Direct production of the metal from the sulfide is represented by reaction (3.28). As in the previous sections, Figure 3.4 presents the construction of the modified diagram for several Damköhler numbers. Considering the stoichiometric coefficients for oxygen and sulfur dioxide, questions can be raised regarding the placement of the lines with respect to the sulfur dioxide axis. However, with a closer observation, the bulk sulfur dioxide partial pressure for a specific composition on the predominance diagram is found to decrease with increasing Damköhler number. Because of the logarithmic scale, this effect is not seen clearly. Also, because the surface concentration is subtracted to obtain the bulk SO_2 partial pressure, a limit exists for the surface sulfur dioxide partial pressure where the bulk partial pressure becomes zero. When setting the bulk partial pressure to zero, equation (3.30), describing the limit is obtained.

$$P_{SO_{2S}} = D_{III} \cdot P_{O_{2S}} \cdot n \tag{3.30}$$

On a logarithmic scale, this equation describes a family of parallel lines on the predominance diagram which varies with D_{III}*n. It is important to note that the sulfur dioxide stoichiometric coefficient in this equation is very important in locating the limit under which, the surface concentrations cannot exist. As the surface concentration approaches this limit, the bulk concentration also approaches zero where its logarithm lies at -∞. The effect of this limit is discussed in the next section.

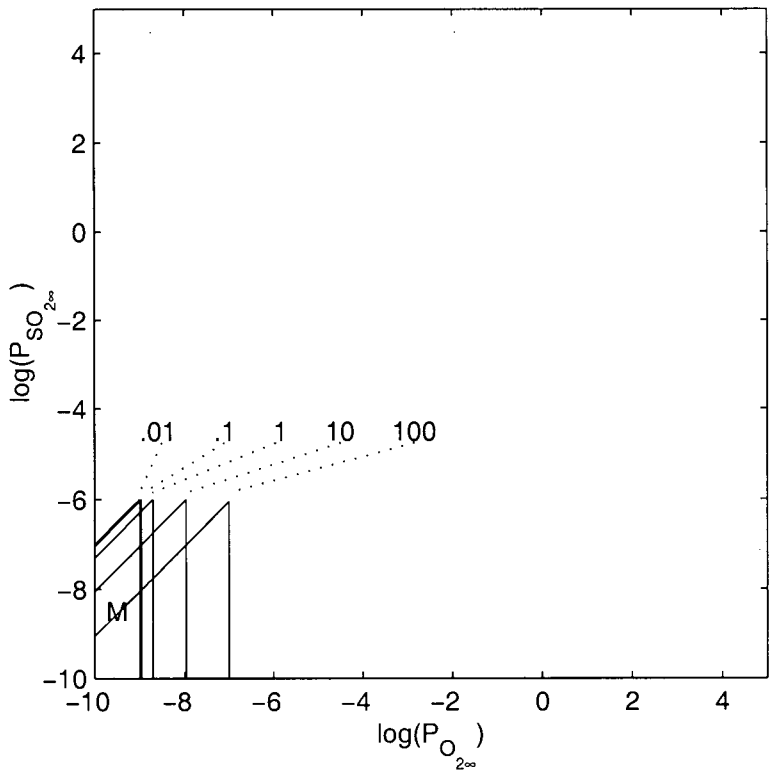

Figure 3.4: Modified predominance diagram construction. M phase. Left to right: D_{III} = 0.01, 0.1, 1, 10 and 100. The thick line on the left consists of lines for Damköhler numbers 0.01 and 0.1.

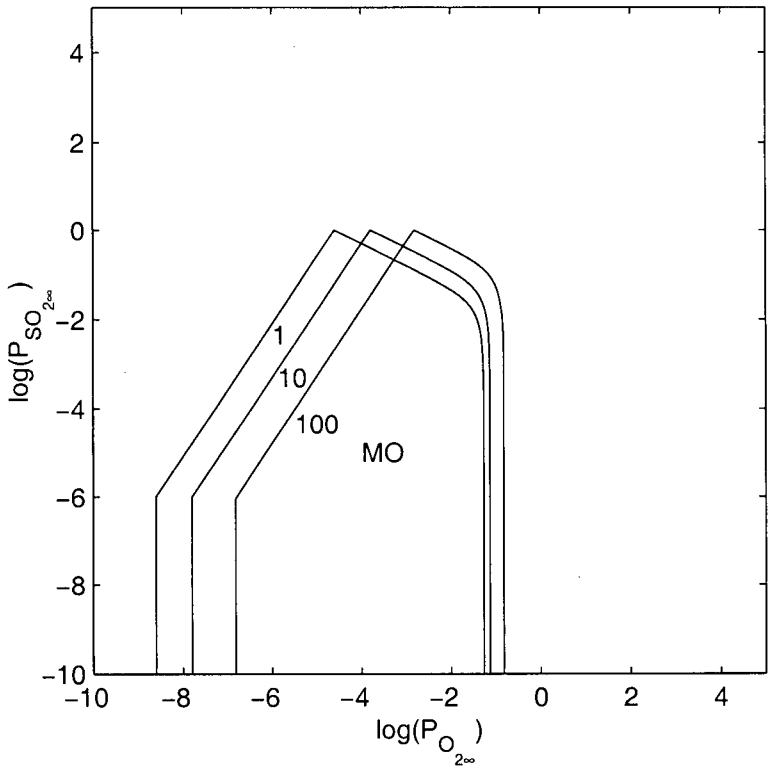

Figure 3.5: Modified predominance diagram construction. MO phase. Left to right D_{III} = 1, 10 and 100.

3.3.4 MS to MO

The last phase to consider in the hypothetical predominance diagram is the oxide. Reaction (3.29) describes the production of the oxide from the sulfide. Figure 3.5 presents the construction of the diagram for relatively high Damköhler numbers. As for the case of the metal and the sulfate, the M-MO and MS-MO lines shift to higher oxygen partial pressures with increasing Damköhler number. However, as discussed above, as the surface concentration approaches the limit created by equation (3.17), the bulk sulfur partial pressure approaches zero (or -∞ on the logarithmic scale). This creates a downward bend in the MO-MSO_4 lines.

Figure 3.6 presents the diagram for lower Damköhler numbers. The thick double line on the left side of the MO region corresponds to all Damköhler numbers. This figure shows that the

limit moves to higher oxygen partial pressures as the Damköhler decreases. Another observation from these two figures is that by increasing the Damköhler number during kinetic control, the MO-MSO_4 boundary moves to lower oxygen partial pressures, while mass transport control causes the boundary to shift to higher oxygen partial pressures.

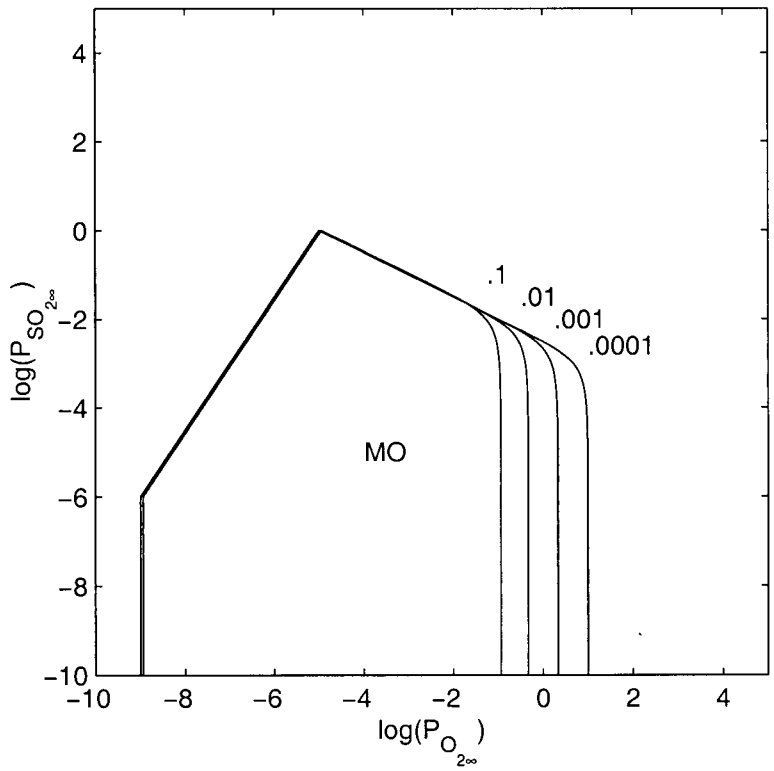

Figure 3.6: Modified predominance diagram construction. MO phase. Left to right D_{III} = 0.1, 0.01, 0.001 and 0.0001.

3.3.5 Two-phase zones

In the last sections, stability regions have been derived for each phase in the diagram. However, when these are combined onto a single diagram such as Figure 3.7 and Figure 3.8, regions appear between each phases.

In these regions, a single equilibrium line on the predominance diagram indicates a mixture of two phases. These new regions can be classified into two types. The first type consists of

oxygen starvation regions between MS and the other phases. The other type consists of binary regions between the MO-MSO_4 lines and between the M-MO lines.

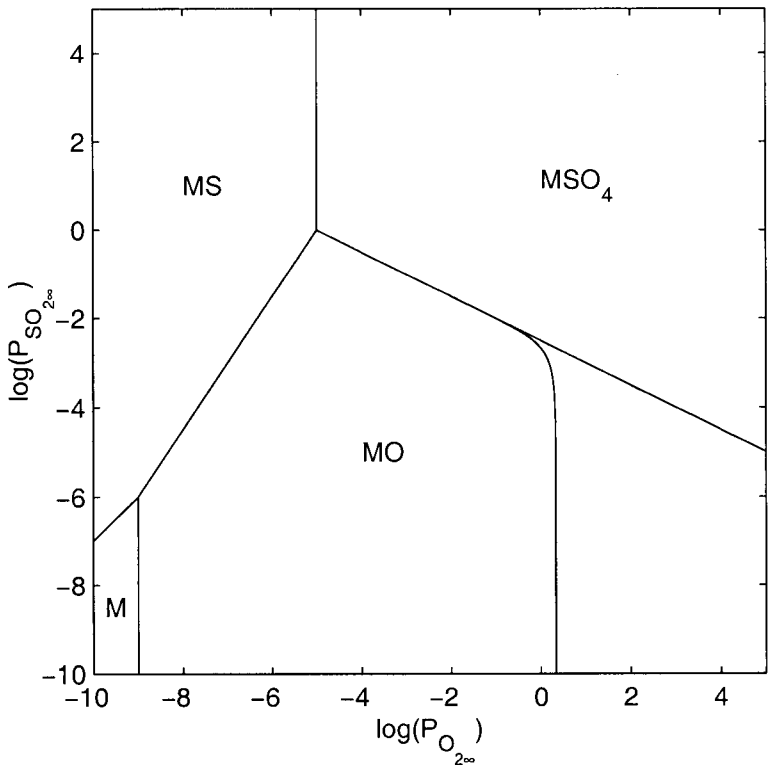

Figure 3.7: Modified predominance diagram construction. Four phases included. $D_{III} = 0.001$.

In all these regions, two solid products are produced, in various amounts and their activity is equal to one. A simple mathematical operation can be carried out to better understand how these regions are described. No assumption was made in equation (3.1) regarding the reaction products. A linear combination between two reactions gives the necessary tool to interpret the two-phase regions. This combination is done by considering the yield of the reaction with respect to each product. The yield of a specific product is defined as the fraction of reactant converted to the specific product.

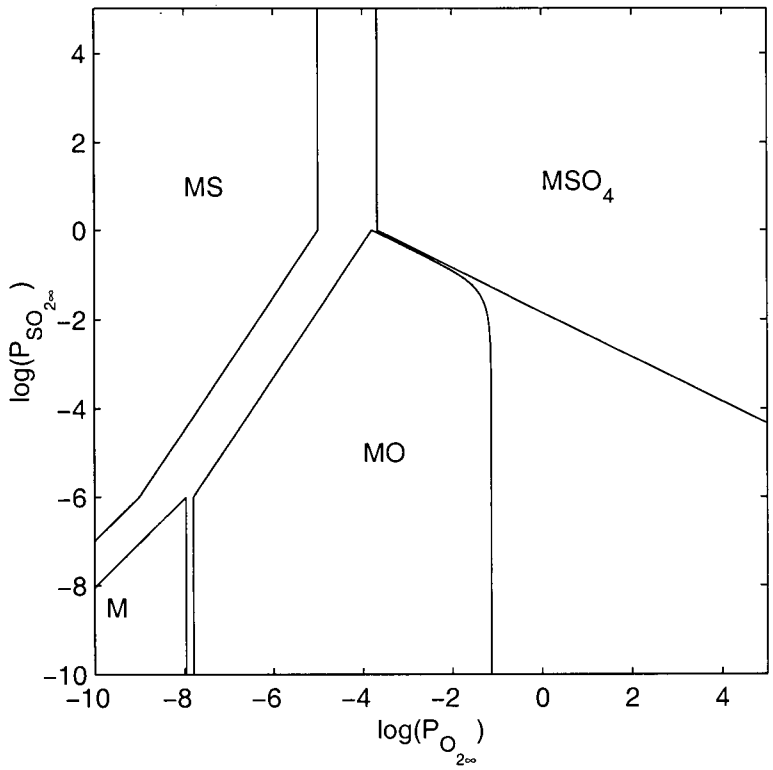

Figure 3.8: Modified predominance diagram construction. Four phases included. $D_{III} = 10$.

In a region where two products are produced, the yield of one product is related to that of the other. Modifying the yield of the reaction will modify the stoichiometric coefficients of the overall reaction. Note that the limit described earlier, moves when changing the yield of the reaction. Iso-compositions can be mapped by carefully varying the yield of a product from 0 to 1. For example, Figure 3.9 presents the complete diagram for a Damköhler number of 0.001 for the hypothetical predominance diagram. The small numbers in the MO-MSO_4 binary phase region indicate the logarithm of the molar fraction of MO in the reaction product. As the oxygen pressure increases, the proportion of MO in the binary phase decreases. The interval between the lines is logarithmic, i.e. 10^{-1}, 10^{-2}, 10^{-3}... Using the dotted lines is simple. For example, the reaction of lead sulfide in an atmosphere containing 10^{3} atm of oxygen with 10^{-8} atm of sulfur dioxide produces MSO_4 containing about 10^{-4} mole fraction of MO.

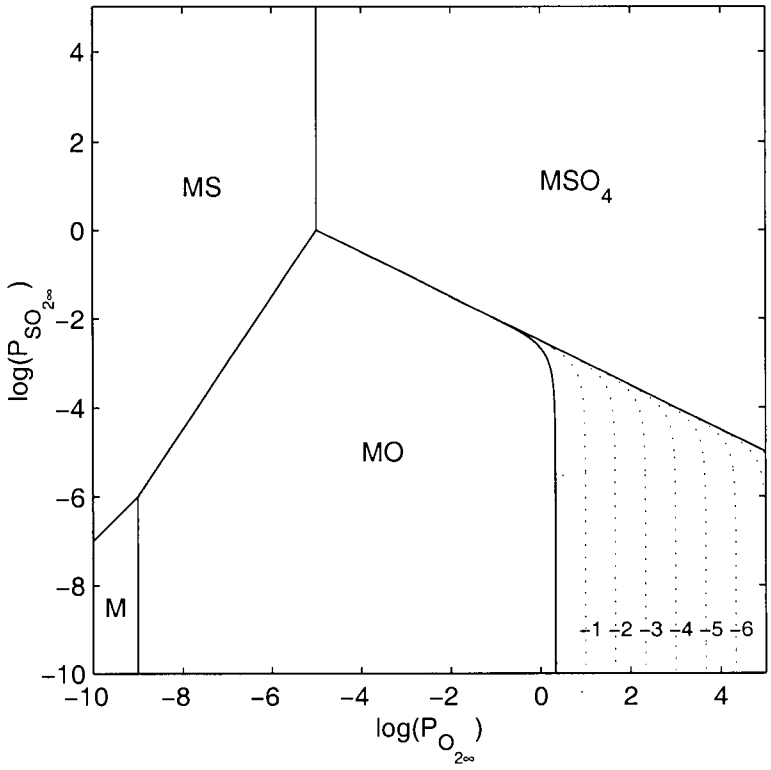

Figure 3.9: Completed modified predominance diagram. Addition of binary phase iso-composition lines. D_{III} = 0.001. Small numbers give logarithms of mole fraction of MO, as explained in the text.

Figure 3.10 is similar to Figure 3.8 except that dotted lines describing the binary regions have been added. The lines in the MO-MSO_4 binary region are similar to those of Figure 3.9. Everywhere in the MO-MSO_4 binary region, the surface concentrations are located on the MO-MSO_4 equilibrium line of the predominance diagram. In this region, the system looses a degree of freedom. The sulfur dioxide concentration at the surface is a function of the oxygen concentration at the surface.

A dotted line has also been added in the M-MO binary region delineating a molar fraction of 0.5 M (or MO). The width of this region being small, only one line has been drawn. Contrary to the MO-MSO_4 region, the lines in this binary region have a linear interval between 0 and 1, i.e. 0, 0.1, 0.2 ... 0.9, 1.

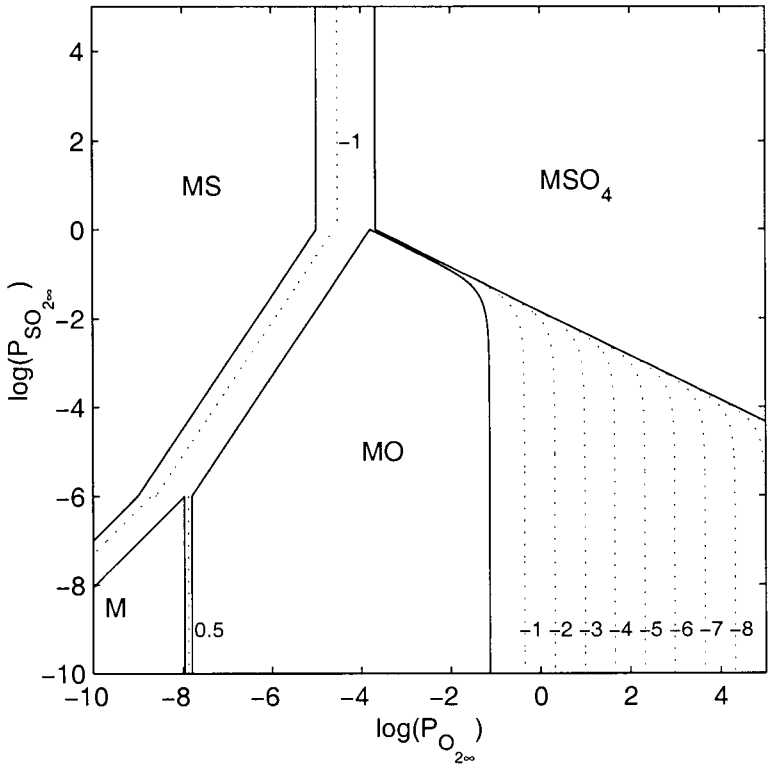

Figure 3.10: Modified predominance diagram construction. Addition of binary phase iso-composition lines for D_{III} = 10.

Dotted lines have also been added to the oxygen starvation region. In these regions, equation (3.18), which describes the oxygen partial pressure difference, does not directly apply. The applicable equations will be discussed in a summary of the assumptions in the next chapter. This binary region, described by an equilibrium line on the predominance diagram, is not a true binary region because one of the reaction products is also a reactant. There is not enough oxygen in the bulk gas phase to support the reaction rates to the prescribed Damköhler number. This region can only be described by artificially reducing the reaction rates. The oxygen starvation region is then a region where the rates are reduced due to insufficient oxygen transport. The dotted line in the oxygen starvation region of Figure 3.10 describes a reduction to 10% of the rates due to oxygen starvation. Other lines could have been drawn, but due to space limitations, only a single line is shown.

3.3.6 Triple points

Triple points can be processed in the same way as the equilibrium lines, except that the composition produced is a variable mixture of three compounds. A triangle is formed by three kinetic transformations applied to a single triple point. Inside the triangle, three solid phases are formed. This triangle, having negligible area, does not have any internal details like the binary regions. The triple points define the transition between two binary regions. For example, in Figure 3.10, some transition must exist between the MO-MS, M-MO and M-MS regions.

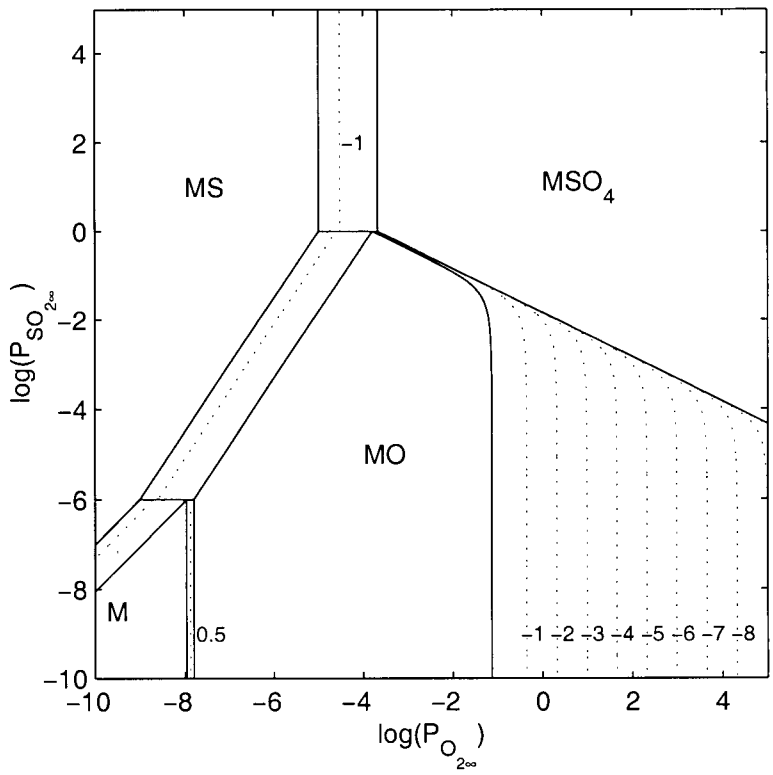

Figure 3.11: Complete modified predominance diagram. D_{III} = 10.

Figure 3.11 is the completed diagram for a Damköhler number of 10, differing from Figure 3.10 only by the addition of the triple point lines. When using the diagram, one can neglect the ternary regions because of their very small influence.

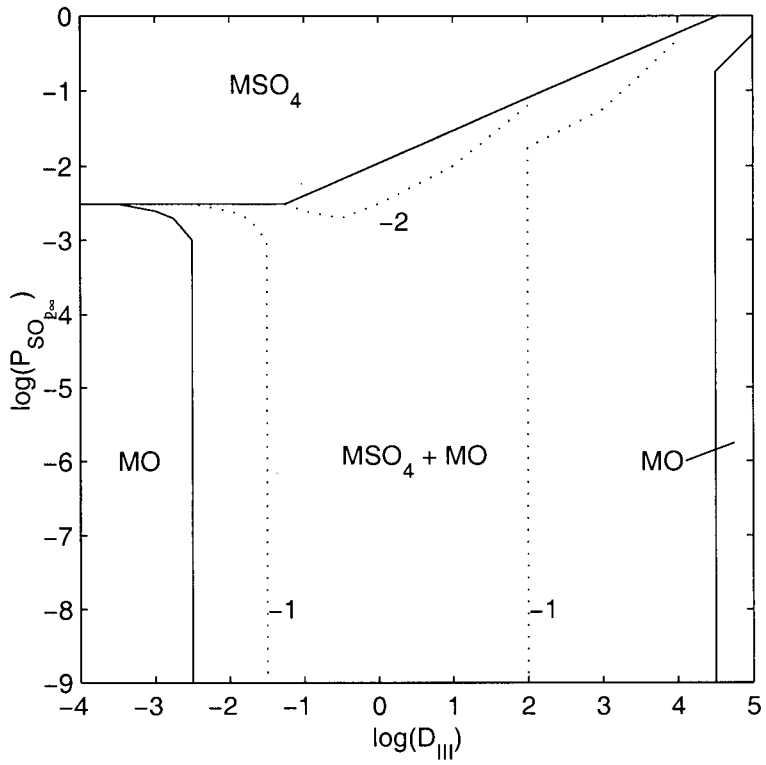

Figure 3.12: Approximate diagram showing a slice of modified predominance diagrams at a constant bulk oxygen partial pressure of 1 atm.

3.3.7 Application of the modified predominance diagram

The modified predominance diagram can be used to answer questions about a reacting system. The first question concerns the conditions under which mass transfer effects can be considered negligible. A criterion is available to consider the effect of mass transfer on the overall rates. However, only the modified predominance diagram can answer the following question: Is there an effect of mass transfer on the reaction path of a system? The answer depends not only on the Damköhler number, but also on the composition of the surrounding atmosphere. For example, referring to Figure 3.6, with a Damköhler number of 0.01 and air ($\log(P_{O2}) = -0.7$), the system produces MO. However, with pure oxygen ($\log(P_{O2}) = 0$), a mixture of MO and MSO_4 is produced. Referring to the same figure, another example of a transition from one region to another can be illustrated. Using pure oxygen ($\log(P_{O2}) = 0$), an

increase in the Damköhler number from 0.001 to 0.01 would again cause a transition from the production of MO to the production of the binary mixture MO-MSO_4. This can be clearly shown by creating Figure 3.12 consisting of a slice at a constant oxygen partial pressure of a series of modified predominance diagrams.

On this figure, one can clearly see that at an oxygen partial pressure of one atmosphere, predictions made by unmodified predominance diagrams are only valid below Damköhler numbers of $10^{-3.5}$. Also, when increasing the Damköhler number, the reaction products goes from the oxide to a mixture of the sulfate and oxide and returns to an oxide production regime when very high Damköhler numbers are used. An increase in the Damköhler number could be caused by the growth of reaction products, which add to the mass transport resistance or to a decrease in the convection in the system, e.g. to a reduction in relative velocity between particles and gas.

Figure 3.12 is an approximate diagram because these diagrams are not simple to compute. No new software has been written to create this diagram, it was created by printing a series of modified predominance diagrams and by manually copying the features onto the new figure. However, automating this process would lead to a very useful tool for the analysis of gas-solid reactions. Using the explicit equations for calculating the composition at the surface would simplify the creation of these diagrams.

These are useful examples, but the application of a hypothetical system is limited. The next chapter presents diagrams for the lead-oxygen-sulfur dioxide system.

4. Modified predominance diagrams for lead sulfide oxidation

The last chapter introduced a transformation that can be made on predominance diagrams to take into account the kinetic regime of reactions. This chapter presents modified predominance diagrams for the oxidation of lead sulfide.

4.1 Predominance diagrams

The lead-sulfur-oxygen system is more complex then the hypothetical system used previously as it has more oxide phases and it has a series of intermediate oxide-sulfate compounds called basic lead sulfates. A typical predominance diagram for the system is presented in Figure 4.1.

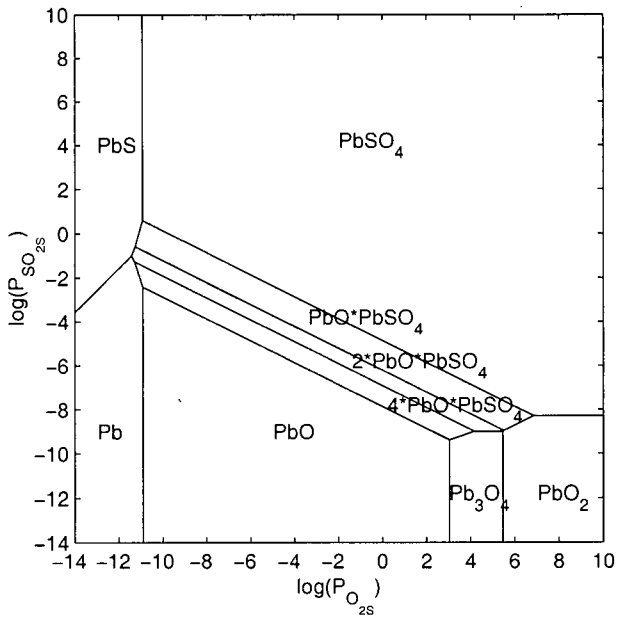

Figure 4.1: Predominance diagram of the Pb-SO_2-O_2 system at 800°C.

This predominance diagram has been chosen because all the compounds present in the Pb-O_2-SO_2 system are represented.

4.2 Modified predominance diagrams

Using the process presented in chapter 3, stoichiometric coefficients can be obtained for each reaction described by the general reaction:

$$PbS + m\ O_2 \rightarrow Products + n\ SO_2$$

The stoichiometric coefficient for each product is shown in Table 4.1.

Table 4.1: Stoichiometric coefficients for each product.

Product	m	n
PbS	0	0
Pb	1	1
PbO	3/2	1
Pb_3O_4	5/3	1
PbO_2	2	1
$PbSO_4$	2	0
$PbO*PbSO_4$	7/4	1/2
$2PbO*PbSO_4$	5/3	2/3
$4PbO*PbSO_4$	8/5	4/5

The modified predominance diagrams can then be created from the predominance diagrams using these stoichiometric coefficients and the equations derived in chapter 3. The modified predominance diagrams in the Pb-SO_2-O_2 system are very similar to those in the hypothetical system. There are however, a few differences because of the presence of the basic lead sulfates and the higher oxides. Figure 4.2 presents a modified predominance diagram for the Pb-O_2-SO_2 system at 800°C with a Damköhler number of 1. To simplify the figure, some of the labels are left out.

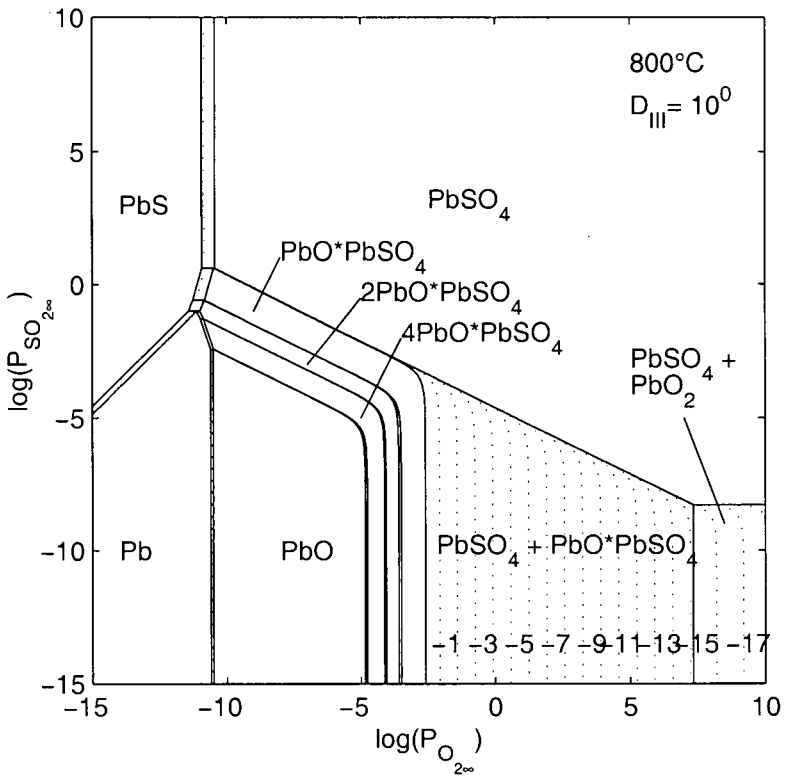

Figure 4.2: Modified predominance diagram at 800°C with a Damköhler number of 1.

The oxygen starvation region is located between the PbS and the other phases. The MSO_4-MO binary region is now composed of a $PbSO_4$-$PbO*PbSO_4$ region and a $PbSO_4$-PbO_2 region. The $PbSO_4$-$PbO*PbSO_4$ region has a boundary on the high oxygen concentration side, created by the presence of the oxide PbO_2. At pressures higher than the $PbSO_4$-$PbO*PbSO_4$-PbO_2 triple point, a $PbSO_4$-PbO_2 binary region exists. The dotted lines have the same meaning as previously. The numbering of the dotted lines in the new binary region is simply the continuation from the adjacent region. For example, if we have, in the $PbSO_4$-$PbO*PbSO_4$ region, iso-composition lines going from -1 to -10, the first line in the $PbSO_4$-PbO_2 will be -11. The binary regions between the basic lead sulfates and the monoxide are regions similar to the M-MO regions described in the last chapter. In this modified predominance diagram, Pb_3O_4 is no longer present. The disappearance is this phase is due to the limit described in the previous chapter. Because there is no equilibrium of Pb_3O_4 with a

phase where n equals zero, the only method of moving the limit so that Pb_3O_4 can be seen is by reducing the Damköhler number.

The modified predominance diagrams must be created for each temperature and each Damköhler number. Appendix 5 contains a collection of modified predominance diagrams for the oxidation of lead sulfide at temperatures of 300,400,500,600,700 and 800°C for various Damköhler numbers, covering a range including chemical kinetics control, mixed control and mass transfer control. The software used to create the diagrams is located in Appendix 3. This software can be used to generate similar diagrams for different temperatures or different Damköhler numbers. If the need to create these diagrams arises for a different system, the software can be modified by changing the data in the thermodynamic procedure and the stoichiometric coefficients in the main program. The software uses the MATLAB [57] programming language, version 5.2.

4.3 Assumptions

Derived from a simple mathematical development based on transport and rate phenomena, the modified predominance diagram demonstrate clearly that under certain conditions, mass transfer can influence the reaction path of a reacting system. However, numerous assumptions have been made and they must be kept in mind when using these diagrams. They are now summarized:

- The sample is reacting according to the predominance diagram. The phase that will be produced will be the one which is in equilibrium with the gas present at the surface of the sample. This assumption is commonly made in various systems.
- Only PbS is reacting to produce other reaction products. If other reactants have to be considered, new diagrams must be created because the reactions and the stoichiometric coefficients for the gases will be different.
- The system is isothermal, and there is no heat transfer or heat generation/utilization. The predominance diagram is an isothermal diagram.

- Activities of the solid products are all unity. No solutions are taken into account. This is a common assumption for the creation of predominance diagrams. This assumption is very useful to characterize the binary regions of the modified predominance diagram.

- The reaction products do not participate in any other reactions such as decomposition, reduction or roast reactions. They also do not influence the reactions.

- The gas-solid reactions are taking place at the solid surface, i.e. gaseous lead sulfide is neglected and there is no gaseous species other than O_2 and SO_2.

- All reactions have the same kinetic rate laws, i.e. the same reaction order (first order) and the same rate constants. This assumption is not strictly valid, as it is probable that the rate laws would differ from one product to another.

- The kinetic law used in the development of the equations is not valid when the concentration of oxygen is close to the equilibrium composition. The difference between the surface gas composition and the composition of the gas in equilibrium with the solid phases is the driving force of the chemical reaction. The following chemical kinetic equation should be used instead:

$$r_{MS} = A \cdot B \cdot e^{-E_a/RT} \cdot \left(P_{O_2 s} - P_{O_2 eq}\right) \tag{4.1}$$

The equilibrium concentrations are described by the sulfide equilibrium lines on the predominance diagram. It is important to note that the equilibrium is between the reactant and the products. The equilibrium lines of two products are not used here. When the partial pressure at the surface is more than two orders of magnitudes higher than the equilibrium concentration, the equilibrium concentrations can be neglected and set to zero. This has already been done in the initial development. The mathematical development and the diagrams are still valid everywhere except where the oxygen partial pressure at the surface is similar to equilibrium oxygen partial pressure. This new equation reduces the reaction rate due to the proximity to the

equilibrium. The rates no longer have to be artificially reduced by changing the yield. However, the diagrams created with the previous equation are very useful to locate the region where the equilibrium concentration should be used.

Using the generalized equation complicate the development of the modified diagrams for one type of lines: the equilibrium lines between the reactant and the products. For all the other lines, the equilibrium concentration is negligible and the previous equation remains. The diagrams created with this new equation will be very similar to the ones presented except that the oxygen starvation zone is no longer clearly defined because some of the lines are no longer represented on the diagram. The equilibrium lines will no longer move right as the Damköhler number increases in the transport controlling regime.

- The influences of other rate-limiting steps such as adsorption, desorption and mass transfer through the pores or through the reaction product layer are neglected. They could be accounted for by redefining the Damköhler number to include some of these.

- The system is considered to be a binary gas system. Ternary gas flow and diffusion have been neglected. The mass transfer coefficients do not vary with composition or species. This is again not strictly valid as the transport properties such as the diffusivity, density and viscosity change with gas composition.

- Bulk flow and high mass transfer rates are neglected. Equations considering these two factors have been developed. The diagrams are different at pressures higher than one atmosphere. At lower partial pressures, the diagrams are virtually unchanged.

Other diagrams could be created to take into account some of these assumptions. For example, if the kinetics of each reaction were known, equations could be derived for each reaction, and diagrams for different mass transfer coefficients could be prepared. However, the quantity of experimental information needed would be prohibitive.

4.4 Validation of the diagrams

After reviewing the assumptions made for the creation of these diagrams, it is doubtful that the diagrams will reflect reality in every situation. They are, however, a good tool when considering the effect of the mass transport on the behaviour of a system.

The novelties brought by the modified predominance diagram are the presence of binary regions and the curvature of some of the lines. The curvature of some of the lines can be easily understood when considering that the sample itself is generating sulfur dioxide. However, some doubts can be raised about the validity of the binary regions because thermodynamics does not predict binary areas as large as the ones presented by the modified predominance diagrams. However, thermodynamics does predict binary phases and they are described as equilibrium lines. It is important to note that for every bulk gas composition in the binary regions, the surface gas composition is lying on the equilibrium line. In order to satisfy both the mole balance and the equilibrium, one degree of freedom is lost. The sulfur dioxide concentration at the surface is then correlated to the oxygen concentration at the surface via the equilibrium line.

There is some experimental evidence, showing that the binary regions do exist. For example, Polyvyannyi et al [58] observed, using IR spectrometry that after reacting PbS in air at 710°C for 15 minutes, the reaction product is a mixture of lead sulfate and monobasic lead sulfate.

It is, however, very difficult to use the current literature to verify the applicability of these diagrams as most studies were conducted for very long periods during which rate-limiting steps changed and the products reacted.

It is important to note that it would be very difficult to verify these diagrams experimentally. One has to control the Damköhler number and the gas composition with precision. Controlling the Damköhler number can only be achieved by varying the gas velocities, effectively changing the mass transfer coefficient. Chemical kinetics cannot be varied without changing the temperature or the composition of the system. Another complicating

factor is that with longer reaction times, the resistances to the reaction can change due to the presence of reaction products. The reaction products produced initially could be used to validate the diagrams, but their small amount would make the identification process difficult. Also, the detection and measurement of the minor compounds in the binary regions would be very difficult because of the very small molar fractions generated under some conditions.

5. Objectives and scope of the experimental work

Chapter 2 has shown that the current state of knowledge of the oxidation kinetics is incomplete. Quantitative and useful results needed for modelling the flash smelting process are unavailable. Therefore, the main objective of this research is to study low temperature oxidation kinetics of lead sulfide.

It has been shown that temperature and the presence of sulfur dioxide are important factors influencing the oxidation kinetics of lead sulfide. A discussion of mass transfer effects has shown that mass transfer is a very important factor that must be taken into account when evaluating experimental data. Each of these factors have to be properly studied. As there is some scatter and uncertainty in the reaction order values found in the literature, an evaluation of the order of reaction with respect to sulfur dioxide and oxygen is also necessary.

The influence of temperature on the reaction rate is described by an Arrhenius plot and its equation. The activation energies found in the literature cannot be used in flash smelting. An evaluation of the temperature dependency of the chemical kinetics is needed.

The reaction products could be lead, lead oxide, lead sulfate or basic lead sulfates. Verification of the reaction products produced during the experiments is also necessary.

The approach taken to meet the objectives consists of performing experiments in a thermogravimetric apparatus where the atmosphere composition and flow rates are controlled. The samples consist of pure lead sulfide pressed into porous pellets. The products are analyzed using X-ray diffractometry (XRD) and scanning electron microscopy (SEM). The experimental data are then analyzed mathematically to extract the relevant kinetic data.

6. Experimental Set-up and Conditions

Various information is needed to characterize the chemical kinetics of lead sulfide oxidation. This thesis seeks to obtain and clarify the activation energy and the pre-exponential constant, the reaction order with respect to oxygen and the reaction order with respect to sulfur dioxide of low temperature lead sulfide oxidation in the presence of sulfur dioxide. To obtain this information, three series of experiments must be performed under experimental conditions of various temperatures, oxygen and sulfur dioxide compositions. In order to carry out these tests, an experimental set-up has been designed. It is capable of:

- Isothermal experiments,
- Quickly switching the gas from an inert atmosphere to a reactive atmosphere,
- Known superficial velocity at the sample,
- Small gas residence times, and as close to plug flow as possible,
- Simultaneous temperature and mass measurement of the sample.

The apparatus chosen is a balance coupled with a temperature controlled vertical tube furnace which can accept multiple samples allowing for simultaneous measurement of the sample mass and temperature during an experiment.

6.1 Experimental set-up

The apparatus used in the experiments is a thermogravimetric balance consisting of a balance, a vertical tube furnace and a gas preparation assembly. A data acquisition system records the information derived from the thermocouples, the balance and the furnace controller. Figure 6.1 shows how each of these is related to the complete apparatus. To simplify the drawing, water cooling has not been shown. Each section is described further below.

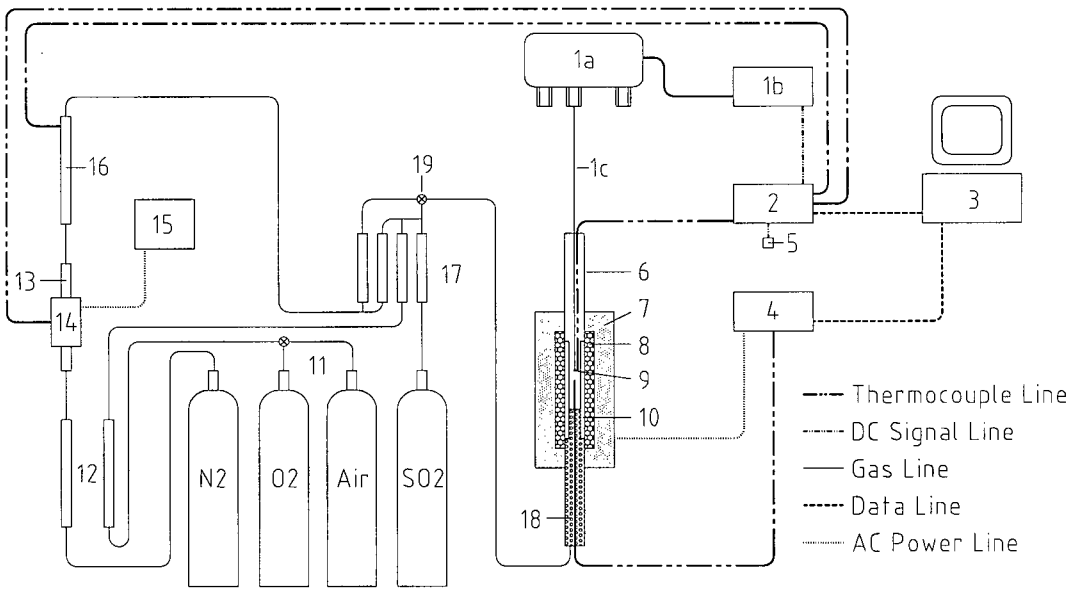

Figure 6.1: Experimental set-up used in this study. The numbers are described in the text.

6.1.1 Balance

The balance is a RG automatic electrobalance from Cahn instruments with a total capacity of 2 grams. It consists of the beam assembly (1a) and the associated electronics (1b). The sample (9) is suspended in the furnace by a thin chromel wire (1c). Tare weights are added to the counterweight side of the beam making the balance useful for measuring mass variations. The output of the balance, usually calibrated and plotted onto a chart recorder, is connected to a high resolution (18 bit) data acquisition system. The balance is calibrated by adding or removing calibration weights. The resulting step change recorded by the data acquisition system is directly proportional to the mass of the calibration weight used. The recorded step

change is then used to transform readings into mass variations. The accuracy of the calibration weights has been verified with a Micro Gram-Atic balance built by Mettler. The balance can measure differences in mass in the range of micrograms. The flowing gas creates noise on the mass measurement larger than the precision of the balance. The factor limiting the sensitivity of the balance is then the noise due to the flowing gas.

6.1.2 Furnace

The vertical tube furnace is installed in an elevator cart guided by two rails and supported by a counterweight. The maximum vertical translation is about 400 mm. Alignment is adjusted by repositioning the balance at the axis of the system. The furnace has been built using two "clamshell" heating elements (8), thermal insulation (7) and a galvanized steel cylinder. The two resistance heating elements are semi-cylindrical helically wound elements, 300 mm (12 inches) long by 60 mm (2.5 inches) internal diameter. The maximum rated temperature for these elements is 1100 °C. The thermal insulation is a high temperature Fiberfrax refractory blanket. The shell of the furnace is a steel cylinder, 400 mm (16 inches) long by 200 mm (8 inches) diameter. The two lids covering the ends of the furnace have a concentric hole for the inner tube. An alumina tube (6), 760 mm (30 inches) long and 57 mm (2.25 inch) outer diameter is placed within the furnace. The inside diameter of the tube is 50 mm (2 inches), large enough to allow positioning of multiple samples. Two stainless steel water-cooled flanges (not shown) are located at the extremities of the tube. The bottom portion of the tube is filled with a bed, containing 12 mm (½ inch) diameter alumina spheres (18) for preheating the gases. A restriction (10) is located at the centre of the furnace. It is a tube with an internal diameter of approximately 29 mm and approximately 250 mm in length, supported by a removable refractory plug. The assembly is inserted into the tube at the centre of the furnace in order to increase the linear velocity of the gases surrounding the pellet. If a new furnace is built for a similar study, one should consider reducing the diameter of the tube to allow higher linear flow rates with reasonable gas volumes.

A gas residence time analysis using a low gas flow rate of 0.5 l/min at room temperature has indicated that the pellet experiences transient conditions for about 1 minute after a step

change in gas concentration. Increasing the gas velocity by a factor of 10 would reduce this transient period by a similar factor. The flow rates chosen for the experiments give a transient regime period of approximately 5 seconds at room temperature. Increasing the temperature of the furnace also decreases the transient regime period.

The temperature of the furnace is controlled by a temperature controller (4) model CN8501-DC1-PC2 supplied by Omega. The controller has an auto-tuning function which optimizes the control of the operating conditions. The control thermocouple is located inside the alumina tube, approximately 12 mm under the pellet.

The pellet location was chosen to be in an isothermal zone, as determined from temperature profiles inside the furnace. The location of the pellet is changed by varying the length of the suspension wire.

6.1.3 Gas System

The gas system consists of the pressurised cylinders and their regulators (11), desiccant (12), an oxygen scrubber (13), and rotameters (17). Compressed air can also be used as the air source.

Nitrogen is fed to the oxygen scrubber after being dried in a fixed bed silica gel. The volume of each bed of desiccant is approximately 1 litre. Either oxygen or air, acting as the oxygen source of the reactive gas, is fed to rotameters after been dried by a second desiccant bed. Sulfur dioxide is fed directly to the rotameters.

The oxygen scrubber is only used for the preparation of nitrogen. The scrubber (13) is made of a 25 mm (1 inch) diameter stainless steel pipe 560 mm long, containing copper filings. The tube is fitted with two reducing unions to allow for the use of small tubing. This assembly is heated to approximately 500°C in a small tube furnace (14) controlled by a variable transformer (15). The hot nitrogen is cooled in a heat exchanger (16) consisting of two concentric copper tubes (1/4 and 1/2 inches, i.e. 6.3 and 12.7 mm) between which cooling water flows. The water cooled section is 430 mm long. The hot gas coming from the

oxygen scrubber flows within the inner tube. The temperature of the gas is monitored by a thermocouple positioned at the exit of the heat exchanger. The temperature of the gas exceeded the room temperature by a few degrees only when the nitrogen flow rate was very high (> 10 l/min).

Nitrogen is fed via two rotameters. One meters the inert gas atmosphere, while the second meters the amount to be mixed with oxygen or air and sulfur dioxide to form the reactive gas. The other gases forming the reactive mixture are also metered with rotameters. A three-way valve (19) allows a step change from an inert atmosphere to a reactive atmosphere.

6.1.4 Data Acquisition System

The data acquisition system consists of the hardware including a data acquisition circuit (2) and a 386 computer (3) running software written specifically for the hardware. A technical description of the hardware and software is presented in Appendix 2. The data acquisition hardware has 8 single-ended 12-bit channels (+4096 levels) and one double-ended 18-bit plus sign channel (+/- 262144 levels). The balance is connected to the 18-bit channel, while all other devices are connected to the 12-bit channels. All 8 channels of the 12-bit section are amplified to a 0-4.096 V level and filtered by a one-pole RC filter before being digitized. The gains of all amplifiers are shown in Table 6.1.

Channels 0 to 5 are used for type K thermocouples. Channel 6 can be used for a pH controller. Channel 7 is used for the room temperature sensor. The software takes the average of several measurements over one second and saves the result into a file. The resulting measurement is less sensitive to electrical noise. Recorded are the set point and temperature of the controller, both read by the data link to the controller, as well as various thermocouples, room temperature and the reading of the balance.

Table 6.1: Gains of the amplifiers used for the 12 bit section.

Channel	0	1	2	3	4	5	6	7
Gain	82.6312	81.9307	83.1328	82.8511	82.6734	82.7618	287.8136	109.98709

The room temperature sensor (5) is a LM35CAZ semiconductor from the National Semiconductors Corporation [59] contained in a TO-92 package. The output varies linearly with temperature by 10.0 mV/°C and has an output of 0 mV at 0°C. Self-heating is negligible in the current application. This measurement is used for cold junction compensation of the thermocouples.

6.2 Materials used

Lead sulfide, ammonium carbonate, nitrogen, oxygen, air and sulfur dioxide are the materials and gases used in this study.

Purchased from Aldrich Chemical Co., the lead sulfide was of high purity (99.9+%) and came from lot # MQ 10415MQ. The average particle size as given on the certificate of analysis is 8 microns. The elemental analysis is presented in Table 6.2. The Brunauer Emmett Teller (BET) surface area measurements were carried out in the department of chemistry on a Micromeritics ASAP 2010 accelerated surface area and porosimetry system. The surface area was determined at 77.4K using krypton as adsorbate. BET krypton surface area measurements performed on the lead sulfide powder resulted in a surface area of approximately 0.4 m^2/g.

Table 6.2: Elemental analysis of lead sulfide.

Ni	Ag	Ca	Al	Cr	Mg	Cu
200 ppm	50 ppm	50 ppm	10 ppm	10 ppm	5 ppm	500 ppm

The ammonium carbonate used as a filler in the pellets, was purchased from Fisher Scientific and is from lot number 965481. It is in the form of lumps, and is crushed with a mortar and pestle before use. Its composition is shown in Table 6.3.

Table 6.3: Analysis for the ammonium carbonate.

Assay (NH_3)	31.0%
Chloride (Cl)	1.2 ppm
Heavy metals (as Pb)	1.2 ppm
Insoluble matter	0.001%
Iron (Fe)	3 ppm
Non-volatile matter	0.004 %
Sulfur Compounds (as SO_4)	0.0005 %

The gases were all of commercial purity. Typical analyses given by the Praxair are presented in Table 6.4.

Table 6.4: Typical analyses of gases used in this study.

N_2	O_2	Air	SO_2
99.0% CO < 10 ppm	99.0% CO < 10 ppm CO_2 < 300 ppm	19.5-23.5 O_2 Balance N_2 CO< 40 ppm CO_2 < 500 ppm SO_2 < 5 ppm $NO+NO_2$ < 2.5 ppm	99.98% H_2O < 100 ppm Residue < 75 ppmw Acid as H_2SO_4 < 25 ppmw

Gas chromatography analysis of the air contained in the air cylinders showed that it contained 22.0%V/V oxygen. The gas chromatograph used is a Varian 3400 equipped with a packed column and a thermal conductivity detector. The injector port, column and detector were maintained at 80°C. The peaks are integrated with a Perkin-Elmer M2 Calculating Integrator previously calibrated with mixtures of nitrogen and oxygen. When compressed air is used in the experiment, a value of 21.0%V/V oxygen is used.

6.3 Sample description

Two pellets (9) are needed for each experiment, one suspended by the balance and the other by a thermocouple. This arrangement gives simultaneous measurement of both weight variation and temperature.

Each pellets was produced by mixing approximately one gram of lead sulfide and 100 milligrams of ammonium carbonate. The ammonium carbonate is used as a volatile filler which takes up space and helps increase the porosity of the pellet after the filler is degassed. The amount of carbonate was chosen to obtain a porosity of 30% to 40%. Before pressing, the mixture of lead sulfide and ammonium carbonate is thoroughly blended with a spatula until no ammonium carbonate grains are visible. The pellets are then pressed with a 9.66 mm cylindrical steel die in a Carver Laboratory Press. After pressing under a force of three metric tons, the pellets are placed in a drying oven at approximately 100°C for one hour. After this degassing period, a X-ray diffraction analysis and the residual mass of the pellet showed that no ammonium carbonate was present. The pellets are then weighted with a GRAM-ATIC balance, and their dimensions are measured with a Mitutoyo micrometer. The bulk density of the pellet is given by dividing the mass of the pellet by the cylindrical volume of the pellet. The porosity of the pellet is given by:

$$\varepsilon_p = 1 - \frac{\rho_p}{\rho_{PbS}} \tag{6.31}$$

The pellets needed for each experiment are matched according to their mass and then porosity, to ensure that two pellets of similar characteristics are used in each experiment.

The BET surface area of the powder and the pellets produced was measured. The surface areas of the pellets was found to be similar to those of the powder, i.e. 0.4 m^2/g. The surface area measurements were carried out on the same machine as those of the powder measurements.

6.4 Experimental conditions

Many experiments were performed with different reaction temperatures and gas compositions. The influence of the furnace temperature, oxygen and sulfur dioxide concentrations were studied one at a time. When the gas composition was varied, the amount of oxygen or sulfur dioxide was varied, and the flow rate of nitrogen was then varied to keep the total gas flow rate to the furnace constant, generally between 7 and 7.5 L/min. The samples used were 9.66 mm diameter and 2.5 to 3 mm in thickness depending on the porosity of the samples. When the sulfur dioxide concentration was held constant, it was kept at approximately 2.7%. When the oxygen concentration was kept constant, it was approximately 20%. The conditions used in each experiment are presented in Appendix 4 and are summarised in Table 6.5

The choice of experimental conditions was limited by a number of factors. The reaction products must not melt, as there is no crucible to retain any liquid. The reaction rate must be high enough to be able to measure it, hence limiting the lowest temperature used. There is then a limited range of temperatures which can be used in our experiment. To be able to compare these experiments with previous studies, an oxygen concentration similar to that of air is used. The concentration of sulfur dioxide has been chosen in order to be certain that the composition of the atmosphere is in the sulfate stability region at all temperatures. The maximum SO_2 content has been chosen to be approximately 10% to ensure that the transport properties are not modified dramatically. This also reduced the volume of sulfur dioxide used during the experiments. The pellet porosity and total flow rate were increased for the reaction order experiments to ensure that gas mass transfer would not influence the measurements.

A series of experiments began with the mounting of the pellets, and the zeroing and calibration of the balance. Calibration is performed with the furnace lowered while the atmosphere of the furnace is thoroughly purged with inert gas. The pellets were suspended by a 36 gauge (0.127 mm) chromel wire wrapped around the pellet. No interactions between

the wire and the pellet were observed until melting of the pellet occurred. The pellets were placed so that the major external surfaces, the flat circular faces, were parallel to the gas flow.

Table 6.5: Summary of experimental conditions.

Series of experiments:	Variable	Constant
Series #1	Temperature °C 269, 309, 346, 373, 416, 434, 508, 546, 607, 645	Porosity 27% 20.4%vol O_2, 2.7%vol SO_2 Bal. N_2 Total flow rate: 5.8 L/min
Series #2	Oxygen concentration %vol 4.4, 7.8, 12.5, 20.6, 36.7, 49.2, 61.5	Porosity 38%, Temperature 390°C 2.2%vol SO_2 Bal. N_2 Total flow rate: 7.3 L/min
Series #3	Sulfur dioxide concentration % vol 0, 1.2, 2.1, 4.4, 6.6, 10.6	Porosity 38%, Temperature 440°C 20.4%vol O_2, Bal. N_2 Total flow rate: 7.3 L/min

To begin an experiment, the furnace was raised to its maximum height above the samples. The samples were preheated in an inert atmosphere until the temperature of the pellets reached thermal equilibrium. The reactive gas mixture was then introduced into the furnace. After the predetermined reaction time, 15 minutes, the inert gas was reintroduced into the furnace until the next experiment. A few minutes were allowed to pass before lowering the furnace to allow the purging and venting of the reactive gases. After lowering the furnace, the sample was air-cooled for a few minutes after which it was removed and stored for later analysis. If an adjustment of the reactive gas composition and flow rates was needed, the furnace was raised to allow the venting of the gases while the rotameters were adjusted. The set point of the temperature controller was also adjusted if needed. Thermal equilibrium of the furnace was achieved before another experiment was performed. After the adjustments needed for the next experiment were done, another set of pellets (two pellets) was installed.

The change in the buoyancy force when changing the inert gas to the reactive gases would cause a mass variation between 7.5 μg (from N_2 to 20.4% O_2, 0% SO_2 at 390°C) and 42.3 μg (from N_2 to 20.4% O_2, 10.6% SO_2 at 390°C). The net effect of the buoyancy is an observed

reduction in the mass and this effect is more important for higher sulfur dioxide concentrations. The transient that the sample experiences has a duration of less than 3 seconds. The buoyancy effect is then localized at the start of the experiment. If the initial rates are determined for longer periods, the buoyancy will be negligible. The buoyancy effect will cause errors of less than 1% of the total mass variations.

6.5 Mathematical treatment of experimental data

After experiments have been performed, the data contained in the saved files are loaded in the Matlab software. The mass variations and temperatures are extracted. The pellet masses and surface areas are entered into the program. Calculation of the initial rates are performed by linear regression of the initial experimental data. The number of data points taken in the linear fit varied according from one experiment to the next. The data points taken were chosen to be in a linear region and their number were usually between 10 and 35. Long term rates are also obtained using a linear regression. In this case, the number of data points did not vary between the experiments.

When rates are compared, a statistical test is performed on all the data available and not only on the fitted rated. The test evaluates if the lines are parallel: H_0 all slopes are equal, H_1 at least one slope is different. This test uses the F distribution with a α of 0.05 and has the advantage of using all the data available and takes into account the incertitude of the regressions.

6.6 X-ray diffraction analysis

The phases formed during an experiment were identified by X-ray diffraction of the reacted pellet. The pellet was inserted in a specially made sample holder and inserted into a Philips diffractometer equipped with a copper source. The divergence and scatter slits commonly used for X-ray diffraction analyses were 1 degree, but to increase the sensitivity of the instrument for the lead-containing samples, the slits were replaced by 2 degree slits. The diffractometer scanned from 15 to 100 degrees. Good results were obtained and identification of the compounds was simplified by covering the XRD chart recorder output by transparencies containing the powder diffraction file data.

The direct use of the reacted pellets in the diffractometer is valid due to the small particle size (8 μm) of the lead sulfide powder. No preferential growth onto the lead sulfide was observed because of the initial random arrangement of the PbS particles.

6.7 Scanning Electron Microscopy

Scanning electron microscopy (SEM) was used to observe the structure of the unreacted and reacted pellets. The microscope used is a Hitachi model S-2300. The backscattered electron detector was used when chemical contrast was needed. The chemical contrast difference between lead sulfide and lead sulfate was sufficient to allow the study of the reaction product distribution in the pores of the pellet. X-ray spectroscopy was not effective to determine the composition of the reaction products because oxygen could not be accurately detected.

When a cross-section of a pellet was needed, it was first mounted in epoxy resin. The mounted sample is then ground to the proper depth and polished using alumina slurries. An optical microscope was used initially, but observations did not allow any feature of the sample to be identified. For use in the electron microscope, the epoxy-mounted samples were carbon coated to make them conductive. The carbon coating did not influence the observations.

7. Experimental results and discussion

Three series of experiments were carried out to clarify the behaviour of lead sulfide oxidation. In each series, the temperature, oxygen concentration and sulfur dioxide concentration were varied. The activation energy and the reaction order were then calculated from the experimental data. This chapter presents the experimental results. Details of the experimental equipment and procedures are presented in the previous chapter.

7.1 Influence of temperature

The experimental temperatures ranged from 269 to 645°C. During each experiment, the mass was recorded as a function of time. The results are presented in Figure 7.1.

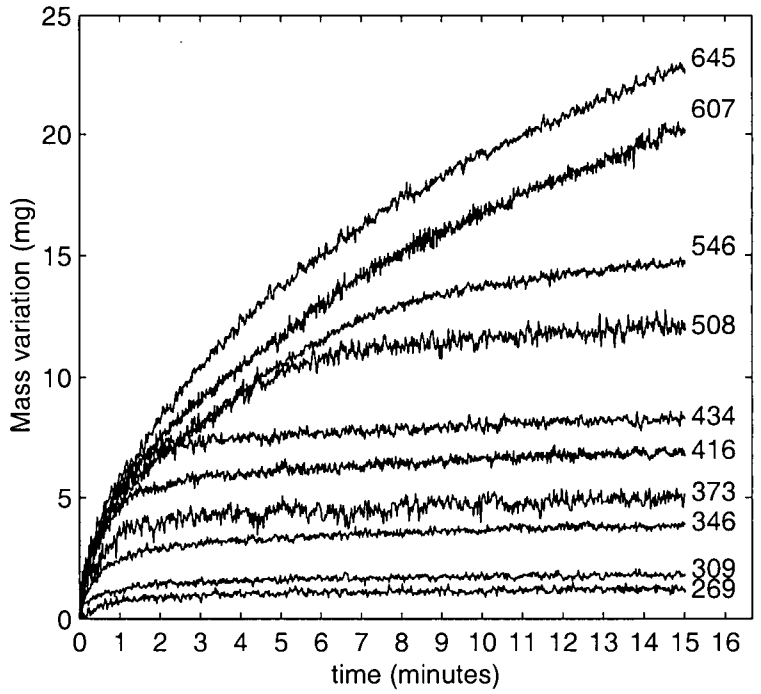

Figure 7.1: Mass variation of pellets as a function of time for experiments at several temperatures with 20.4% O_2 and 2.7% SO_2.

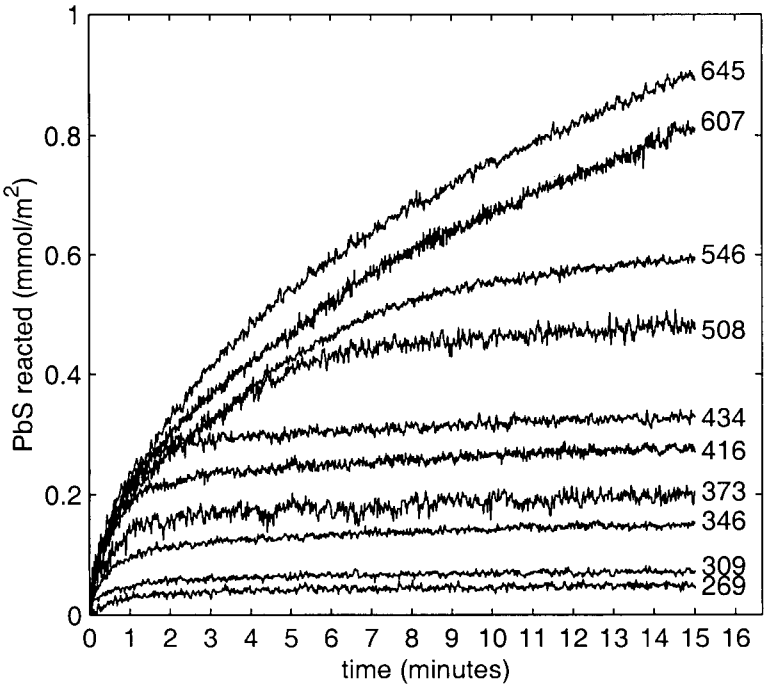

Figure 7.2: PbS reacted as a function of time for experiments at several temperatures with 20.4% O_2 and 2.7% SO_2.

Table 7.1: Initial reaction rates as a function of temperature.

Reaction rate (mmol $m^{-2}s^{-1}$)	Temperature (°C)
0.00105	269
0.00174	309
0.00329	346
0.00380	373
0.00515	416
0.00784	434
0.00667	508
0.00570	546
0.00432	607
0.00651	645

For each experiment, pellets having a porosity of 27.2 +/- 1.6% were used. Each pellet weighed 0.982 +/- 0.013 g. The atmosphere contained 2.7% sulfur dioxide, 20.4% oxygen and the balance nitrogen. The temperatures shown on the right side of the figure are the initial pellet temperatures in degrees Celsius. These temperatures are the actual pellet temperatures as measured by the second pellet after they reached thermal equilibrium in an inert atmosphere. When the gas is switched from the inert to the reactive atmosphere, the transient regime that the pellet experiences has been calculated to be less than 3 second at the lowest experimental temperature.

XRD analysis showed that the reaction product was $PbSO_4$ in all experiments. SEM observations of reacted samples showed that the reaction products were present through the sample. The total surface area of the pellet should therefore be used in determining the reaction rate constant rather than the external surface as measured by a micrometer. Electron microscope observations and image analysis also confirmed the porosity measurements. The mass variation can be related to the number of moles of lead sulfide reacted per unit surface area knowing the original mass of the pellets, the approximate surface area of all pellets, determined by BET to be 0.4 m^2/g, and the molar mass difference between PbS and $PbSO_4$ (64 g/mol). The results are presented in Figure 7.2. Figures 7.1 and 7.2 differ only in their scale.

At least three rate-limiting phenomena are represented in these figures. The mass transport resistance through the product layer causes the reaction to be very slow after a few minutes. This can be seen at low temperatures (269-508°C) after prolonged reaction times. The second mass transport controlling mechanism is the gas phase mass transfer limitation which can be observed at high temperature (508-645°C). The maximum initial rate is limited by gas mass transfer. The last rate-limiting mechanism seen in the figure is due to chemical kinetics. This can be seen by comparing the initial rates for the low temperature experiments (269-434°C) which increased as the temperature increased. The activation energy and the pre-exponential constants can be determined by plotting the logarithm of the rates as a function of the inverse of the absolute temperature, as presented in Table 7.1 and Figure 7.3.

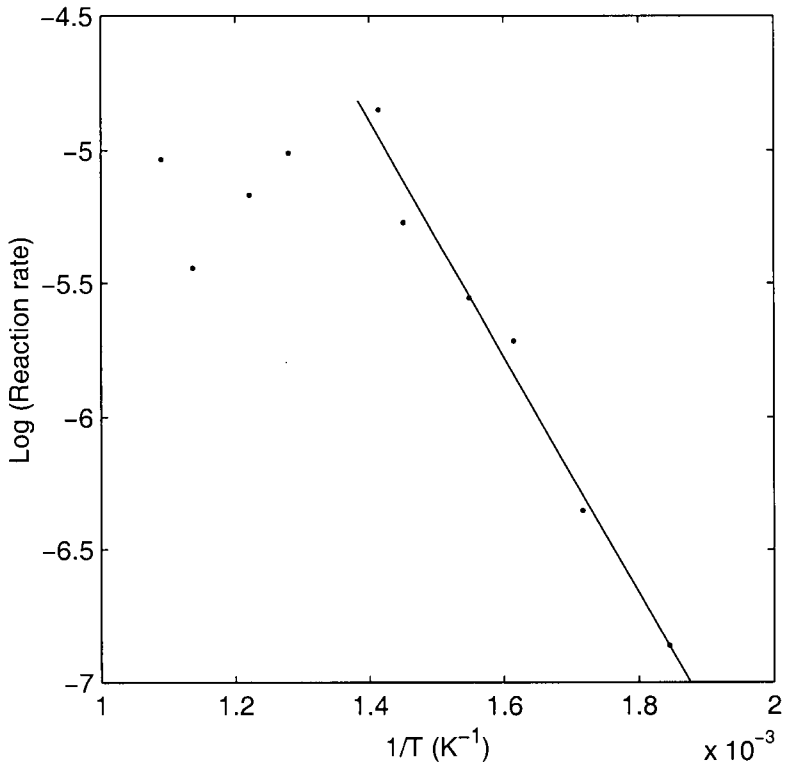

Figure 7.3: Arrhenius plot for the initial reaction rates.

The initial rates are indicated on the graph. The linear fit gives the Arrhenius parameters for the low temperature oxidation leading to an activation energy of 36.8 +/- 5.6 kJ/mol. The pre-exponential constant, which includes the effect of the gas concentration, is 3.7 (+7.3 - 2.45) mmol m^{-2} s^{-1}. Note that the error is not symmetric due to the linear fit using logarithmic values. On this plot, the transition at relatively high temperatures, from chemical kinetic control to mass transfer control is evident. This activation energy is much lower than those reported in other studies conducted at higher temperatures and for longer times. This indicates that the reaction probably occurs by another mechanism. One should however be careful when using activation energies obtained from long term experiments because many other reactions could be occurring. Phenomena occurring simultaneously could, for example, include high temperature oxidation of lead sulfide and reduction of the products by gaseous lead sulfide. Being at lower temperatures and only using the initial reaction rates, the rates obtained in this study are probably not influenced by other reactions.

The Damköhler number calculated from the experimental rates is $2.6*10^{-6}$. This low Damköhler number indicates that the film mass transfer resistance is negligible. Thiele modulus calculations also show that pore resistance is negligible. (See Appendix 1, section 3 for calculations) However, these calculations are only valid initially as they do not take into account any influence of product layer diffusion. However, concentration gradients within the pellet are likely negligible because the porosity is not reduced significantly as the reaction proceeds. This is due to the very small amount of reaction, i.e. a conversion of less than one percent which would correspond at most to a drop in porosity of a few percent.

An interesting observation is the increase in the rates with temperature at relatively long times, i.e. from 10 to 15 minutes. An effective diffusivity can be obtained by using the shrinking core model for ash diffusion control. An Arrhenius plot for these diffusivities appears in Figure 7.4.

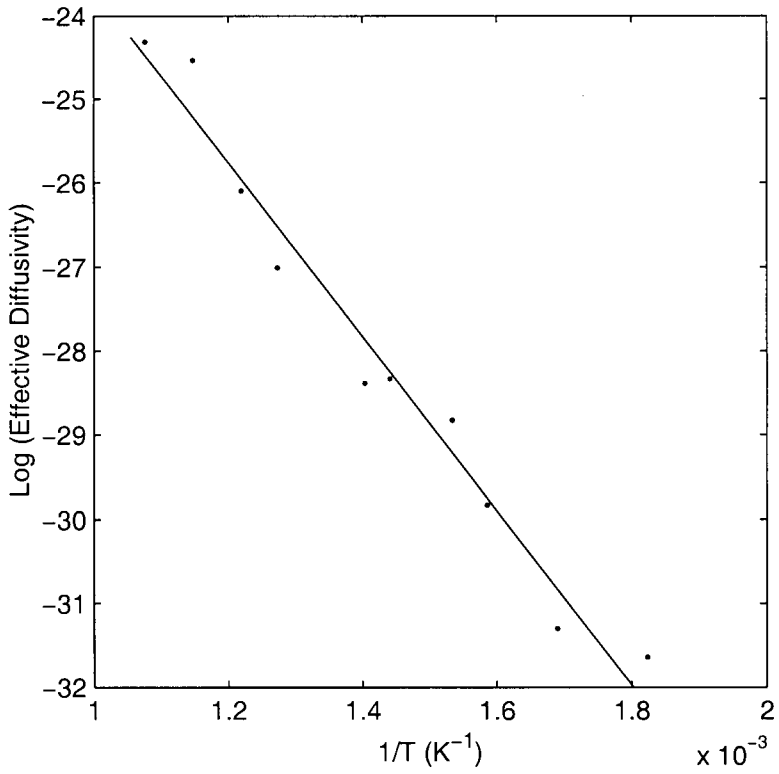

Figure 7.4: Arrhenius plot for the effective diffusivity.

In this case, the observed activation energy is 86 +/- 10 kJ/mol. This value is relatively low for the activation energy of a solid-state diffusion process. However, it is too high for a gas diffusion process.

7.2 Influence of oxygen concentration

A series of experiments was conducted to illustrate the effect of oxygen concentration on the reaction of lead sulfide. Figure 7.5 presents the experimental results. Because they are very similar, the curves are plotted individually. The porosity of the pellets was 38 +/- 2 % and their mass was 0.981 +/- 0.016 g. XRD analysis revealed that the reaction product was $PbSO_4$.

As in the last section, the reaction is initially rapid and slows as the product layer grows. The experimental curves show much more similarity than the curves for different temperatures, except for the initial slopes. When the initial rates are plotted as a function of the oxygen partial pressure as in Figure 7.6, the effect of oxygen on the reaction rate is evident. The reaction order is undeniably positive because increasing the oxygen concentration increases the oxidation rate of lead sulfide. Statistical analysis demonstrated that the observed reaction order differs from one. From a log-log plot, the reaction order has been found to be 0.43 +/- 0.22. Fractional reaction orders have already been observed in other sulfide oxidation systems [55] such as in the oxidation of zinc sulfide. Fractional reaction orders can be explained using oxygen adsorption models. The model that fitted best the experimental data was the single-site dissociative adsorption model. The rate constant and the equilibrium constant obtained for the curve were 0.026 mmol $m^{-2}s^{-1}$ and 0.28, respectively.

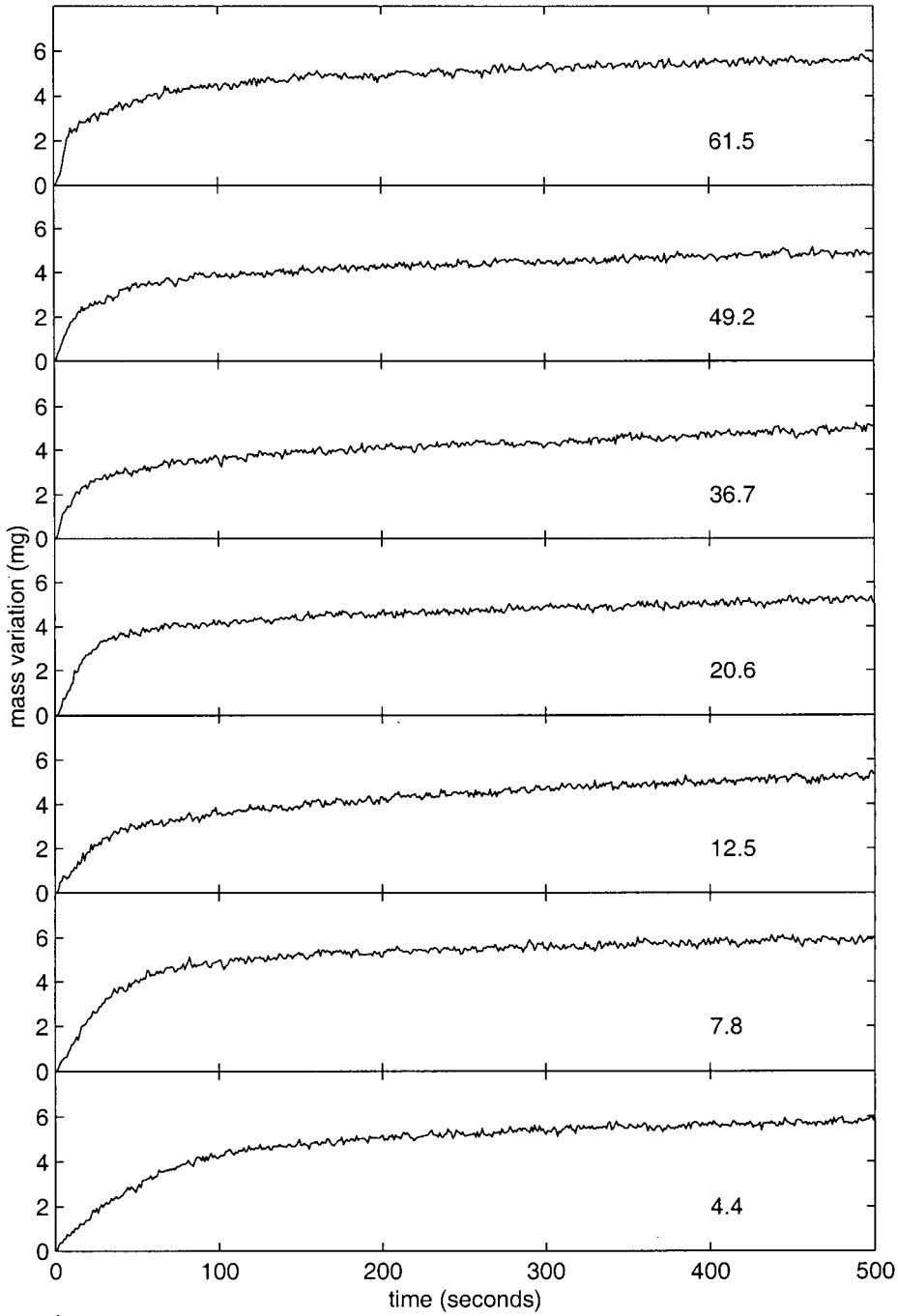

Figure 7.5: Experimental results for different oxygen concentrations with 2.2% SO_2 at 390°C.

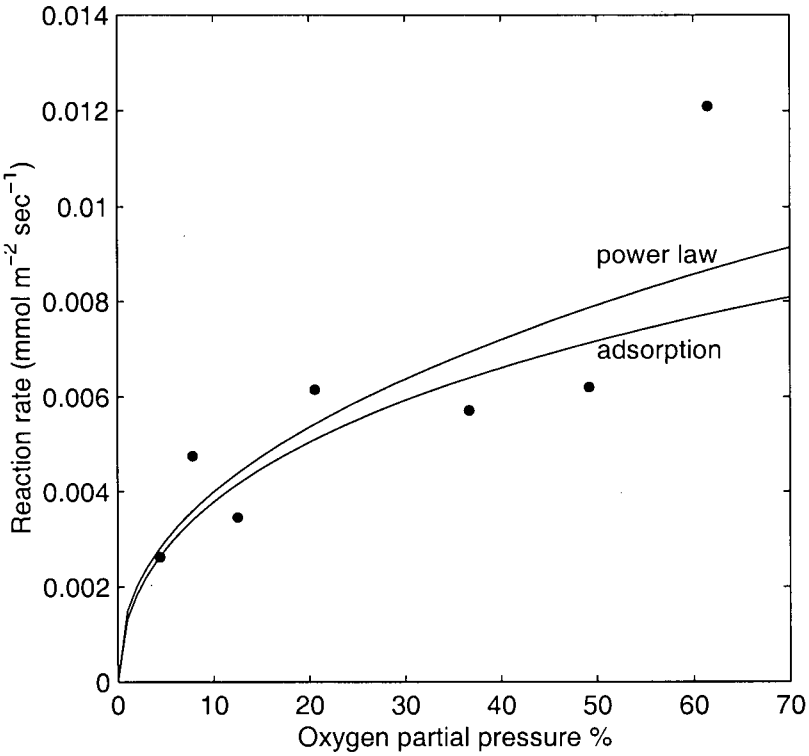

Figure 7.6: Plot of the reaction rate as a function of oxygen partial pressure.

A statistical analysis showed that there was no statistically significant difference between the reaction rates after 300 seconds. The test used was a test to verify for the parallelism of experimental lines. There might be an influence at lower oxygen concentrations but this cannot be verified. The lack of influence of oxygen concentration could be explained by the fact that the rates are controlled by a process which does not depend on the oxygen concentration, e.g. ionic diffusion through the sulfate layer.

7.3 Influence of sulfur dioxide concentration

In the next set of experiments, only the sulfur dioxide concentration was varied. The furnace temperature, oxygen concentration and pellet porosity were kept nearly constant at

approximately 440°C, 20.3% and 38.5 +/- 2.9%, respectively. The pellet masses were 0.979 +/- 0.01 g.

Figure 7.7 presents the experimental results for this series of experiments. The initial rates are very similar from one experiment to the next. Statistical analysis on the data of the initial reaction indicates that the influence of sulfur dioxide concentration on the rates is negligible. The test done is a test for the parallelism of experimental lines. The variations can be attributed to minor variations in experimental conditions such as the porosity of the pellets, gas flow rates and temperatures. More experiments have to be performed to clearly state that the sulfur dioxide concentration does not have any effect on the reaction rates. Another observation from this figure is that, with the exception of the experiment without any sulfur dioxide, the rates long after the transition to diffusion control are nearly identical. In fact, a statistical analysis at a confidence level of 0.95 could not reject the hypothesis that the rates for the experiments with sulfur dioxide are all equal. However, the same analysis at the same level of confidence, including the experiment with 0% sulfur dioxide rejected this hypothesis. The reaction rates for the experiment without SO_2 is therefore different from those with sulfur dioxide. X-ray diffraction analysis showed that all the samples contained unreacted lead sulfide and some lead sulfate. The XRD of the sample produced with 0% sulfur dioxide was difficult to analyse due to the small amount of lead sulfate present. However, only lead sulfate could be identified as a reaction product. The effect of sulfur dioxide seems to be on the rates of the diffusion limited regime. When there is no sulfur dioxide, a sharp knee occurs and the reaction stops. On the other hand, when sulfur dioxide is present, the amount of sulfate produced is much higher, and the reaction still proceeds.

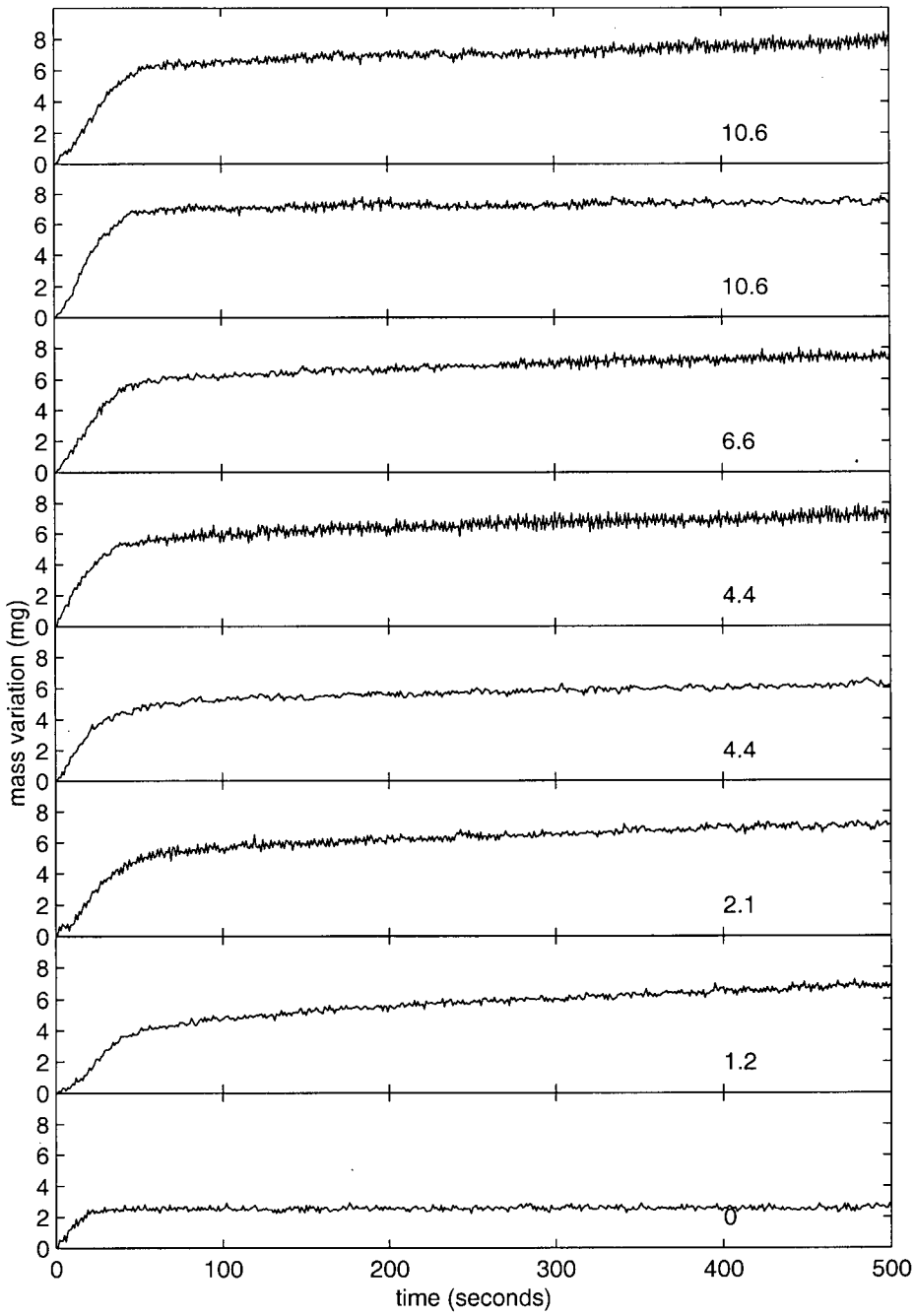

Figure 7.7: Experimental data for different SO_2 concentrations with 20.4% O_2 at 440°C.

7.4 Experimental errors and repeatability

Some of the experiments were performed multiple times (see previous figure) and the results were similar. There is however, some minor differences between the experiments. These can be attributed to variations between pellets and to variations in pellet temperatures. Obtaining reliable initial kinetics information is difficult because very little data can be used as initial rate data. Also, the amount of reaction products produced during this period is small and the transient regime between the inert and the reactive gas probably causes errors. The switching causes vibrations in the balance due to temporarily turning off the gas flow. Also, minute differences in gas velocities between experiments and between the inert gas and the reactive gases are present. The furnace in the current configuration has a slow response (due to the insert). A faster response would allow less temperature variations.

7.5 Reaction mechanism

From the present experiments, at least two regimes appear to be at play. The first one relates to the initial oxidation of the surface of the lead sulfide, and the second, to the growth of the sulfate layer.

From our observations, the initial oxidation appears to depend on the oxygen concentration, but not on the sulfur dioxide concentration. The fractional reaction order suggests that an ionic diffusion process or an oxygen adsorption process prevails. Adsorption models (single site non dissociative, single site dissociative, dual site dissociative) were tested. Their correlation coefficients were very similar to the one obtained from the power law. However, all the regressions gave correlation coefficients between 0.86 and 0.89, with the single site dissociative model giving the highest value. To obtain the exact mechanism and the correct temperature dependence of the parameters, many more experiments would have to be performed under various temperatures and at various oxygen partial pressures. Adsorption models have at least two parameters that vary with temperature, i.e. the rate constant and the adsorption equilibrium constant. The hypothesis of an adsorption process seems plausible as it has been discussed by Bugajska et al [35], and it has been observed for the oxidation of zinc sulfide [55].

The experiments showed that the growth of a sulfate layer depends mainly on the presence of sulfur dioxide. Its concentration did not affect the growth rates. The oxygen concentration also did not influence the rates, but its absence was not tested. However, it might be prudent to assume that the presence of oxygen is necessary to the growth of the sulfate layer. These observations tend to indicate that the sulfur dioxide which could be present at the surface of the sample helps in the growth of the sulfate layer. The sulfur dioxide probably affects the mechanism of the reaction or modifies the rate-limiting step. However, due to the fact that there is no difference in the initial rates for the experiments with and without sulfur dioxide, it is probable that either the mechanism or the rate-limiting steps are different.

This behaviour can be explained when considering the growth mechanism of the sulfate layer proposed in previous studies [43,46,53]. It has been observed by Gray et al [46] that the sulfate layer grows outwards. This means that lead and sulfur ions must migrate through the sulfate layer before reacting with the atmosphere. However, because diffusion of the sulfur ions is slower than diffusion of lead ions [39], the reaction rates would be limited by the diffusion of sulfur through the sulfate layer. Another source of sulfur at the outer surface, such as adsorbed sulfur dioxide, could simply enhance the reaction rates. This scenario would explain why the rates were higher when sulfur dioxide was present. However, the rate would now be limited by the diffusion of the lead ions, creating the effect that further increasing the sulfur dioxide concentration would no longer affect the growth rate.

The reaction mechanism proposed here can explain the experimental observations. However, it cannot be verified with the present experiments.

7.6 Verification of modified predominance diagrams

The experiment conducted without sulfur dioxide can be used to try to validate the modified predominance diagrams. The Damköhler number calculated from the experimental rates is $2.6*10^{-6}$. The modified predominance diagram for the experimental conditions corresponding to the experiments shows that under an air atmosphere with very small amounts of sulfur dioxide, lead sulfate would be produced with undetectable amounts of lead oxide. If somewhat higher sulfur dioxide concentrations were present (still very low), only

lead sulfate would be produced. The experiment performed with no sulfur dioxide in the atmosphere produced lead sulfate. On a logarithmnic scale, it is impossible to clearly determine the exact concentration of sulfur dioxide during the experiment. Adsorbed sulfur dioxide on the equipment that slowly desorbs would probably be enough to change dramatically the concentration of SO_2.

As it is practically impossible to directly control concentrations below 10^{-4} atm, other systems or other methods could be used to verify the modified predominance diagrams. Also, the lead system is a complex system where many compounds exist and several reactions which can modify the nature of the oxidation products can occur, such as roast reactions and vaporization of lead sulfide . It would also be advantageous to use a system where a ratio of gaseous compounds could be set to better define the concentrations. The CO/CO_2 ratio is a good example of a method which can control the oxygen potential to very low levels.

8. Conclusions and Recommendations

8.1 Experimental

The review of the literature has shown that little is known with certitude about the behaviour of lead sulfide oxidation, even though numerous studies have been done on the subject. Most studies have neglected the effect of sulfur dioxide, gas phase mass transport, reaction products reactions, gaseous lead sulfide and the diffusion of gases through a porous sample. The order of the reaction reported in previous works with respect to both oxygen and sulfur dioxide is very variable, with different studies finding negative, positive or no effect of the oxygen or sulfur dioxide compositions.

The experimental section of this work has clarified the oxidation kinetics of lead sulfide between 250 and 450°C. Under all the condition tested, lead sulfate was the reaction product. The observed activation energy was 36.8 +/- 5.6 kJ/mol and the pre-exponential constant was 3.7 (+7.3 -2.45) $*10^{-3}$ mol $m^{-2}s^{-1}$. This activation energy is lower than previously published but higher than activation energies for gas diffusion.

The initial reaction rates showed a fractional reaction order with respect to the oxygen concentration. After prolonged times, no effect of oxygen concentration has been observed. Sulfur dioxide did not seem to have an effect on the initial oxidation kinetics. However, when a sufficient lead sulfate layer was produced, the presence of sulfur dioxide influenced the growth rate of the product layer. In the absence of sulfur dioxide, the reaction was very slow. With the addition of sulfur dioxide, the rates were small compared with the initial rates, but not negligible.

It has been shown that under the conditions tested, pore and gas film resistances were negligible. The observed characteristics are then controlled by surface reaction and growth of the reaction products.

Our observations can be explained by using an adsorption and ionic diffusion mechanism. Initially, adsorption of oxygen is rate-limiting. As the sulfate layer grows, sulfur and lead ion diffusion through the product layer becomes rate limiting. Because the diffusivity of sulfur ions is lower than that of lead ions, ionic sulfur diffusion is rate-controlling if no sulfur is available at the outer surface. However, if sulfur is available at the outer surface as sulfur dioxide, ionic lead diffusion becomes rate-limiting. The overall rate would then be higher when sulfur dioxide is present in the system. Its initial influence would be negligible because the rate is not limited by the presence of sulfur at the outer surface.

The current experiments cannot verify the proposed reaction mechanism. Experiments designed to investigate the influence of various parameters on surface adsorption of the gases and on ionic diffusion in the sulfate layer are necessary to fully evaluate the proposed mechanism.

8.2 Diagrams

A simple mathematical model was derived from basic transport and rate phenomena theories in an attempt to follow the gas concentration at the surface of a sample, and to try to predict the reaction path of a reacting system. Two simple equations were obtained describing the gas composition differences between the surface of the sample and the bulk gas phase as a function of the kinetic conditions. These equations can be used to modify predominance diagrams by including kinetic information described in a single dimensionless number, the third Damköhler number.

The modified predominance diagrams were not validated experimentally but they are an innovative tool in the study of gas-solid reactions which should prove very useful in systems where a gaseous reaction product can influence the atmosphere surrounding a sample. This includes (but is not limited to) most metal-sulfur-oxygen systems. For instance, sulfur dioxide is produced by the oxidation reactions of sulfides. However, if no sulfur dioxide is introduced in the reactive gas flow, generation of sulfur dioxide would dramatically change the atmosphere at the surface.

Hydrometallurgical systems can also be analyzed by the same method, as in the case of Pourbaix diagrams (Eh-pH diagrams) where reactions are consuming or producing acid (pH) or where reactions can affect the local potential by modifying the ferric-to-ferrous ratio.

8.3 Recommendations on experimental studies

The kinetic diagrams and their governing equations have shown that under certain conditions, mass transfer can have a significant effect on the reaction path of a reacting system. In addition, the literature review clearly pointed out that when different studies are compared, any conclusion must be evaluated carefully. The following recommendations regarding the experimental study of gas-solid reactions are proposed:

- Mass transfer conditions must be clearly defined, including the effect of the atmosphere composition on the transport properties, the superficial velocity in the vicinity of the sample, the sample porosity and surface area. When porous samples (pellet or small heap) are used, the Thiele Modulus of the sample must be considered when analysing experimental data.

- The gas flow behaviour should be as close as possible to plug flow. This ensures that any step change in gas composition will provide a rapid change in gas composition at the sample. It also ensures that the output gas response is adequate. Tracer studies and residence time distributions are useful tools in characterizing an experimental set-up.

- The influence of the gaseous reaction products must not be neglected even when the system is not under mass transport rate-controlling conditions. The modified predominance diagrams clearly showed that under certain conditions where chemical kinetics are rate-limiting, the reaction products differ from those predicted by the predominance diagram.

- Isothermal and non-isothermal experiments must be compared cautiously as the reactions observed in both cases could be very different.

- Non-isothermal experiments must be analysed very carefully. Phenonema observed at higher temperatures could be valid only for the reaction products.

- Isothermal experiments must also be analysed prudently if long term experiments are to be used to represent a short term system. For example, reaction products could modify the behaviour of a system by contributing to other reactions, e.g. roast reactions between lead sulfide and reaction products. Also, the rate-limiting steps of two similar systems could very well be different. The present study is a very good example. When ionic diffusion is limiting, the rate-limiting step is either ionic lead or ionic sulfur diffusion, depending on whether or not sulfur dioxide is present at the outer surface.

- Gaseous species locally generated by the sample must be considered. These include reaction products, such as sulfur dioxide and gaseous reactants, such as gaseous lead sulfide.

8.4 Further work

A mechanism for the oxidation of lead sulfide has been proposed. It has, however, not been verified. Experimental verification and extension of this mechanism would allow the modelling of lead sulfide oxidation. Sulfur dioxide, which seems beneficial to the reaction under by solid state diffusion control, will have to be considered in any modelling work of lead sulfide oxidation. However, due to the very fast heating rates in flash smelting, solid state diffusion control might simply not occur before melting. Further experiments will have to be performed to gain better confidence in the initial oxidation kinetics mechanism. Because the initial reaction seems to be limited by oxygen adsorption, the exact type of adsorption and the temperature dependence of the adsorption parameters must be determined. An accurate model will then be available for the initial oxidation stage of the lead flash smelting process. The parameters obtained in this study could be used for the first stage of the flash smelting model. An analysis of the sensitivity of the flash smelting model to the initial oxidation parameters would determine whether further research is needed.

Modified predominance diagrams have only been used to consider the behaviour of the oxidation of lead sulfide. Their application to other systems could provide an insight into the effect of mass transfer on reaction paths. Experimental verification of the modified predominance diagrams is needed in order to provide some confidence in their applicability.

References

1 Jan H. Reimers and John C. Taylor, "The Future of Lead Smelting", Advances in Sulfide Smelting, 1983 Fall Extractive and Process Metallurgy Meeting of the Metallurgical Society of AIME and 1983 International Sulfide Smelting Symposium, San Francisco, California, November 6-9 1983, pp.529-551.

2 H.Y.Sohn, V. Ramachandran, "Advances in Sulfide Smelting - Technology, R&D, and Education",Sulfide Smelting '98: Current and Future Practices, Proceedings of symposium held at 1998 TMS Annual Meeting, San Antonio, Texas, February 16-19, 1998, pp.3-37.

3 A.G.Matyas, P.J. Mackey,"Metallurgy of the Direct Smelting of Lead", Journal of Metals (JOM), November 1976. pp.10-15.

4 J. E. Hoffman,"Update on Emerging Lead Smelting Processes", Journal of Metals (JOM), September 1984, pp .29-35.

5 N.J. Themelis,"Pyrometallurgy Near the End of the 20th Century", JOM, August 1994, pp.51-57.

6 P.Bryk, R.Malmstrom and E.Nyholm, "Flash Smelting of Lead Concentrates", Journal of Metals, December 1966, pp.1298-1302.

7 Y.I. Sannikov, M.A. Liamina, V.A. Shumskij, Y.A. Grinin, "A Physical and Chemical Description of the Kivcet Lead Flash Smelting Process", CIM Bulletin, Vol. 91 No 1022, July/August 1998, pp.76-81.

8 D.W.Ashman,"Pilot Plant and Commercial Scale Test Work in the Kivcet Process for Cominco's New Lead Smelter", Zinc and Lead Processing, Proceedings of International Symposium on Zinc and Lead Processing, Calgary, Canada, August 16-19, 1998, pp.783-794.

9 A.R. Babcock, R.A. Franco, A.C. Mikrovas, S.Bharmal and M.I. Cecchini,"Preparation and Start-up of Cominco's New Lead Smelter", Zinc and Lead Processing, Proceedings of International Symposium on Zinc and Lead Processing, Calgary, Canada, August 16-19, 1998, pp.795-809.

10 F.R.A.Jorgenson, "Combustion of Chalcopyrite, Pyrite, Galena and Sphalerite under Simulated Suspension Smelting Conditions", Australia Japan Extractive Metallurgy Symposium, Sydney Australia, 1980, pp.41-51.

11 A.M. Salomon de Friedberg, "Kinetics of Lead Concentrate Oxidation in a Stagnant Gas Reactor", M.A.Sc. Thesis, University of British Columbia, 1987.

12 A.K. Kyllo, A.M. Salomon de Friedberg, G.G. Richards and J.K. Brimacombe "Kinetics of Lead Concentrate Oxidation in a Stagnant Gas", Proc. Intl. Symp. on Primary and Secondary Lead Processing, ed. M.L. Jaeck, CIM, Pergamon Press, Toronto, 1989, pp.27-38.

13 A.Jokilaakso, "Behavior of Various Sulfidic Raw Materials under Simulated Flash Smelting Conditions", in Rate Phenomena in Pyrometallurgical Processes, June 10-11 1996 Espoo Finland, Helsinki University of Technology, Report TKK-V-B121, pp.1-22.

14 V.K. Condina, F.R.A. Jorgensen, F.J. Moyle, T.M. Turner,"Ignition of Elura Lead Concentrate under Flash Drying Conditions" Symp. Ser. - Australas. Inst. Min. Metall. 1987, 51(Res. Dev. Extr. Metall.) pp.61-68 CAS 107:202752k.

15 N.E. Tuffrey, G.G. Richards and J.K. Brimacombe: "Two-Wavelength Pyrometry Study of the Combustion of Sulfide Minerals: Part II. Galena and Commercial Lead Concentrates" Metall. Mater. Trans., 1995, vol. 26B, pp. 943-958.

16 J.J. Lander,"The Basic Sulfates of Lead", Trans. Electrochem. Soc., 1949, vol 95 p 174-186.

17 HSC Chemistry, Ver. 2.03, Thermodynamical Software, Outokumpu Research Oy, Pori, Finland.

18 H.W. Billhardt, "New Data on Basic Lead Sulfates",J.Electrochem.Soc., Vol 117 no 5, May 1970, pp. 690-692.

19 S. J. Merrick, "A Study of the Roast-Reaction of Lead Sulfide", University of British Columbia, Master of Applied Science Thesis, Department of Mining and Metallurgy, August 1957.

20 S.K.El-Rahaiby, Y.K. Rao, "Kinetics of Vaporization of Lead Sulfide", Metallurgical Transactions B, volume 13B, No 4, December 1982, pp.633-641.

21 V.D.Ponomarev, I.R.Polyvyannyi, "Kinetics of the Interaction of Lead Sulfide with Lead Sulfate", Izvest. Akad. Nauk. Kazarh. S.S.R., Ser. Gornogo Dela, Met. Stroitel. i Stroimaterialov, 1956, No. 9, pp 35-46 (in Russian), CAS (1958):13505e.

22 C. Malinowski, "Analysis of the Chemical Reaction between $PbSO_4$ and PbS", Thermochimica Acta, 119(2), 1987, pp.329-336, CAS 108:12098z.

23 C.Malinowski, K.Malinowska,"Analysis of the Course of Reactions between Lead Sulfide and Lead Sulfate and Zinc Sulfate based on Thermogravimetric Studies", Zesz. Nauk. Akad. Gorn.-Hutn. im. Stanislawa Staszica, Metal. Odlew., 1987 no 109 pp.113-124, CAS 109:58797a.

24 H.Kiuchi, I.Nakamura, T.Tanaka,"Mutual Reaction of Lead Sulfide with Lead Sulfate",Nippon Kogyo Kaishi, 1980, 96(1108) pp.417-422, (Japanese), CAS 96:184907n.

25 H. Vander Poorten, L. Meunier, "Les réactions d'oxydation du sulfure de plomb: Première partie: Etude thermogravimetrique de l'oxydation du sulfure de plomb" "Oxidation reactions of lead sulfide. I. Thermogravimetric study", Metallurgie (Mons, Belgium) Vol 3 no 1, 1962, pp 15-25 (In French) CAS 62:2499c.

26 F. Ajersch, M. Benlyamani, "Thermogravimetric Identification and Analysis of Reaction Products During Oxidation of Solid or Liquid Sulfides", Thermochimica Acta, vol 143 (1989), pp 221-237.

27 V.K. Condina, F.R.A. Jorgensen, F.J. Moyle, T.M. Turner,"Ignition of Elura Lead Concentrate under Flash Drying Conditions" Symp. Ser. - Australas. Inst. Min. Metall. 1987, 51(Res. Dev. Extr. Metall.) pp61-68 CAS 107:202752k.

28 E.M. Kurian, R.V. Tamhankar, "A Thermodynamic and Kinetic Investigation of some Transformations in M-S-O Systems", Transactions of Indian Institute of Metals, December 1970, vol 23 no 4 p 59-64 CAS 74:89930b.

29 T.Nakamura, F. Noguchi, Y.Ueda, H. Ito," A Basic Study on the Oxidation Smelting of Lead Sulfide", Symp. Ser. - Australas. Inst. Min. Metall. 1987, 51(Res. Dev. Extr. Metall.) pp85-94 CAS 107:202755p.

30 G.W. Reimers, K.E. Hjelmstad, "Analysis of the Oxidation of Chalcopyrite, Chalcocite, Galena, Pyrrhotite, Marcasite and Arsenopyrite" 1987, Reports of Investigations, Bureau of Mines, vol 9118, 19 pages.

31 P. Balaz, H. Heegn, T.G. Korneva, K.Matheova, "Effect of Mechanical Activation on the Thermal Behaviour of Sulfidic Minerals", Proceedings of the 1st Conference on Mechanochemistry, 1993, p 157-161 CAS 121:184116p.

32 J.R. Tuffley, B.Russell,"The Oxidation of Lead Sulfide", J. Australian Inst. Metals, Vol 7, 1962, pp 122-129 CAS 14706d.

33 J.R. Tuffley, B.Russell, "Sulfate Formation during the Roasting of Lead Sulfide", Trans. AIME, vol 230 no 5, pp950-956, CAS 61:14220f.

34 H. Vander Poorten, L. Meunier, "Les réactions d'oxydation du sulfure de plomb Deuxième partie: Etude structurale des couches d'oxydation du sulfure de plomb massif" "Oxidation reactions of lead sulfide. II. Structural study of oxidation layers of massive lead sulfide", Metallurgie (Mons, Belgium) Vol 3 no 2, 1962, pp 41-48 (In French) CAS 62:6136f.

35 M.Bugajska, T.Karwan, "Characteristics of the Oxidation Products of Spherical Samples of Lead Sulphide in the Temperature Range 773-1023K" Thermochimica Acta, Vol 33, 1979 pp 41-50, CAS91:185869k.

36 M.Bugajska, T.Karwan, "Termograwimetryczne Badania Procesu Utleniania Siarczku Olowiawego w interwale Temperatur 500-750C" "Thermogravimetric study of lead sulfide oxidation in the temperature range 500-750C", Zesz. Nauk. Akad. Gorn.-Hutn. Im Stanislawa Staszica, Zesz. Spec. 1978, vol 57, pp 77-90 CAS 89:218328x.

37 K.Sarveswara Rao, R.P. Das, "Reaction Sequence during Oxidation of Multimetal Sulfides", International Conference on Base Metals Technology, 8-10 February, Jamshed pur India, 1989 pp 131-139.

38 K.Sarveswara Rao, B.Sarangi, H.S. Ray, "Application of Thermal Analysis in the Study of Oxidation of Sulfide Minerals" Proceedings 9th National Symposium on Thermal Analysis: Goa University, Goa November 8-10, 1993 p 57-60 CAS 121:138171e.

39 N.A.Kolobrodova, Z.A.Eremina, G.V.Indenbaum, E.V.Marchenko, "Product Structure and Kinetics of Low Temperature Oxidation of Lead Sulfide Single Crystals at the Boundaries of Homogeneity Regions", Izv. Akad. Nauk. SSSR, Neorg. Mater., 1991, vol 27 no 2 pp 238-243 (eng translation pp 168-172) CAS 116:11733.

40 D.H. Kirkwood, J. Nutting, "An Electron Metallographic Investigation of the Oxidation of Lead Sulfide in Air Between 200° and 350°C", Trans AIME, Vol 233 no 4, 1965, pp 708-713, CAS 63:239f.

41 S.A.A. Jayaweera, P.Sleeman,TG and DTA Studies of the Oxidation of Lead Sulfide" Proc. Eur. Symp. Therm. Anal. 1st, 1976, pp 287-290 CAS 87:47542q.

42 O. Levenspiel, "Chemical Reaction Engineering", 2nd ed.,1972, John Wiley & Sons, Inc., Chapter 14.

43 R.C.Culver, N.B.Gray, E.C.R.Spooner,"Oxidation of Galena to Lead Sulfate", Nature, April 1, 1961, Vol 190 no 4770, pp78-79.

44 A.G.Gaivoronskii, I.R. Polyvyannyi, "Effect of the Concentration of Sulfur Dioxide in a Gas Mixture on the Oxidation of Lead Sulfide", Vestn. Akad. Nauk. Kaz. SSR, 1967, Vol 23 no 10 pp 11-19 CAS 68:90255t.

45 I.R. Polyvyannyi, "Effect of Sulfurous Anhydride on Lead Oxidation", Izvest. Akad. Nauk. Kazakh. S.S.R. Ser. Met., Obogashchniya i Ogneuporov, 1958, no 3 pp 61-70, CAS 54:207115i.

46 N.B.Gray, N.W.Stump W.S.Boundy R.V.Culver, "The Sulfation of Lead Sulfide",Trans. Met. Soc. AIME 1967, vol 239 no 11 pp 1835-1840 CAS 68:33640r.

47 Haldun N. Terem, M. Ilhan Arslan, "Studies on the Oxidation of Lead Sulfide", Chimica Acta Turcica, 1975, Volume 3, No 3, pp 163-178 CAS 85:127650x.

48 V.D.Ponomarev, I.R.Polyvyannyi, "Kinetics of the Oxidation of Lead Sulfide with Oxygen of the Air", Izvest. Akad. Nauk. Kazarh. S.S.R., Ser. Gornogo Dela, Met. Stroitel. i Stroimaterialov, 1956, No. 9, pp 3-34 (in Russian), CAS (1958):13505g.

49 R. Dimitrov, B. Boyanov, "A Study of Metal Sulfides and Sulfide Concentrates Oxidation",Proc. Eur. Symp. Therm. Anal., 1981, 2nd, pp340-343 CAS 96:126911y.

50 R. Dimitrov, B. Boyanov, "Investigation of the Oxidation of Metal Sulphides and Sulphide Concentrates" Thermochimica Acta, vol 64 (1983) pp 27-37 CAS 99:25904e.

51 T.Hattori, Y.Iwadate, T.Sato, "Densification of Lead Selenide and Lead Sulfide by Hot Isostatic Pressing", J.Am.Ceram.Soc., vol 73 no 1, 1990 pp 140-141.

52 R.Paunova, T.Nikolov, V. Levina, L.Dimanova, V.Kolchanov, D.Ryzhonkov, "Mechanism and Kinetics of Oxidation of Zinc, Cadmium, and Lead Sulfides under Nonisothermal Conditions"

God. Vissh. Khim.-Tekhnol. Inst. Sofia, 1979 (pub. 1980) vol 26 no 3 pp 200-208 CAS 97:79663c.

53 R.V.Culver, N.B. Gray, E.C.R. Spooner, "The Kinetics of the Oxidation of Galena", J.Australian Inst. Metals, Vol 7, No2, 1962, pp130-135 CAS 15857c.

54 A.V.Spasov, Al.Lenchev, G.Stanchev, "Oxidation of a Bricket of Lead Sulfide" God. Sofii. Univ. Khim. Fak. 1967-1968 (Pub 1970) vol 62 pp 157-169 CAS 73:136925v.

55 Ore A. Sofekun, L.K.Doraiswamy, "High-Temperature Oxidation of Zinc Sulfide: Kinetic Modeling under Conditions of Strict Kinetic Control", Ind.Eng.Chem.Res. 1996, vol 35 pp 3163-3170.

56 R.B.Bird, W.E.Stewart, E.N.Lightfoot, "Transport Phenomena", John Wiley & Sons. 1960, Chapter 21.

57 MATLAB 5.2, The MathWorks, Inc. 24 Prime Park Way, Natick, MA, 01760-1500, http://www.mathworks.com.

58 Polyvyannyi, I.R., Zhubanova, N.Kh., Kuanyshev, A. Sh., "Oxidation mechanism of lead sulfide", Kompleksn. Ispol'z. Miner. Syr'ya, 1988 (8), 92-94, in Russian, CAS 110: 27021j.

59 National Semiconductor Corporation. Datasheets for the LM35 are available online at: http://www.national.com.

60 R.B.Bird, W.E.Stewart, E.N.Lightfoot, "Transport Phenomena", John Wiley & Sons. 1960, Chapter 21.

61 O. Levenspiel, "Chemical Reaction Engineering", 3rd edition, John Wiley & Sons, 1999 Chapter 18.

62 D.R.Poirier, G.H.Geiger,"Transport phenomena in materials processing" The Minerals, Metals & Materials Society, 1994

63 Maxim Integrated Products, 120 San Gabriel Drive, Sunnyvale CA 94086, (408) 737-7600, Datasheets available online at: http://www.maxim-ic.com/.

64 National Semiconductor Corporation. Datasheets for the LM35 are available online at: http://www.national.com.

65 C.Brereton, "Fluid mechanics of high velocity fluidised beds ", Ph.D. Thesis, U.B.C., 1987

Appendix 1 : Equations

Section 1 : Surface area of sample of constant mass

Assuming that the particles in a powdered sample are spherical, non porous and monosized, it can be shown that the surface area of a given mass of particles (m_s) is inversely proportional to the particle diameter (d_p or $2r_p$).

Volume of a spherical particle (V_p): $V_p = \frac{4}{3}\pi r_p^3$

Outer surface area of a spherical particle (A_p): $A_p = 4\pi r_p^2$

Particulate volume of sample (V_s): $V_s = \frac{m_s}{\rho_s}$ where ρ_s is the density of the particles

Number of particles in sample (N_s): $N_s = \frac{V_s}{V_p}$

Total surface area of sample (A_s): $A_s = N_s A_p = \frac{3 \cdot 4 \cdot \pi \cdot r_p^2 \cdot m_s}{4 \cdot \pi \cdot r_p^3 \cdot \rho_s} = \frac{3 \cdot m_s}{r_p \cdot \rho_s} = \frac{6 \cdot m_s}{d_p \cdot \rho_s}$

The surface area of a powdered sample is therefore proportional to the inverse of the diameter.

Section 2 : Development of kinetic equations

As in chapter 3, a general oxidation reaction such as equation (A1.1) is used for our analysis.

$$1\ PbS + m\ O_2 \rightarrow Products + n\ SO_2 \tag{A1.1}$$

From equation (A1.1), the overall reaction rate can be related to the mass transfer by the use of the stoichiometric coefficients.

$$r_{Overall_{PbS}} = r_{PbS} = -\frac{W_{O_2}}{m} = \frac{W_{SO_2}}{n} \tag{A1.2}$$

The variables r and W are the molar rates over the entire surface. The rate of PbS consumption is considered to be first order with respect to oxygen, i.e.

$$r_{PbS} = A \cdot B \cdot e^{-E_a/RT} \cdot P_{O_{2S}} \tag{A1.3}$$

where A is the surface area, B the pre-exponential constant in the Arrhenius equation, E_a the activation energy, R the gas constant, T the temperature and $P_{O_{2S}}$ is the oxygen partial pressure at the surface. The mass transport rate of SO_2 from the surface to the bulk gas is:

$$W_{SO_2} = \theta_{SO_2} \cdot k \cdot A \cdot \left(\frac{P_{SO_{2S}}}{P_t} - \frac{P_{SO_{2\infty}}}{P_t} \right) + \left(W_{SO_2} + W_{O_2} \right) \cdot \frac{P_{SO_{2S}}}{P_t} \tag{A1.4}$$

where k is the mass transfer coefficient, θ is the mass transfer correction factor, P_t is the total system pressure and W represents molar rates over the entire surface. Similarly the mass transport rate of O_2 is:

$$W_{O_2} = \theta_{O_2} \cdot k \cdot A \cdot \left(\frac{P_{O_{2S}}}{P_t} - \frac{P_{O_{2\infty}}}{P_t} \right) + \left(W_{SO_2} + W_{O_2} \right) \cdot \frac{P_{O_{2S}}}{P_t} \tag{A1.5}$$

These equations take into account any bulk flow which can be important at high mass transfer rates. The mass transfer rates can be isolated by using equation (A1.2) relating the two gas molar rates.

$$W_{SO_2} = \frac{\theta_{SO_2} \cdot k \cdot A \cdot \left(P_{SO_{2S}} - P_{SO_{2\infty}}\right)}{P_t - P_{SO_{2S}} \cdot (1 - \frac{m}{n})} \tag{A1.6}$$

$$W_{O_2} = \frac{\theta_{O_2} \cdot k \cdot A \cdot \left(P_{O_{2S}} - P_{O_{2\infty}}\right)}{P_t - P_{O_{2S}} \cdot \left(1 - \frac{n}{m}\right)} \tag{A1.7}$$

From equations (A1.2), (A1.3) and (A1.4), we can show that:

$$B \cdot e^{-E_a/RT} \cdot P_{O_{2S}} = \frac{\theta_{SO_2} \cdot k}{n} \cdot \frac{\left(P_{SO_{2S}} - P_{SO_{2\infty}}\right)}{P_t - P_{SO_{2S}} \cdot \left(1 - \frac{m}{n}\right)} \tag{A1.8}$$

Dividing through by the mass transfer coefficient, recognizing the Damköhler number and rearranging the equation to the same form as obtained in chapter 3, we obtain:

$$\left(P_{SO_{2S}} - P_{SO_{2\infty}}\right) = D_{III} \cdot P_{O_{2S}} \cdot n \cdot \left(\frac{P_t - P_{SO_{2S}} \cdot \left(1 - \frac{m}{n}\right)}{\theta_{SO_2}}\right) \tag{A1.9}$$

Similarly for oxygen we can derive:

$$\left(P_{O_{2\infty}} - P_{O_{2S}}\right) = D_{III} \cdot P_{O_{2S}} \cdot m \cdot \left(\frac{P_t - P_{O_{2S}} \cdot \left(1 - \frac{n}{m}\right)}{\theta_{O_2}}\right) \tag{A1.10}$$

These equations are very similar to those obtained in chapter 3 where high mass transfer rates and bulk flow are neglected. In each of these equations, the numerator of the right-hand term in parenthesis is the correction for bulk flow, while the denominator corrects for high mass transfer rates.

The correction factor for high mass transfer rates, θ_{AB}, can be approximated using film theory [60], giving:

$$\theta_{AB} = \frac{\ln(R_{AB}+1)}{R_{AB}} = \frac{\phi_{AB}}{e^{\phi_{AB}}-1} = \frac{\phi_{AB}}{R_{AB}} \tag{A1.11}$$

where R_{AB} is the flux ratio and ϕ_{AB} is the rate factor for mass transfer. These two variables are dimensionless numbers derived from the film theory [60]. R_{AB} can be calculated as follows:

$$R_{AB} = \frac{x_{A_0} - x_{A\infty}}{\frac{N_{A_0}}{N_{A_0}+N_{B_0}} - x_{A_0}} \tag{A1.12}$$

Replacing the generic subscripts by those required for our problem:

$$R_{SO_2} = \frac{P_{SO_{2S}} - P_{SO_{2\infty}}}{\frac{P_t \cdot W_{SO_2}}{W_{SO_2}+W_{O_2}} - P_{SO_{2S}}} \tag{A1.13}$$

The mass transport rates can be replaced using equation (A1.2) to obtain

$$R_{SO_2} = \frac{P_{SO_{2S}} - P_{SO_{2\infty}}}{\frac{P_t}{1-\frac{m}{n}} - P_{SO_{2S}}} \tag{A1.14}$$

Using equations (A1.9), (A1.11) and (A1.14) and equating the partial pressure difference, we obtain:

$$R_{SO_2} \cdot \left(\frac{P_t}{1-\frac{m}{n}} - P_{SO_{2S}} \right) = D_{III} \cdot P_{O_{2S}} \cdot n \cdot \left(P_t - P_{SO_{2S}} \cdot \left(1-\frac{m}{n}\right) \right) \cdot \frac{R_{SO_2}}{\phi_{SO_2}} \tag{A1.15}$$

Simplifying and isolating ϕ gives:

$$\phi_{SO_2} = D_{III} \cdot P_{O_{2S}} \cdot n \cdot \left(\frac{P_t - P_{SO_{2S}} \cdot \left(1 - \frac{m}{n}\right)}{\frac{P_t}{1 - \frac{m}{n}} - P_{SO_{2S}}} \right) \tag{A1.16}$$

Further simplification leads to:

$$\phi_{SO_2} = D_{III} \cdot P_{O_{2S}} \cdot (n - m) \tag{A1.17}$$

A parallel analysis for the oxygen equations leads to:

$$\phi_{O_2} = D_{III} \cdot P_{O_{2S}} \cdot (n - m) \tag{A1.18}$$

Equations (A1.17) and (A1.18) are used with equation (A1.11) to obtain the correction factor for the mass transfer coefficient.

When considering a total pressure of 1 atmosphere or more, the bulk flow and mass transfer coefficient corrections significantly modify the kinetic diagram for pressures above 1 atm. However, the diagrams for partial pressures below 1 atmosphere are virtually the same as those without corrections.

Section 3: Calculation of transfer conditions

Damköhler number

The Damköhler number is used to determine if mass transfer resistance through the gas film at the surface of a sample is significant or negligible. The Damköhler number is defined as the ratio of the chemical rate constant to the mass transfer coefficient (see chapter 3). Using the Activation energy and pre-exponential constant obtained experimentally and considering the reaction to be first order, we obtain Damköhler numbers of $3*10^{-10}$ and $2*10^{-9}$ for 700 and 1000K respectively. Because the rate constants are based on the actual surface area of the pellets and not on the external surface of the pellets, a correction must be made to the values obtained previously. When correcting for the external surface which is approximately 1800 times smaller than the actual surface area, we obtain Damköhler numbers of $5.4*10^{-7}$ and $2.9*10^{-6}$. The mass transfer coefficients used for these calculations were 12 and 20 cm s^{-1} which are typical values for the experimental conditions used. These two Damköhler numbers show clearly that the gas film is not rate limiting.

Thiele modulus

The Thiele modulus was developed to evaluate the importance of pore diffusion for solid catalytic reactions. In our case, it can also be used for gas-solid reaction as long as it is only for the initial moments of the reaction. At longer times, reaction products block direct access of the gas to the surface. For the theory behind the Thiele modulus, the reader is referred elsewhere [61].

When using the definition of the Thiele Modulus for a first order reaction, and replacing the characteristic length by the ratio of the volume of the pellet to the external pellet surface, the effective diffusivity by the gas diffusivity, the pellet porosity and the tortuosity, and the volumetric rate constant by the surface rate constant, we obtain the expression:

$$mL = \frac{1}{S_P}\sqrt{\frac{\tau \cdot S_A V_P k_r}{D_{AB}\varepsilon_P}}$$

where mL is the Thiele modulus, S_P is the external pellet surface, S_A is the pellet surface area, V_P is the pellet volume, ε_P is the pellet porosity, τ is the tortuosity, k_r is the reaction rate constant expressed per surface area, and D_{AB} is the gas diffusivity.

For the experiments described in this thesis, typical values are: for diffusivity (0.7 cm^2s^{-1}) [62], tortuosity (4) [62] and porosity (0.27) . Typical dimensions of a pellet are 2.5 mm for the thickness and 9.66 mm for diameter giving a volume of 0.183 cm^3 and an external area of 2.98 cm^2. A surface area of 0.4 m^2/g (4000 cm^2/g), as measured by BET surface area analysis, has been used. Using the values for the activation energy (36.8 kJ/mol) and the pre-exponential coefficient (3.7 mmol m^{-2} s^{-1}) obtained experimentally, as well as a temperature of 700K, we obtain a reaction rate constant of $3.3*10^{-9}$ mol $cm^{-2}s^{-1}$ and a Thiele modulus of 0.002. Being below 0.4, we can assume that concentration gradients are negligible within the pellet. Calculations at higher temperatures (1000K) mL also revealed to be below 0.4. If one would have used a fractional reaction order, as observed experimentally, the modulus would simply have been smaller, making the internal diffusionnal resistance even lower.

Appendix 2 : Data Acquisition System

Hardware

The data acquisition hardware is based on the typical applications in the MAXIM datasheets[63] for the MAX186 and MAX132 analog to digital converter chips. These chips are 8 single-ended inputs at 12 bit resolution and one differential-input at 18 bits plus sign resolution analog-to-digital converters. All the connections between the computer and the external board are through the parallel port. The functions of each pin of the parallel port are described in Table 1.

Table A2.1 Connections between the computer and the data acquisition hardware

LPT1 Pin name	Function	System
Strobe	None	
Data 0	SCLK	12,16,18 bits
Data 1	CS	18 bits
Data 2	CS	12 bits
Data 3	CS	16 bits
Data 4	DIN	18 bits
Data 5	DIN	12 bits
Data 6	CONV	16 bits
Data 7	RESET	16 bits
ACK	EOC	16 bits
Busy	DOUT	12 bits
Paper Empty	DOUT	18 bits
Select	DOUT	16 bits
Autofeed	none	
Error	EOC	18 bits
Init	none	
Selection	none	

A 16 bit system based on the MAX195BCPE chip is part of the hardware but has been deactivated to reduce noise and power consumption. The power supply needed for this

system is a simple +/- 5V. It is regulated by a MC7805C, and the negative voltage is generated by a MAX1044CPA DC-DC converter. The data connection between the computer and the furnace temperature controller is via the RS-232 serial port.

Low resolution section

The low resolution section of the data acquisition hardware is based on the MAX186ACPP chip. It has 8 single-ended constant gain 12-bit channels giving 4096 different levels. Channels 0 to 5 are used for type K thermocouples. Channel 6 can be used for the output of a pH controller. Channel 7 is used for the room temperature sensor. Operational amplifiers are used to amplify the signals to a 0-4.096V level.. To minimize noise, single pole RC filters with a cutoff frequency of 2.63 Hz are used between the MXL1014DN operational amplifiers and the MAX186. The gain of each channel has been measured with an Omega PCL 422 handheld calibrator and a Hewlett Packard multimeter. The maximum sampling rate of the chip is 133kHz. However, the effective maximum sampling rate is limited by the software. The reference voltage used by this section has been measured to be 4093.3 mV.

Table A2.2: Measured gains of the operational amplifiers

Channel	0	1	2	3	4	5	6	7
Gain	82.6312	81.9307	83.1328	82.8511	82.6734	82.7618	287.8136	109.98709

The room temperature sensor used in the system is a LM35CAZ semiconductor from the National Semiconductors Corporation[64] and is contained in a TO-92 package. The output varies linearly with temperature by 10.0 mV/°C and has an output of 0 mV at 0°C. Self-heating is negligible in the current application. This device is located near the terminal block connecting the thermocouple. This allows software compensation of the cold junction of the thermocouple.

High resolution section

The high resolution section is based on the MAX132CNG chip which gives one double-ended 18 bit plus sign channel (+/- 262144 levels). It is an integrating analog-to-digital converter which integrates the input over one AC line cycle minimizing 60 Hz noise. The maximum sampling rate of this section is limited by the 32768 Hz crystal to 16 Hz. The software and the speed of the interface between the computer and the hardware reduce the acquisition rate to about 10 Hz. The voltage reference used is a MX580KCSA132 which drives a voltage divider giving the MAX132 a constant 545.0 mV, set with a high accuracy Hewlett Packard voltmeter. This section is labelled channel number 8. It has an offset which is read by the software once per second. The offset has been given channel 11. The offset takes one complete measurement cycle and can be considered as invariant.

Furnace controller

The furnace controller is connected to the computer by a RS-232 serial connection. Both the set point and furnace temperature are read by the computer. These readings are given channel numbers 9 and 10 for the temperature and set point respectively. The reader is referred to the CN8500 Series Operator's Manual for the details of the controller.

Software

Structure of the software

The software is written in Borland C, specifically for the hardware used. It is compiled to be used in DOS. It can probably be compiled with other DOS compilers with little or no modification to the source code. To simplify the software, the code is written in many small sections:

Level1.c: Direct access to the parallel port and basic data transfer routines.

Level2.c: Implementation of the hardware specific commands.

Levec3.c: Implementation of a single function to interface the software and the hardware.

Comm.c: Implementation of communication to temperature controller routines.

Adcv3.c: Main program.

Before going into the main program loop, the following steps are taken:

1- Modification of the clock tick interval. The software modifies the internal clock of the computer to obtain a better time resolution. It has been modified from the usual 18 ticks per second to 100 ticks per second. The usual real-time clock functions are no longer reliable because the clock ticks are much faster. The program has an internal counter which counts the number of ticks since initiation of recording. Each clock tick being 10 ms, the time in seconds is simply the value of the counter divided by 100. Verification of the timekeeping capabilities of this counter was confirmed when the program saved the right number of seconds in a day, suggesting that the software is sufficiently accurate for recording events over time. This verification has been done on a 386 AST computer and must be performed again if another computer is used.

2- Implantation of the clock interrupt routine. The clock interrupt has also been modified so that it checks the status of the 18-bit section at every clock tick. When the interrupt has detected that new data is available, it sets a flag indicating that the hardware has finished its acquisition cycle. The clock interrupt also updates the program's time counter.

3- Implantation of the communication routine. The necessary routines to handle serial port communications by using the interrupt are installed and the port initialized.

4- Initialization of variables and constants. The gains, buffers and various counters are initialized.

After the initialization steps, the program enters a loop which ends only when the user needs to quit the software and return to DOS. The main program loop consists of the following steps:

1- The software checks if a keyboard command has been entered and processes it accordingly. The following commands are available: Start and stop recording to the test.out file, change the setpoint temperature, suspend or return to DOS and toggle the recording status of each channel.

2- Verification of the hardware state flag. This flag is modified by the clock tick interrupt routine if the data acquisition hardware has completed its acquisition and is ready for a new command.

3- If the hardware is ready, new acquisition is started. The time elapsed since the last save is verified and, if one half second has passed, it requests the controller for the set point. If a second has passed, the software sends a command to the temperature controller to return the furnace temperature and calculates the averages of the data acquired during the last second, saving them to file if they are recorded.

4- If the data acquisition hardware is not ready for a new command, the acquisition buffer is emptied, its data sorted and displayed onto the screen.

When the program exits, the following steps are taken:

1- Removal of clock interrupt,

2- Modification of the clock tick interval to its original value.

3- Removal of the communication interrupt,

4- The data acquisition hardware is switched to a sleep mode.

Note that the time and date are not set to the correct values.

The software and its source are stored on the computer currently in use for this data acquisition system.

Structure of saved data

The structure of the data that is saved into the file named "test.out" is given below.

Time (secs)

-1	Channel number	Channel number	Channel number
-1	Gain of channel	Gain of channel	Gain of channel
1	Dumped data	Dumped data	Dumped data
2	Good data	Good data	Good data
...	Good data	Good data	Good data

This is a simple text file and can be read by most software. The first column is the time of the reading. The following columns (one per channel) contain the raw data for each channel. The raw data consist of the numerical value obtained by the data acquisition system. For channels 0 to 7, the values vary between 0 and 4096. For the 18-bit system, the values vary between -262144 and +262144. For the controller, the recorded value is the temperature. The three first lines are control data. The first line is the channel number and the second line is its gain. The third line contains data that are being dumped. The next lines contain valid data being recorded.

The name of the file cannot be changed from within the software. To save this file for later analysis, it is recommended that it be copied to another filename as soon as the acquisition has been completed. This ensures that the data are saved and cannot be deleted.

Summary of the data acquisition channels

Channel	Resolution	Gain	Vref	Range	Sensor
0	12 bits	82.6312	4093.3 mV	0-49.5 mV	Type K
1	12 bits	81.9307	4093.3 mV	0-49.9 mV	Type K
2	12 bits	83.1328	4093.3 mV	0-49.2 mV	Type K
3	12 bits	82.8511	4093.3 mV	0-49.4 mV	Type K
4	12 bits	82.6734	4093.3 mV	0-49.5 mV	Type K
5	12 bits	82.7618	4093.3 mV	0-49.4 mV	Type K
6	12 bits	287.8136	4093.3 mV	0-14.22 (pH)	pH Controller
7	12 bits	109.98709	4093.3 mV	0-37.2 (°C)	LM35
8	+/- 18 bits		545.0 mV	+/ 512 mV	Balance
9	0-1200°C				Temperature
10	0-1200°C				Set point
11	+/- 18 bits		545.0 mV		Offset

Appendix 3 : Modified predominance diagram software

```
function out = realdiag(Dam,temperature,drawphases,D0,fig_handle,axes_handle)
%    function out = realdiag(Dam,temperature,drawphases,D0,fig_handle,axes_handle)
%
%    MODIFIED PREDOMINANCE DIAGRAMS
%
%    Written in MATLAB 5.2 by Pierre Constantineau
%    ARGUMENTS
%    Dam                        Damköhler number
%    temperature          Temperature (C)
%
%    OPTIONAL ARGUMENTS
%    drawphases           Phases to draw enter 511 for all phases
%    D0                   If =0 do not draw predom diagram if =1, draw it
%    fig_handle           handle of figure to draw
%    axe_handle           handle of axes to draw

if nargin<5
   axes_handle=0;
   fig_handle=0;
   if nargin<4
      D0 = 0; % 1 if we want the thermodynamic diagram
      if nargin <3
         drawphases=511;
         if nargin<2
            error('Must have Damköhler number and temperature as inputs')
         end
      end
   end
end

drawtext=0;              % 0 =Do not put phase labels in figures

%Assign a binary value to each phase

MS=1;                    %PbS              1
M=2;                     %Pb               2
MO=4;                    %PbO              4
M2O4=8;                  %Pb3O4            8
MO2=16;                  %PbO2             16
MSO4=32;                 %PbSO4            32
MOMSO4=64;               %PbO*PbSO4        64
MO2MSO4=128;             %*2PbO*PbSO4      128
MO4MSO4=256;             %*4PbO*PbSO4      256
```

```
% Get predoinance diagram from thermodynamic procedure
[triplepoints,data,limits,steps]=thermodata(temperature);

if D0~=0  % create figure and plase labels for the predominance diagrams
   psd=createfigure('Phase Stability Diagram',limits,steps,steps,'', 'log(P_{O_{2S}})','log(P_{SO_{2S}})',
      [(limits(2)-limits(1)) (limits(4)-limits(3)) 1],[0.25 1.5 4.5 4.5]);
   if temperature == 400
      text(-25.5,-20,'Pb')
      text(-25.5,0,'PbS')
      text(-10,0,'PbSO_4')
      text(-15,-20,'PbO')
      text(4,-23,'PbO_2')
      text(-0.5,-23,'Pb_3O_4')
      text(-7,-14,'PbO*PbSO_4')
      text(-4,-18,'4*PbO*PbSO_4')
   end
   if temperature == 600
      text(-17.5,-12,'Pb')
      text(-17.5,2,'PbS')
      text(-5,2,'PbSO_4')
      text(-9,-12,'PbO')
      text(5,-16,'PbO_2')
      text(1.7,-16,'Pb_3O_4')
      text(-3,-9,'PbO*PbSO_4')
      text(-2.5,-11,'4*PbO*PbSO_4')
   end
   if temperature == 800
      text(-13,-9,'Pb')
      text(-13,4,'PbS')
      text(-2,4,'PbSO_4')
      text(-5,-9,'PbO')
      text(7,-12,'PbO_2')
      text(3,-12,'Pb_3O_4')
      text(-3.4,-4,'PbO*PbSO_4')
      text(-1.4,-6,'2*PbO*PbSO_4')
      text(0.2,-8,'4*PbO*PbSO_4')
   end
end

if fig_handle==0  % if no handle of figure entered, create a new figure
   kpd=createfigure('Kinetic Phase Diagram',limits,steps,steps,'', 'log(P_{O_{2\infty}})',
      'log(P_{SO_{2\infty}})', [(limits(2)-limits(1)) (limits(4)-limits(3)) 1],[0.25 1.5 3 3]);
   kpdaxes=gca;
else
   kpd=fig_handle;
   kpdaxes=axes_handle;
end
```

```
%% define stoichiometric coefficients m and n
%% p is a coefficient for converting yield into molar fractions
%% i is the phase ID

        %   i  m   n p
phases = [  1  0   0  1;
            2  1   1  1;
            4 3/2  1  1;
            8 5/3  1  1;
            16  2  1  1;
            256 1.6 0.8  0.2;
            128 5/3 2/3  1/3;
            64 7/4 1/2  1/2;
            32  2  0  1];

for indexdam = 1:length(Dam)
   D=Dam(indexdam);
   for i = 1:length(data)
      % find phases
      phaseno1=0;
      for j = 1:length(phases)
         if twophase(data(i,1),phases(j,1))==1
            if phaseno1==0
               phaseno1=j;
            else
               phaseno2=j;
            end
         end
      end

      m1=phases(phaseno1,2);          % data for one side of the line
      n1=phases(phaseno1,3);
      p1=phases(phaseno1,4);
      m2=phases(phaseno2,2);          % data for the other side of the line
      n2=phases(phaseno2,3);
      p2=phases(phaseno2,4);
      ph1=phases(phaseno1,1);
      ph2=phases(phaseno2,1);

      if twophase(data(i,1),MOMSO4+MSO4)==2
         between=sort([0 10.^(-30:0)]);
      else
         if twophase(data(i,1),MS+MSO4)==2
            between=sort([0 1 .9]);
         else
            if twophase(data(i,1),MO+MS)==2
               between=sort([0 1 .9]);
            else
               if twophase(data(i,1),M+MS)==2
                  between=sort([0 1 .9]);
               else
                  if twophase(data(i,1),MO2+MSO4)==2
                     between=sort([0 10.^(-40:0)]);
                  else
```

```
                if twophase(data(i,1),MOMSO4+MS)==2
                    between=sort([0 1 .9]);
                else
                    if twophase(data(i,1),MO2MSO4+MS)==2
                        between=sort([0 1 .9]);
                    else
                        between=sort([0 1 0.5]);
                    end
                end
            end
        end
    end
end

for j = 1:length(between)
    mf=between(j);
    if twophase(ph1+ph2,drawphases)>=1
        mfcorr=mf*p2/(p1*(1-mf)+p2*mf); % correction to obtain %molar in products
        m=mfcorr*m1+(1-mfcorr)*m2;
        n=mfcorr*n1+(1-mfcorr)*n2;
        X=[data(i,2) data(i,4)];  % data for the line
        Y=[data(i,3) data(i,5)];          % data for the line
        if D0  % to draw predominance diag.
            set(0,'CurrentFigure',psd);
            H=line(X,Y);
            set(H,'color','g')
        end
        if (X(1)>X(2)) % sort X
            X=[X(2) X(1)];
            Y=[Y(2) Y(1)];
        end
        if X(1)==X(2) % vertical
            if (Y(1)<Y(2)) % sort Y
                X=[X(2) X(1)];
                Y=[Y(2) Y(1)];
            end
            Yspace=linspace(Y(1),Y(2),1000);
            Xspace=X(1)*ones(size(Yspace));
            linedata=calculation(D,[10.^Xspace' 10.^Yspace'],m,n);
            if(any(any(isnan(linedata))))
            [locationi,locationj]=find(isnan(linedata));
            if locationi(1)>1  % if we went under the limit of pso2inf =0, refine end of line
                outofplot=0;
                counteroutofplot=0;
                newYspace=Yspace;
                newlinedata=linedata;
                while ~outofplot  % loop to refine the line up to the limit (PSO2inf =0)
                    counteroutofplot=counteroutofplot+1;
                    [locationi,locationj]=find(isnan(newlinedata));
                    delta=newYspace(locationi(1)-0)-newYspace(locationi(1)-1);
                    newYspace=linspace(newYspace(locationi(1)-1),newYspace(locationi(1)-1)+delta,100);
                    newXspace=X(1)*ones(size(newYspace));
                    newlinedata=calculation(D,[10.^newXspace' 10.^newYspace'],m,n);
```

```
            linedata=[linedata; newlinedata];  % store new line data
            if any(any(isnan(linedata)))  % remove bad points (not a number)
               linedata(any(isnan(linedata)'),:)=[];
            end
            if delta <=10*eps
               % Stop if the variation is smaller than 10 times the smallest number available in matlab
               outofplot=1;
            end
            if (counteroutofplot==40)  % Stop if we have gone through the loop 40 times
               outofplot=1;
               disp('forcing out of adding vertical')
            end
         end
      end
   end

else % not vertical   See above for explanations
   Xspace=linspace(X(1),X(2),1000);
   Yspace=interp1q(X',Y',Xspace')';
   linedata=calculation(D,[10.^Xspace' 10.^Yspace'],m,n);
   if any(any(isnan(linedata)))
      [locationi,locationj]=find(isnan(linedata));
      if locationi(1)>1
         outofplot=0;
         counteroutofplot=0;
         newXspace=Xspace;
         newlinedata=linedata;
         while ~outofplot
            counteroutofplot=counteroutofplot+1;
            [locationi,locationj]=find(isnan(newlinedata));
            delta=newXspace(locationi(1)-0)-newXspace(locationi(1)-1);
            newXspace=linspace(newXspace(locationi(1)-1),
               newXspace(locationi(1)-1)+delta,100);
            newYspace=interp1q(X',Y',newXspace')';
            newlinedata=calculation(D,[10.^newXspace' 10.^newYspace'],m,n);
            linedata=[linedata; newlinedata];
            if any(any(isnan(linedata)))
               linedata(any(isnan(linedata)'),:)=[];
            end
            if delta <=10*eps
               outofplot=1;
            end
            if (counteroutofplot==40)
               outofplot=1;
               disp('forcing out of adding not vertical')
            end
         end
      end
   end
end
if any(any(isnan(linedata))) % delete any bad numbers
   linedata(any(isnan(linedata)'),:)=[];
end
newX=log10(linedata(:,1));
```

```
            newY=log10(linedata(:,2));
            set(0,'CurrentFigure',kpd);
            axes(kpdaxes)
            H=line(newX,newY); % draw line
            if (j==1) | (j==(length(between)))
               set(H,'linestyle','-')
            else
               set(H,'linestyle',':','linewidth',0.1)
               set(H,'color','r') % change color of
            end
         end
      end
   end
end
% let's take care of the triple points...
for i = 1: size(triplepoints,1)
   x1=triplepoints(i,2);
   y1=triplepoints(i,3);
   k=1;
   for j = 1:length(phases)
      if twophase(triplepoints(i,1),phases(j,1))==1
         m(k)=phases(j,2);
         n(k)=phases(j,3);
         k=k+1;
      end
   end
   point1=log10(calculation(D(1),[10.^x1 10.^y1],m(1),n(1)));
   point2=log10(calculation(D(1),[10.^x1 10.^y1],m(2),n(2)));
   point3=log10(calculation(D(1),[10.^x1 10.^y1],m(3),n(3)));
   if ((isnan(point1(2)))) % if we have NAN, it is because PSO2inf is negative, put it very small
      point1(2)=-100;
   end
   if ((isnan(point2(2))))
      point2(2)=-100;
   end
   if ((isnan(point3(2))))
      point3(2)=-100;
   end

   set(0,'CurrentFigure',kpd);
   axes(kpdaxes)
   H=line([point1(1) point2(1) point3(1) point1(1)],[point1(2) point2(2) point3(2) point1(2)]);
   set(H,'linestyle','-');
end
%%%%%%%%%%%%%%%%%%%%%%%%%%%%%%%%%%%%%%%%%%%%%%%%%%%%%%%%%% %%
%%   END OF MAIN FUNCTION                                                                                           %%
%%%%%%%%%%%%%%%%%%%%%%%%%%%%%%%%%%%%%%%%%%%%%%%%%%%%%%%%%% %%
```

```
%%%%%%%%%%%%%%%%%%%%%%%%%%%%%%%%%%%%%%%% %%
%%  Calculation                                              %%
%%  This is the two equations                                %%
%%       derived in chapter 3 of Pierre Constantineau's MASC Thesis  %%
%%  D  :  Damköhler number                                   %%
%%  PS :  Pressures (Po2s PSO2s)                             %%
%%  m  :  coefficient for oxygen                             %%
%%  n  :  coefficient for SO2                                %%
function out=calculation(D,PS,m,n)
   PO2S=PS(:,1);
   PSO2S=PS(:,2);
   PO2=PO2S+(D.*PO2S.*m);
   PSO2=PSO2S-(D.*PO2S.*n);

   out=[PO2 PSO2];
   i=find(out<=0);
   out(i)=nan;
%%  END OF calculation FUNCTION      %%
%%%%%%%%%%%%%%%%%%%%%%%%%%%%%%%%%%%%%%%%%%

%%%%%%%%%%%%%%%%%%%%%%%%%%%%%%%%%%%%%%%% %%
%%  twophase                                                 %%
%%       Counts the number of phases both in a and b         %%
%%  a  :  data                                               %%
%%  b  :  phases to check                                    %%
function out=twophase(a,b)
   out=0;
   temp=bitand(a,b);
   for index = 1:9
      if odd(temp)
         temp=(temp-1)/2;
         out=out+1;
      else
         temp=temp/2;
      end
   end
%%  END OF twophase FUNCTION       %%
%%%%%%%%%%%%%%%%%%%%%%%%%%%%%%%%%%%%%%%%%%

%%%%%%%%%%%%%%%%%%%%%%%%%%%%%%%%%%%%%%%%
%%  odd                                              %%
%% Returns true if odd, false if even                %%
%%  in  :  input                                     %%
function out=odd(in)
   if floor(in/2)==floor((in-1)/2)
      out=1;
   else
      out=0;
   end
%%  END OF odd FUNCTION                                      %%
%%%%%%%%%%%%%%%%%%%%%%%%%%%%%%%%%%%%%%%% %%
```

```
%%%%%%%%%%%%%%%%%%%%%%%%%%%%%%%%%%%%%%%%%%%%%%%%%%%%%%%%%%%%%%%%%% %%
%% thermodata (temperature in C)                                  %%
%% Data from HSC thermodynamical software                         %%
%% It outputs the triplepoints coordinates, lines end points and  %%
%% preset limits and stepsize for displaying the graph            %%
%%%%%%%%%%%%%%%%%%%%%%%%%%%%%%%%%%%%%%%%%%%%%%%%%%%%%%%%%%%%%%%%%% %%
function [triplepoints,data,limits,step]=thermodata(Temp)
if Temp==300
  limits=[-35 5 -35 5];
  step=5;
  triplepoints=[ 2+4+256   -29.5307   -11.4930;
            2+256+1   -29.7279   -10.9012;
            4+8+256    -1.8413   -25.3376;
            16+64+8     1.0020   -24.4226;
            16+64+32    3.6519   -23.0977;
            8+64+256    0.9365   -24.4117;
            64+256+1  -28.9993    -9.4438;
            64+1+32   -28.3313    -7.1061];

 al=[2+4        -29.5307   -50.0000   -29.5307   -11.4930       ;
 2+1            -68.8267   -50.0000   -29.7279   -10.9012  ;
 4+8             -1.8413   -50.0000    -1.8413   -25.3376  ;
 16+8             1.0020   -50.0000     1.0020   -24.4226  ;
 16+32           50.0000   -23.0977     3.6519   -23.0977  ;
 1+32           -28.3313    35.0000   -28.3313    -7.1061  ];

end

if Temp==400
  limits=[-25 5 -25 5];
  step =5;
  triplepoints=[ 2+4+256   -23.5860    -8.5346;
            2+256+1   -23.8605    -7.7110;
            4+8+256    -0.2147   -20.2202;
            16+64+8     2.4230   -19.4734;
            16+64+32    4.6985   -18.3357;
            8+64+256    2.1582   -19.4293;
            64+256+1  -23.3441    -6.6781;
            64+1+32   -22.7532    -4.6098];

 al=[2+4        -23.5860   -50.0000   -23.5860    -8.5346       ;
 2+1            -50.0000   -33.8504   -23.8605    -7.7110  ;
 4+8             -0.2147   -50.0000    -0.2147   -20.2202  ;
 16+8             2.4230   -50.0000     2.4230   -19.4734  ;
 16+32           30.0000   -18.3357     4.6985   -18.3357  ;
 1+32           -22.7532    30.0000   -22.7532    -4.6098  ];

end
if Temp==500
  limits=[-20 10 -20 10];
  step = 5;
  triplepoints=[ 2+4+256   -19.1621    -6.3741;
            2+256+1   -19.5087    -5.3344;
```

```
            4+8+256     0.9554    -16.4329;
            16+64+8      3.4762    -15.8087;
            16+64+32     5.4615    -14.8161;
            8+64+256     3.0440    -15.7367;
            64+256+1   -19.1591     -4.6352;
            64+1+32    -18.6267     -2.7720];


al=[2+4          -19.1621    -50.0000    -19.1621     -6.3741          ;
2+1             -50.0000    -35.8257    -19.5087     -5.3344   ;
4+8               0.9554    -50.0000      0.9554    -16.4329   ;
16+8              3.4762    -50.0000      3.4762    -15.8087   ;
16+32            50.0000    -14.8161      5.4615    -14.8161   ;
1+32            -18.6267     50.0000    -18.6267     -2.7720   ];

end

if Temp==600
  limits=[-20 10 -20 10];
  step = 5;
  triplepoints=[ 2+4+256    -15.7635     -4.7281;
            2+256+1    -16.1165     -3.5193;
            4+8+256      1.8302    -13.5250;
            16+64+8      4.2882    -12.9936;
            16+64+32     6.0398    -12.1178;
            8+64+256     3.7122    -12.8976;
            64+256+1   -15.9421     -3.0705;
            64+1+32    -15.4562     -1.3698];

al=[2+4          -15.7635    -50.0000    -15.7635     -4.7281          ;
2+1             -50.0000    -37.3528    -16.1165     -3.5193   ;
4+8               1.8302    -50.0000      1.8302    -13.5250   ;
16+8              4.2882    -50.0000      4.2882    -12.9936   ;
16+32            30.0000    -12.1178      6.0398    -12.1178   ;
1+32            -15.4562     30.0000    -15.4562     -1.3698   ];

end

if Temp==700
  limits=[-15 10 -15 10]; % limits of figures
step=5;
triplepoints=[ 2+4+256          -13.0748     -3.4410;
            2+256+1          -13.5239     -2.0936;
            4+8+256          2.5037    -11.2302;
            16+8+64          4.9340    -10.7711;
            16+64+32          6.4918     -9.9922;
            8+64+128    4.6279    -10.7201;
            8+128+256  4.0342    -10.7201;
            64+128+1      -13.3639     -1.7242;
            64+1+32          -12.9489     -0.2718;
            128+256+1    -13.4628     -1.9715];


%lines
```

```
al=[2+4          -13.0748   -30.0000   -13.0748    -3.4410      ;
2+1             -30.0000   -18.5697   -13.5239    -2.0936   ;
4+8               2.5037   -30.0000     2.5037   -11.2302   ;
16+8              4.9340   -30.0000     4.9340   -10.7711   ;
16+32            40.0000    -9.9922     6.4918    -9.9922   ;
1+32            -12.9489    40.0000   -12.9489    -0.2718   ];


end

if Temp==800
  limits=[-15 10 -15 10]; % limits of figures
step=5;
triplepoints=[ 2+4+256    -10.8978    -2.4148;
               2+128+256  -11.2793    -1.2704;
               2+128+1    -11.4219    -0.9851;
               4+8+256      3.0346    -9.3810;
               16+8+128     5.4614    -8.9996;
               16+64+128    5.5015    -8.9594;
               16+64+32     6.8545    -8.2829;
               8+128+256    4.1791    -8.9996;
               64+128+1   -11.2594    -0.5790;
               64+1+32    -10.9212     0.6049];

%lines

al=[2+4          -10.8978   -50.0000   -10.8978    -2.4148;
2+1             -50.0000   -39.5632   -11.4219    -0.9851   ;
4+8               3.0346   -50.0000     3.0346    -9.3810   ;
16+8              5.4614   -50.0000     5.4614    -8.9996   ;
16+32            70.0000    -8.2829     6.8545    -8.2829   ;
1+32            -10.9212    70.0000   -10.9212     0.6049   ];

end
%routine to find all the other lines...
k=1;
for i = 1:(length(triplepoints)-1)
   for j= i+1:length(triplepoints)
      if twophase(triplepoints(i,1),triplepoints(j,1))==2% if 2 phases
         newlines(k,:)=[  bitand(triplepoints(i,1),triplepoints(j,1)) triplepoints(i,2) triplepoints(i,3)
            triplepoints(j,2) triplepoints(j,3)];
         k=k+1;
      end
   end
end
data = [al;newlines];
```

```
function handle=createfigure(windowtitle,limits,xtick,ytick,graphtitle,xtitle,ytitle,aspect,size)
no_axes=0;
no_of_inputs=nargin;
if no_of_inputs<8
   aspect=[1 1 1];
end

if no_of_inputs<9
   size=[0.25 1.5 4.5 4.5];
      if no_of_inputs<2;
         no_axes=1;
         size=[1.25 1 6.25 9];
      end
end


handle=figure;
set(handle,'PaperOrientation','portrait','PaperPosition',size,'Name',windowtitle);
uimenu('Label','Print in EPS','Callback',['printfigure(' num2str(handle) ')'])
if no_axes==1
  disp('no axes given');
else
   axes('box','on','Xtick',(limits(1):xtick:limits(2)),'Ytick',(limits(3):ytick:limits(4)),'DataAspectRatio',aspect);
   axis(limits)
   title(graphtitle)
   xlabel(xtitle)
   ylabel(ytitle)
end
```

Appendix 4 : Experimental conditions

Experiments to determine the influence of temperature

Pellet	Thickness	Mass	Porosity
B11	2.46	0.9814	27.4
	2.44	0.9780	27.1
B12	2.43	0.9720	27.2
	2.48	0.9899	27.4
B14	2.45	0.9730	27.7
	2.45	0.9750	27.6
B15	2.48	0.9855	27.7
	2.46	0.9819	27.3
B16	2.44	0.9683	27.8
	2.49	0.9864	27.9
B17	2.48	0.9893	27.4
	2.50	0.9815	28.5
B18	2.49	0.9905	27.6
	2.48	0.9819	28.0
B19	2.45	0.9815	27.1
	2.46	0.9853	27.1
B20	2.44	0.9789	27.0
	2.46	0.9807	27.5
B21	2.47	0.9824	27.6
	2.46	0.9833	27.3
B22	2.46	0.9791	27.6
	2.43	0.9720	27.2
B23	2.42	0.9829	26.1
	2.41	0.9848	25.7
B24	2.42	0.9982	25.0
	2.41	0.9856	25.6

For all experiments: Air from cylinders, reading of 90 on 604 rotameter, SO_2 reading of 30 on Ω3, giving 5732 mL/min air + 160 cc/min SO_2. Overall composition: 2.7% SO_2, 21.4% O_2 Balance N_2. Masses: 0.982 +/- 0.013 g. Porosity: 27.2 +/- 1.6 %

Experiments to determine oxygen reaction order

Pellet	Thickness (mm)	Mass (g)	Porosity (%)	Gas	Reading	Rotameter	Flowrates mL/min air	Flowrates mL/min	Conc. % Vol.
1998	2.84	0.9909	36.5	O_2	60	ΩL	1590	1514	36.7
110901	2.84	0.9873	36.8	SO_2	30	Ω3	240	160	2.2
				Air	90	604	5732	5732	
1998	2.91	0.9723	39.2	O_2	100	ΩL	2745	2614	49.2
110902	2.91	0.9710	39.3	SO_2	30	Ω3	240	160	2.2
				Air	70	604	4419	4419	
1998	2.90	0.9763	38.8	O_2	150	ΩL	4106	3910	61.5
110903	2.91	0.9786	38.8	SO_2	30	Ω3	240	160	2.1
				Air	55	604	3470	3470	
1998	2.88	0.9719	38.6	O_2	0	ΩL	0	0	20.6
110904	2.89	0.9728	38.7	SO_2	30	Ω3	240	160	2.1
				Air	120	604	7603	7603	
1998	2.92	0.9805	38.9	Air	90	604	5732	5732	16.4
110905	2.89	0.9699	38.9	SO_2	0	Ω3	0	0	0
				N_2	60	ΩL	1590	1622	83.6
1998	2.88	0.9777	38.2	Air	70	604	4419	4419	12.5
110906	2.90	0.9859	38.2	SO_2	30	Ω3	240	160	2.2
				N_2	100	ΩL	2745	2801	85.3
1998	2.91	0.9860	38.4	Air	100	ΩL	2745	2745	7.8
110907	2.92	0.9836	38.7	SO_2	30	Ω3	240	160	2.2
				N_2	70	604	4419	4509	90
1998	2.86	0.9946	36.7	Air	60	ΩL	1590	1590	4.4
110908	2.84	0.9883	36.7	SO_2	30	Ω3	240	160	2.1
				N_2	90	604	5732	5849	93.5
1998	2.82	0.9886	36.2	O_2	90	604	5732	5459	75.4
110909	2.80	0.9833	36.1	SO_2	30	Ω3	240	160	2.2
				N_2	60	ΩL	1590	1622	22.4
1998	2.85	0.9719	38.0	O_2	120	604	7603	7241	97.8
110910	2.90	0.9912	37.8	SO_2	30	Ω3	240	160	2.2
				N_2	0	ΩL	0	0	0

Masses: 0.981 +/-0.016 g, Porosity: 38.0 +/-2 %

Experiments to determine sulphur dioxide reaction order

Pellet	Thickness (mm)	Mass (g)	Porosity (%)	Gas	Reading	Rotameter	Flowrates mL/min air	Flowrates mL/min	Conc. % Vol.
9901	2.90	0.9744	38.9	O_2	60	ΩL	1590	1514	20.1
	2.90	0.9750	38.8	SO_2	30	Ω3	240	160	2.1
				N_2	90	604	5732	5849	77.8
9902	2.97	0.9737	40.4	O_2	60	ΩL	1590	1514	20.3
	2.97	0.9715	40.5	SO_2	15	Ω3	135	90	1.2
				N_2	90	604	5732	5849	78.5
9903	2.95	0.9818	39.5	O_2	60	ΩL	1590	1514	20.5
	2.95	0.9784	39.7	SO_2	60	Ω3	490	327	4.4
				N_2	85	604	5404	5514	75.1
9904	2.95	0.9743	39.9	O_2	60	ΩL	1590	1514	20.2
	2.96	0.9735	40.2	SO_2	150	Ω3	1190	793	10.6
				N_2	80	604	5076	5180	69.2
9905	2.83	0.9827	36.8	O_2	60	ΩL	1590	1514	20.2
	2.83	0.9823	36.9	SO_2	150	Ω3	1190	1190	10.6
				N_2	80	604	5076	5180	69.2
9906	2.82	0.9802	36.8	O_2	60	ΩL	1590	1514	20.1
	2.82	0.9799	36.8	SO_2	90	Ω3	745	497	6.6
				N_2	85	604	5404	5514	73.3
9907	2.84	0.9842	37.0	O_2	60	ΩL	1590	1514	20.5
	2.84	0.9843	37.0	SO_2	60	Ω3	490	327	4.4
				N_2	85	604	5404	5514	75.1
9908	2.86	0.9807	37.6	O_2	60	ΩL	1590	1514	20.1
	2.86	0.9816	37.6	SO_2	30	Ω3	240	160	2.1
				N_2	90	604	5732	5849	77.8
9909	2.85	0.9838	37.2	O_2	60	ΩL	1590	1514	20.3
	2.86	0.9873	37.2	SO_2	15	Ω3	135	90	1.2
				N_2	90	604	5732	5849	78.5
9910	2.96	0.9740	40.1	O_2	60	ΩL	1590	1514	20.6
	2.94	0.9678	40.1	SO_2	0	Ω3	0	0	0
				N_2	90	604	5732	5849	79.4

Masses: 0.979 +/-0.010 g , Porosity: 38.5 +/- 2.9 %

Appendix 5: Modified predominance diagrams

This appendix contains a collection of modified predominance diagrams for the reaction of lead sulfide, based on the equations developed in chapter 3.

Temperatures of 300,400,500,600,700 and 800°C are presented. For each temperature, an unmodified predominance diagram ($D_{III}=0$), and modified predominance diagrams from Damköhler numbers of 10^{-17} to 10^{5} are shown.

The purpose of this collection of diagrams is to allow the creation of approximate diagrams such as in Figure 3.12 which describes the phases produced as a function of the Damköhler number for a constant bulk oxygen concentration.

All these diagrams, with the exception of the unmodified predominance diagrams, only apply to the following reaction:

$$PbS + m\ O_2 \rightarrow Products + n\ SO_2$$

If other reactions need to be considered, for example the sulfation or sulfidation of oxides, other modified predominance diagrams have to be derived.

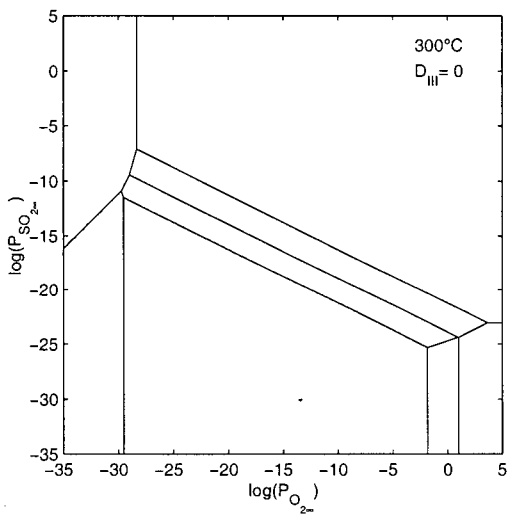
300°C
D_{III}= 0
$\log(P_{SO_{2\infty}})$
$\log(P_{O_{2\infty}})$

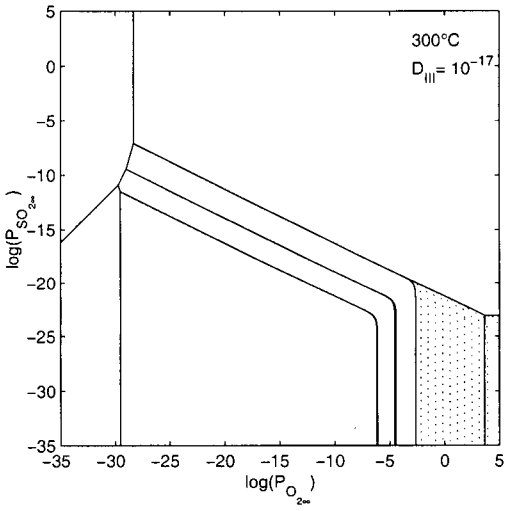
300°C
D_{III}= 10^{-17}
$\log(P_{SO_{2\infty}})$
$\log(P_{O_{2\infty}})$

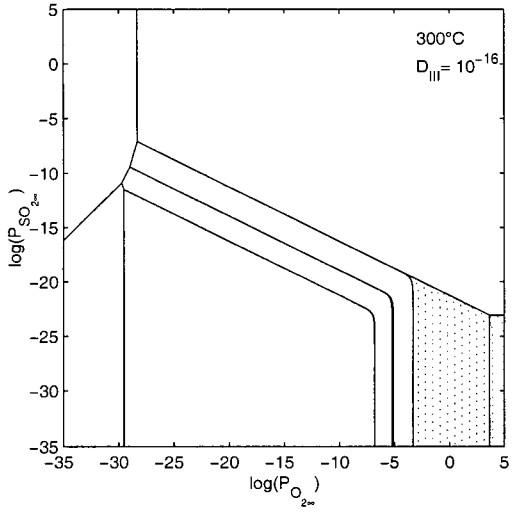
300°C
D_{III}= 10^{-16}
$\log(P_{SO_{2\infty}})$
$\log(P_{O_{2\infty}})$

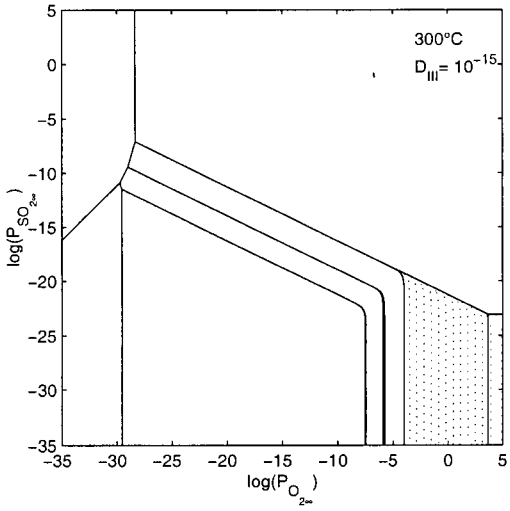
300°C
D_{III}= 10^{-15}
$\log(P_{SO_{2\infty}})$
$\log(P_{O_{2\infty}})$

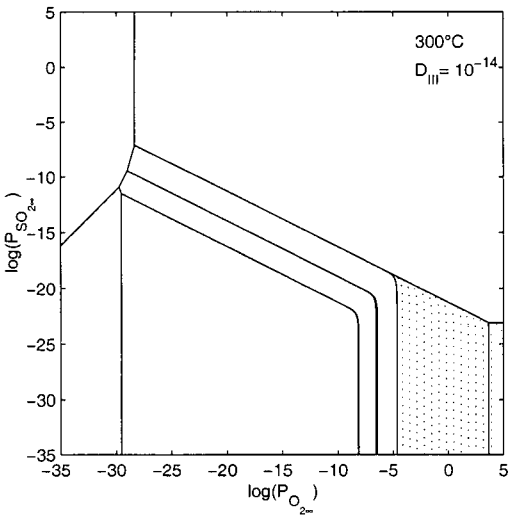
300°C
D_{III}= 10^{-14}
$\log(P_{SO_{2\infty}})$
$\log(P_{O_{2\infty}})$

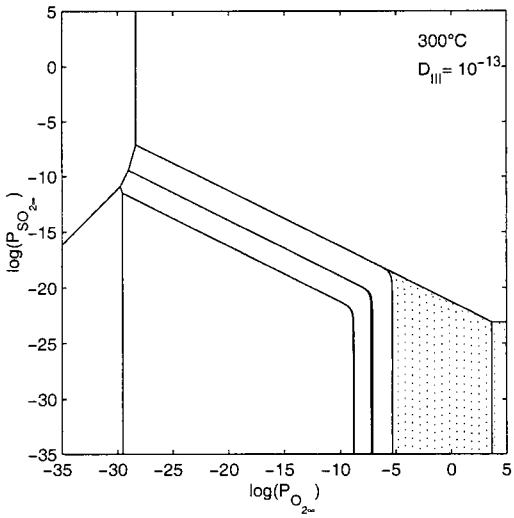
300°C
D_{III}= 10^{-13}
$\log(P_{SO_{2\infty}})$
$\log(P_{O_{2\infty}})$

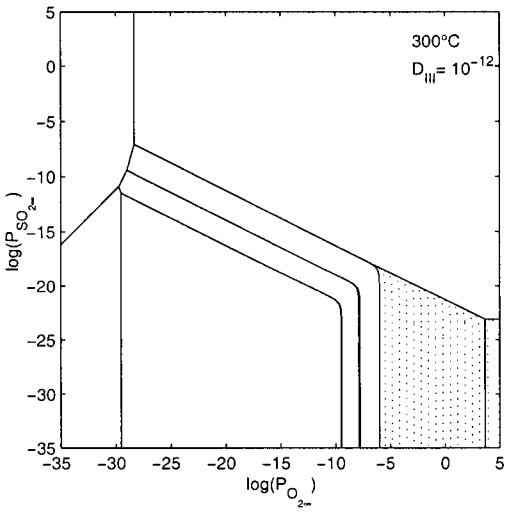
300°C
$D_{III}= 10^{-12}$
$\log(P_{SO_{2\infty}})$
$\log(P_{O_{2\infty}})$

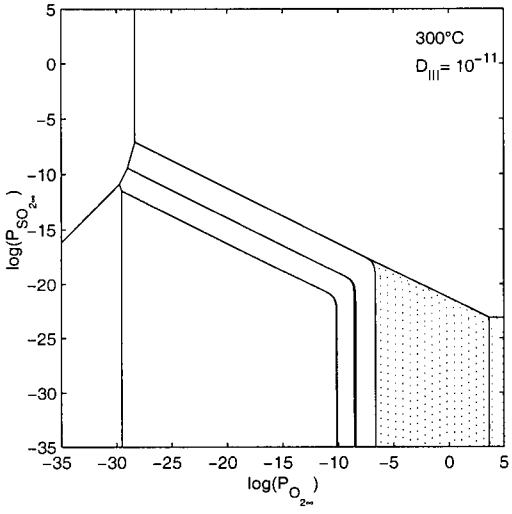
300°C
$D_{III}= 10^{-11}$
$\log(P_{SO_{2\infty}})$
$\log(P_{O_{2\infty}})$

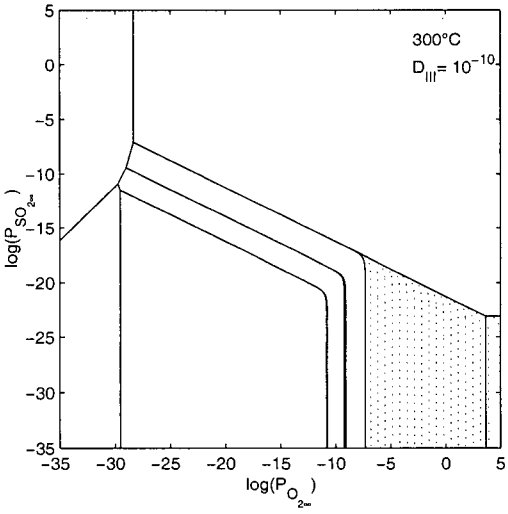
300°C
$D_{III}= 10^{-10}$
$\log(P_{SO_{2\infty}})$
$\log(P_{O_{2\infty}})$

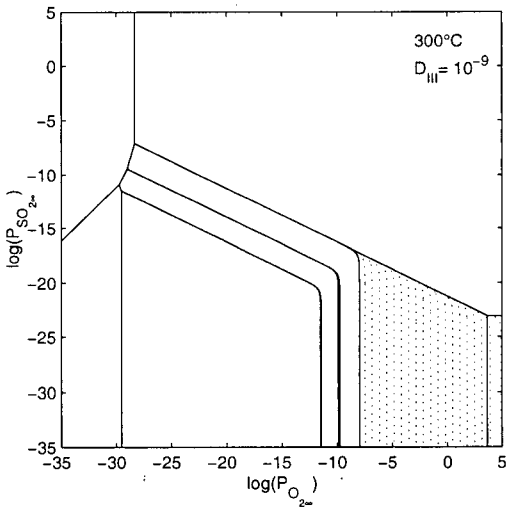
300°C
$D_{III}= 10^{-9}$
$\log(P_{SO_{2\infty}})$
$\log(P_{O_{2\infty}})$

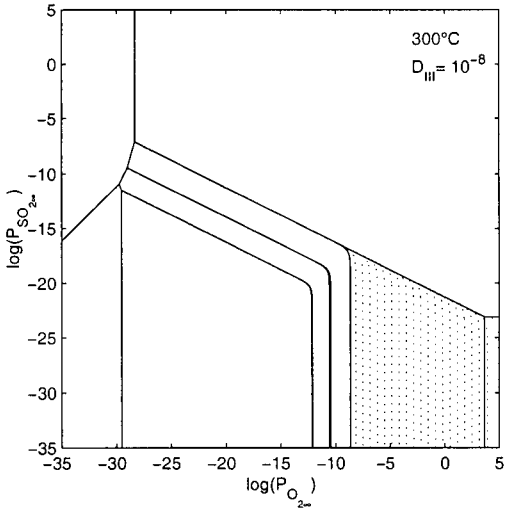
300°C
$D_{III}= 10^{-8}$
$\log(P_{SO_{2\infty}})$
$\log(P_{O_{2\infty}})$

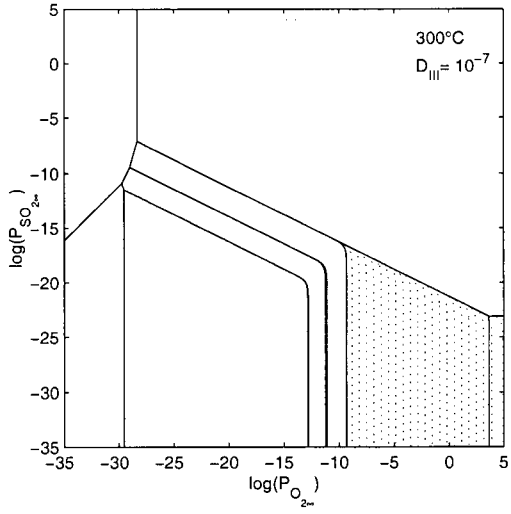
300°C
$D_{III}= 10^{-7}$
$\log(P_{SO_{2\infty}})$
$\log(P_{O_{2\infty}})$

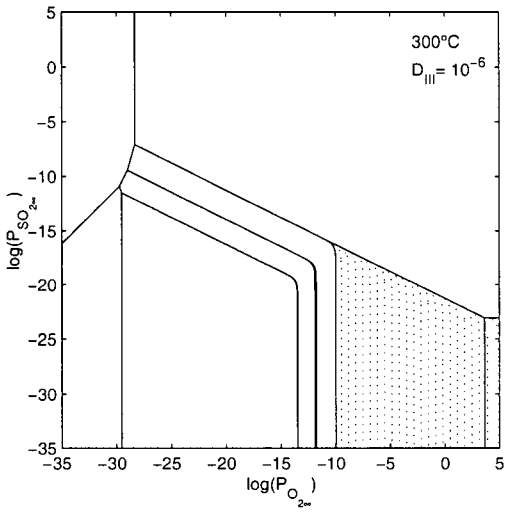
300°C
$D_{III}= 10^{-6}$
$\log(P_{SO_{2-}})$
$\log(P_{O_{2-}})$

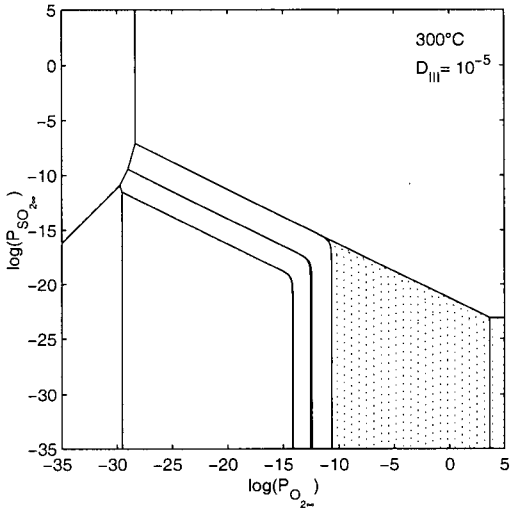
300°C
$D_{III}= 10^{-5}$
$\log(P_{SO_{2-}})$
$\log(P_{O_{2-}})$

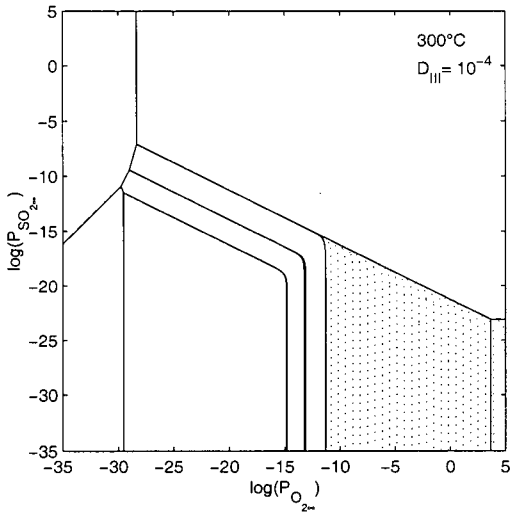
300°C
$D_{III}= 10^{-4}$
$\log(P_{SO_{2-}})$
$\log(P_{O_{2-}})$

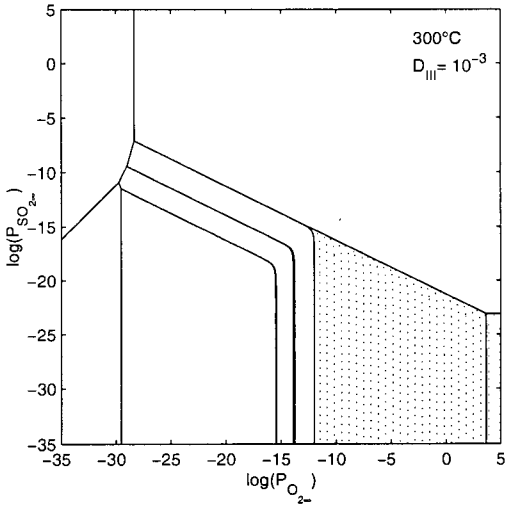
300°C
$D_{III}= 10^{-3}$
$\log(P_{SO_{2-}})$
$\log(P_{O_{2-}})$

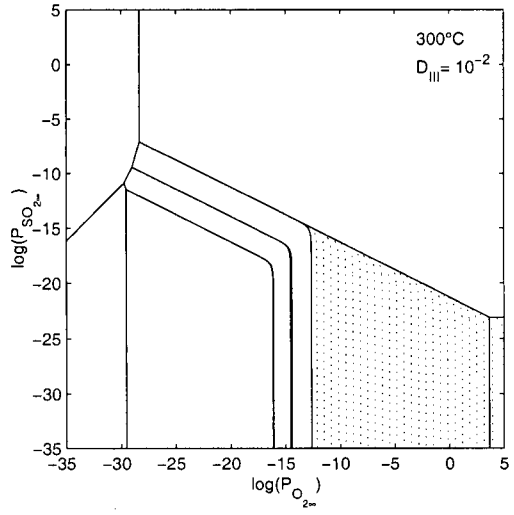
300°C
$D_{III}= 10^{-2}$
$\log(P_{SO_{2-}})$
$\log(P_{O_{2-}})$

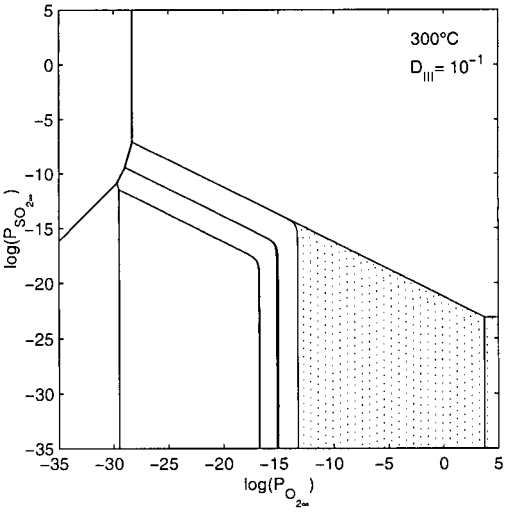
300°C
$D_{III}= 10^{-1}$
$\log(P_{SO_{2-}})$
$\log(P_{O_{2-}})$

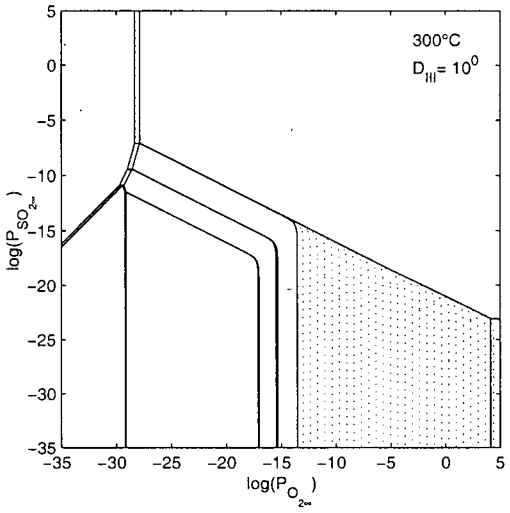
300°C
$D_{III}= 10^{0}$
$\log(P_{SO_{2\infty}})$
$\log(P_{O_{2\infty}})$

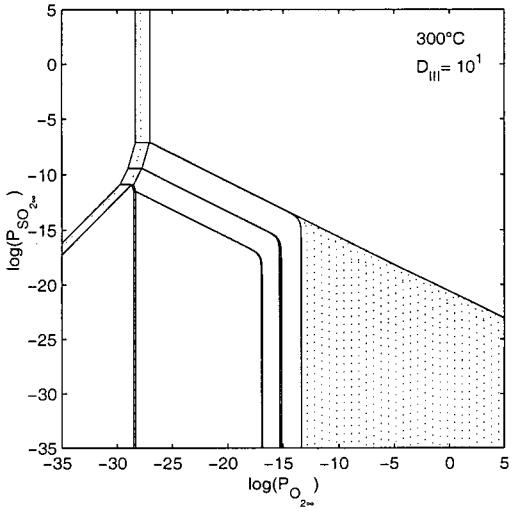
300°C
$D_{III}= 10^{1}$
$\log(P_{SO_{2\infty}})$
$\log(P_{O_{2\infty}})$

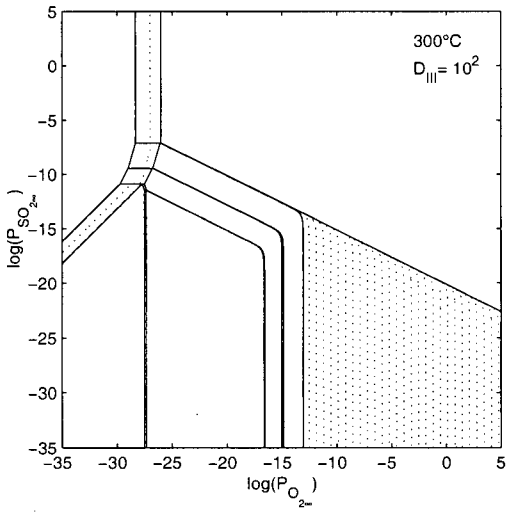
300°C
$D_{III}= 10^{2}$
$\log(P_{SO_{2\infty}})$
$\log(P_{O_{2\infty}})$

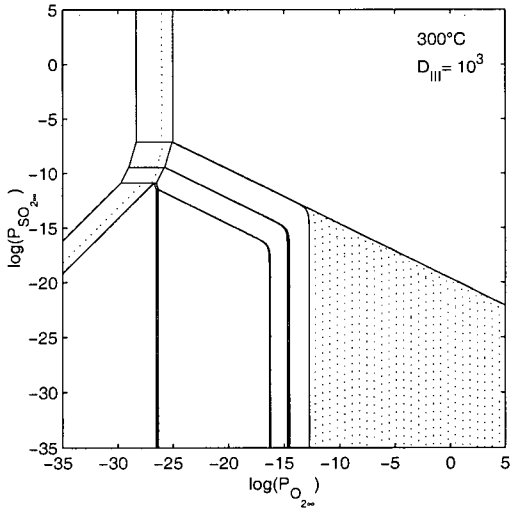
300°C
$D_{III}= 10^{3}$
$\log(P_{SO_{2\infty}})$
$\log(P_{O_{2\infty}})$

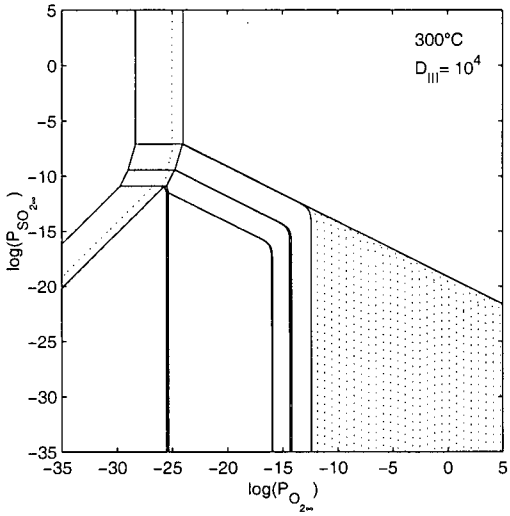
300°C
$D_{III}= 10^{4}$
$\log(P_{SO_{2\infty}})$
$\log(P_{O_{2\infty}})$

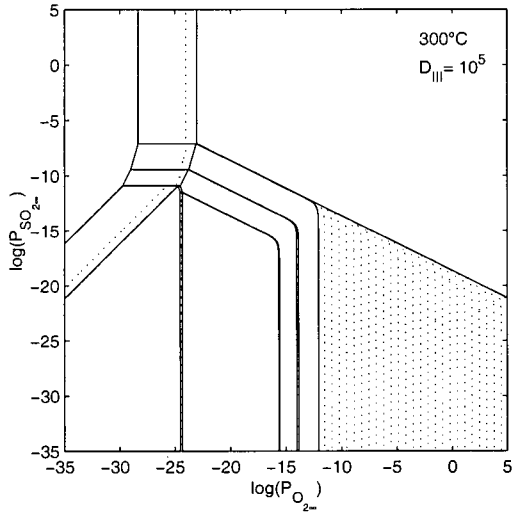
300°C
$D_{III}= 10^{5}$
$\log(P_{SO_{2\infty}})$
$\log(P_{O_{2\infty}})$

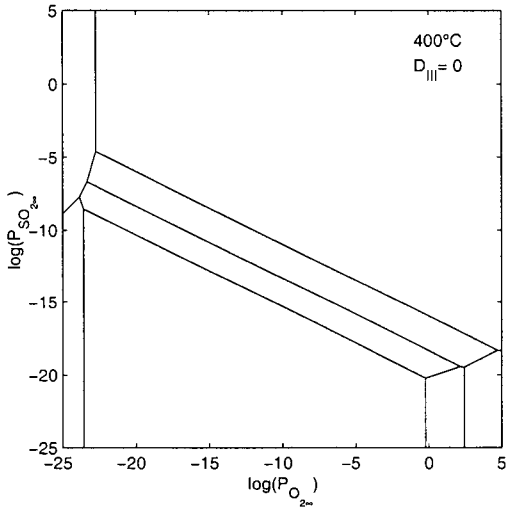
400°C
D_{III}= 0
$\log(P_{SO_{2\infty}})$
$\log(P_{O_{2\infty}})$
5
0
-5
-10
-15
-20
-25
-25 -20 -15 -10 -5 0 5

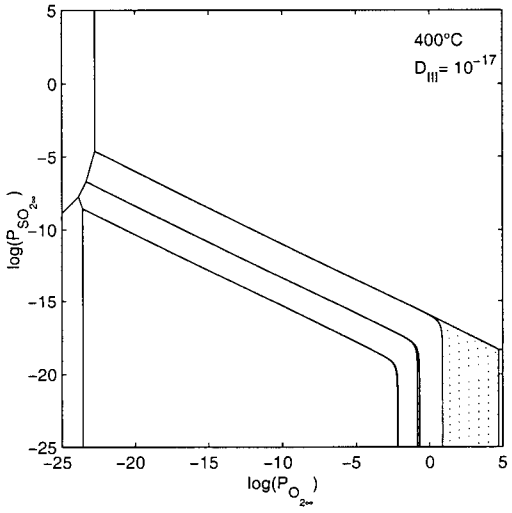
400°C
D_{III}= 10^{-17}
$\log(P_{SO_{2\infty}})$
$\log(P_{O_{2\infty}})$
5
0
-5
-10
-15
-20
-25
-25 -20 -15 -10 -5 0 5

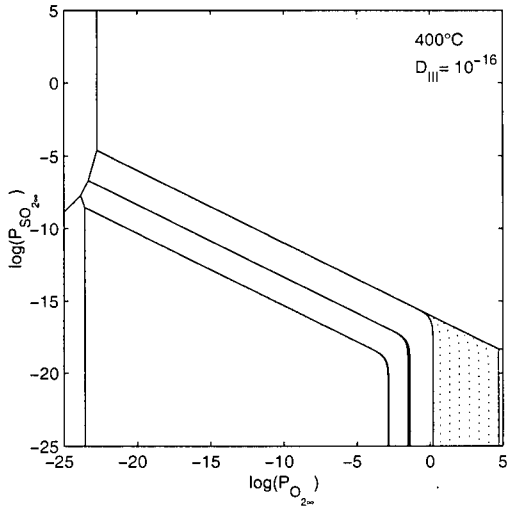
400°C
D_{III}= 10^{-16}
$\log(P_{SO_{2\infty}})$
$\log(P_{O_{2\infty}})$
5
0
-5
-10
-15
-20
-25
-25 -20 -15 -10 -5 0 5

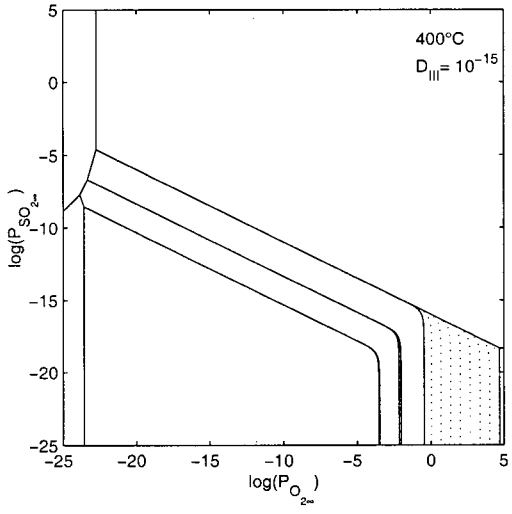
400°C
D_{III}= 10^{-15}
$\log(P_{SO_{2\infty}})$
$\log(P_{O_{2\infty}})$
5
0
-5
-10
-15
-20
-25
-25 -20 -15 -10 -5 0 5

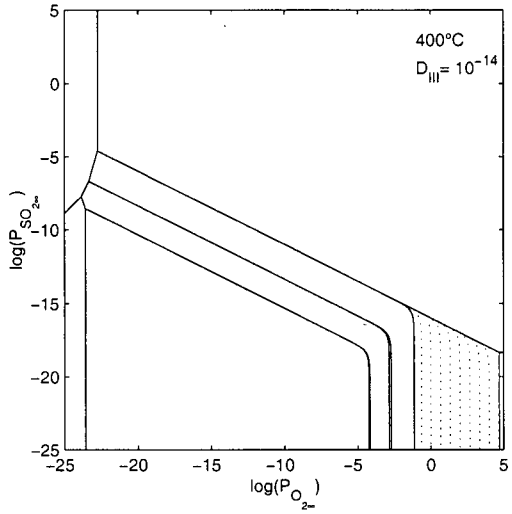
400°C
D_{III}= 10^{-14}
$\log(P_{SO_{2\infty}})$
$\log(P_{O_{2\infty}})$
5
0
-5
-10
-15
-20
-25
-25 -20 -15 -10 -5 0 5

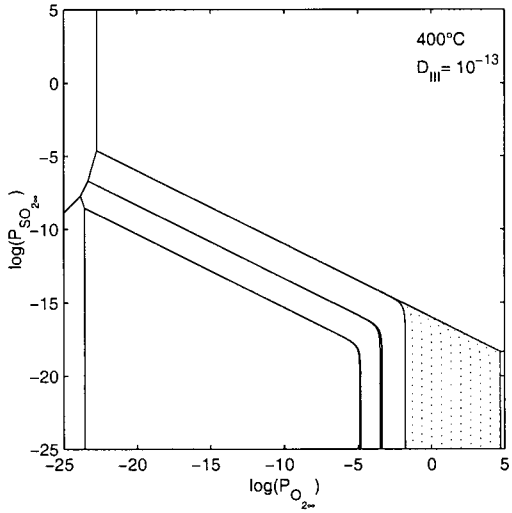
400°C
D_{III}= 10^{-13}
$\log(P_{SO_{2\infty}})$
$\log(P_{O_{2\infty}})$
5
0
-5
-10
-15
-20
-25
-25 -20 -15 -10 -5 0 5

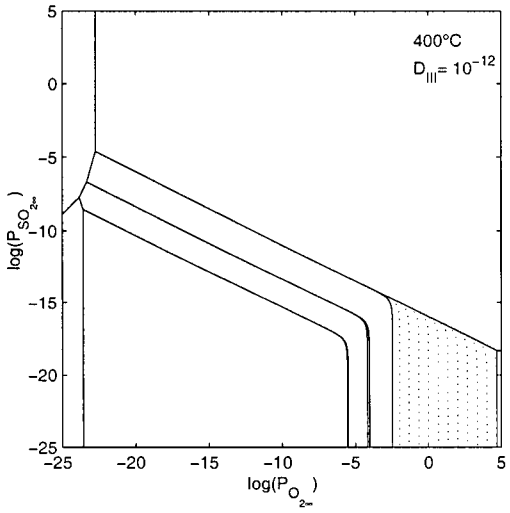
400°C
$D_{III}= 10^{-12}$
$\log(P_{SO_{2\infty}})$
$\log(P_{O_{2\infty}})$

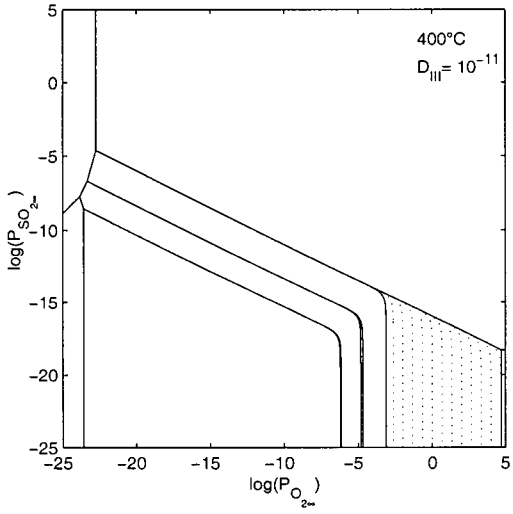
400°C
$D_{III}= 10^{-11}$
$\log(P_{SO_{2\infty}})$
$\log(P_{O_{2\infty}})$

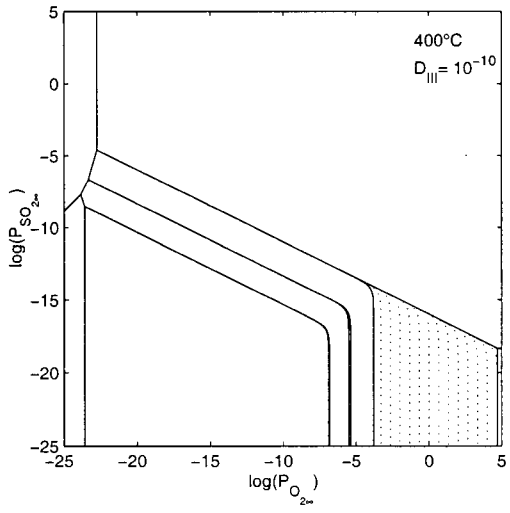
400°C
$D_{III}= 10^{-10}$
$\log(P_{SO_{2\infty}})$
$\log(P_{O_{2\infty}})$

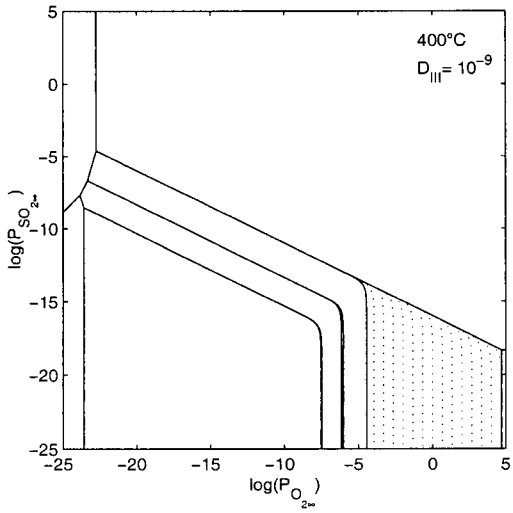
400°C
$D_{III}= 10^{-9}$
$\log(P_{SO_{2\infty}})$
$\log(P_{O_{2\infty}})$

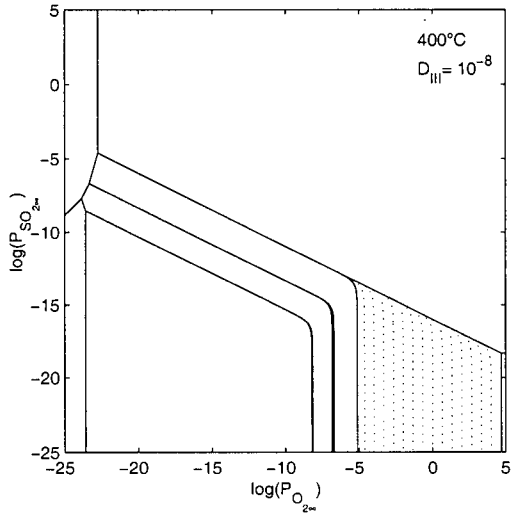
400°C
$D_{III}= 10^{-8}$
$\log(P_{SO_{2\infty}})$
$\log(P_{O_{2\infty}})$

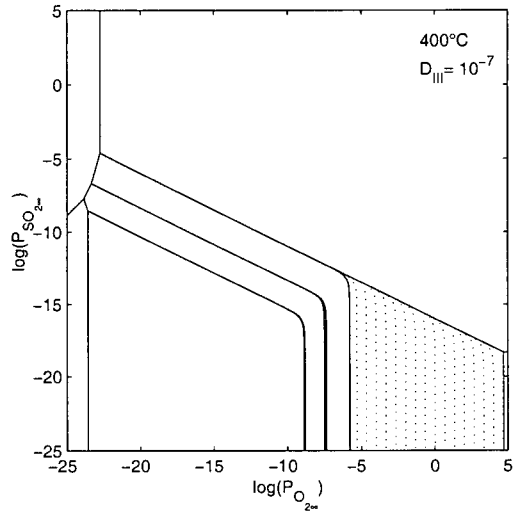
400°C
$D_{III}= 10^{-7}$
$\log(P_{SO_{2\infty}})$
$\log(P_{O_{2\infty}})$

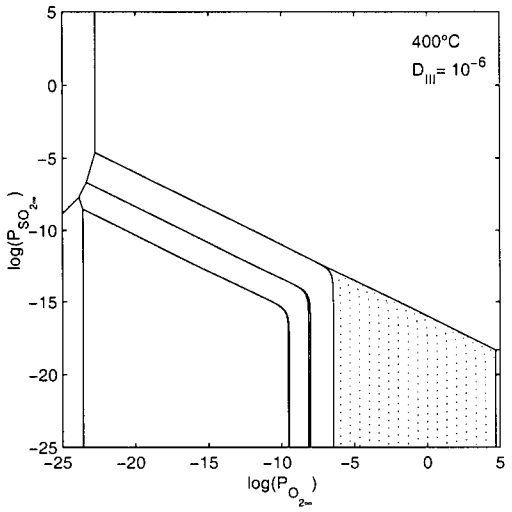
400°C
$D_{III}= 10^{-6}$
$\log(P_{SO_{2\infty}})$
$\log(P_{O_{2\infty}})$
5
0
−5
−10
−15
−20
−25
−25 −20 −15 −10 −5 0 5

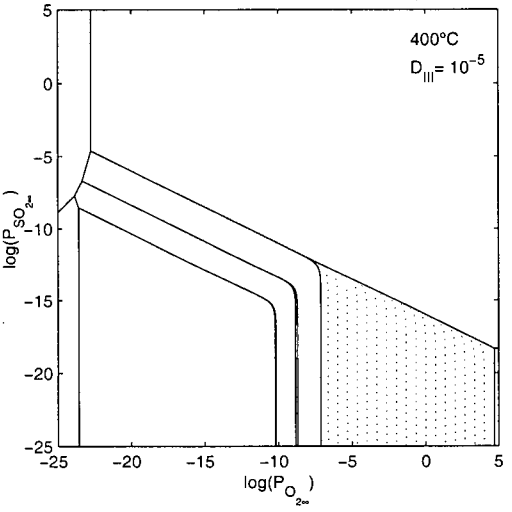
400°C
$D_{III}= 10^{-5}$
$\log(P_{SO_{2\infty}})$
$\log(P_{O_{2\infty}})$
5
0
−5
−10
−15
−20
−25
−25 −20 −15 −10 −5 0 5

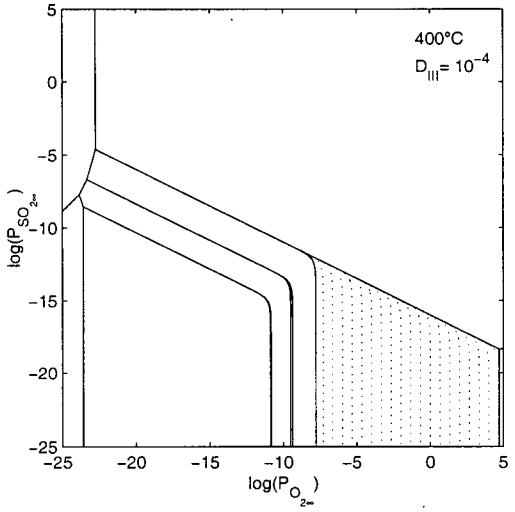
400°C
$D_{III}= 10^{-4}$
$\log(P_{SO_{2\infty}})$
$\log(P_{O_{2\infty}})$
5
0
−5
−10
−15
−20
−25
−25 −20 −15 −10 −5 0 5

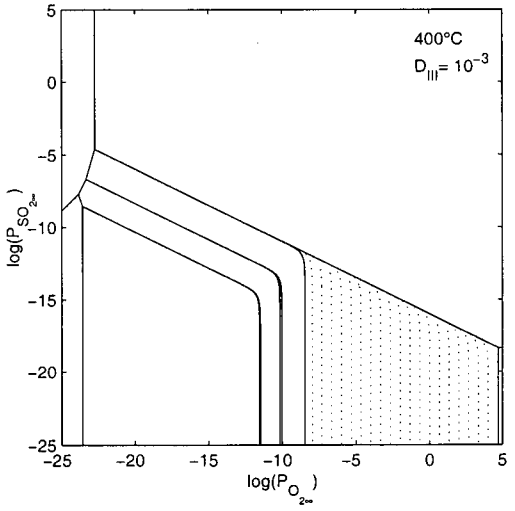
400°C
$D_{III}= 10^{-3}$
$\log(P_{SO_{2\infty}})$
$\log(P_{O_{2\infty}})$
5
0
−5
−10
−15
−20
−25
−25 −20 −15 −10 −5 0 5

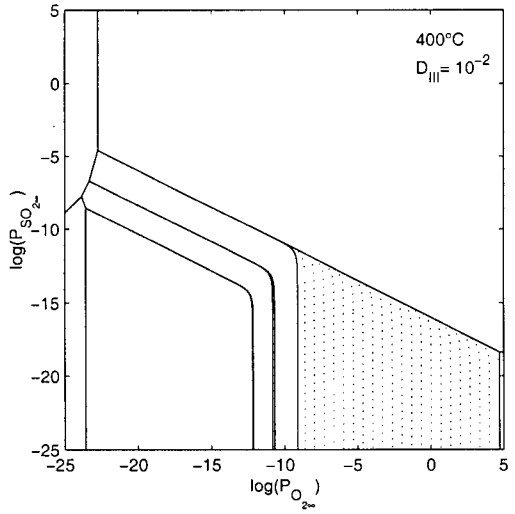
400°C
$D_{III}= 10^{-2}$
$\log(P_{SO_{2\infty}})$
$\log(P_{O_{2\infty}})$
5
0
−5
−10
−15
−20
−25
−25 −20 −15 −10 −5 0 5

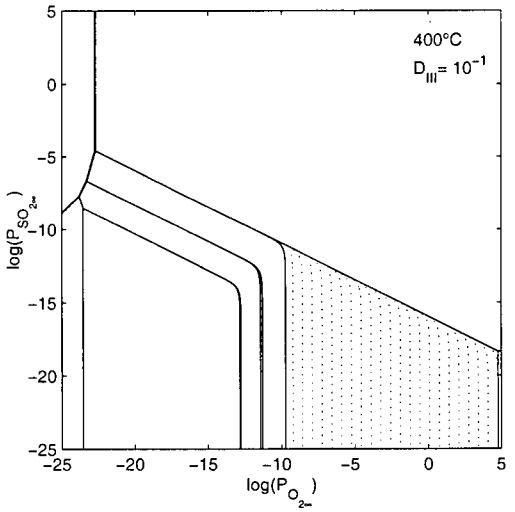
400°C
$D_{III}= 10^{-1}$
$\log(P_{SO_{2\infty}})$
$\log(P_{O_{2\infty}})$
5
0
−5
−10
−15
−20
−25
−25 −20 −15 −10 −5 0 5

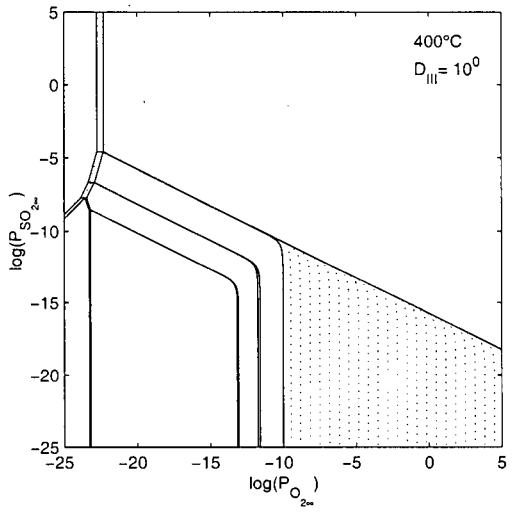
400°C
$D_{III}= 10^0$
$\log(P_{SO_{2-}})$
$\log(P_{O_{2-}})$

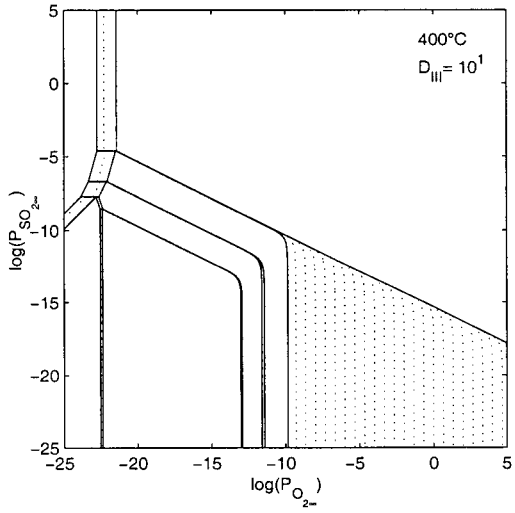
400°C
$D_{III}= 10^1$
$\log(P_{SO_{2-}})$
$\log(P_{O_{2-}})$

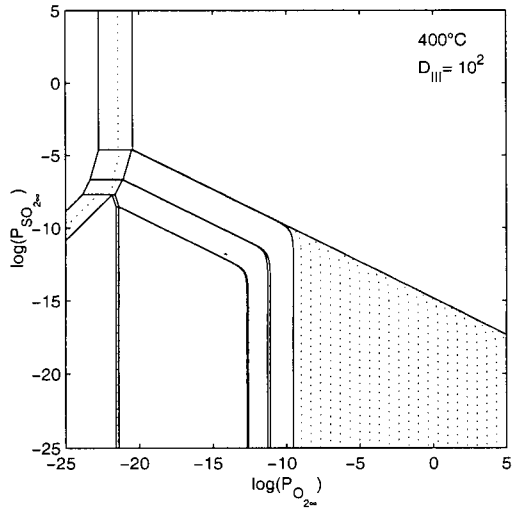
400°C
$D_{III}= 10^2$
$\log(P_{SO_{2-}})$
$\log(P_{O_{2-}})$

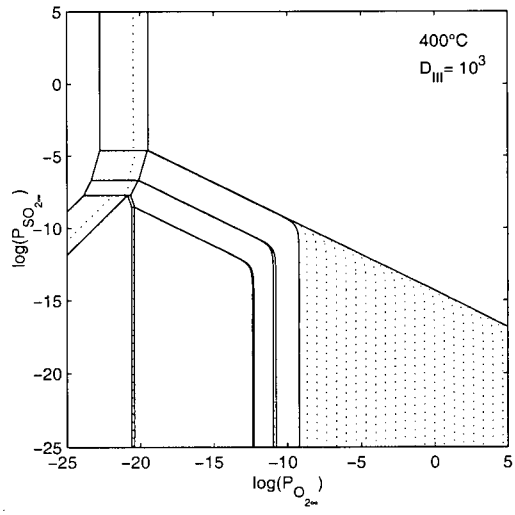
400°C
$D_{III}= 10^3$
$\log(P_{SO_{2-}})$
$\log(P_{O_{2-}})$

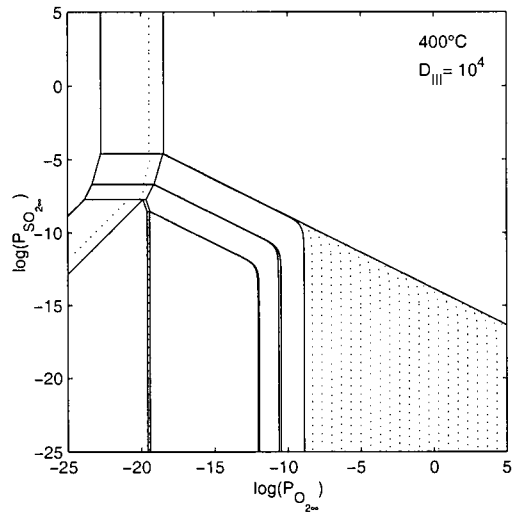
400°C
$D_{III}= 10^4$
$\log(P_{SO_{2-}})$
$\log(P_{O_{2-}})$

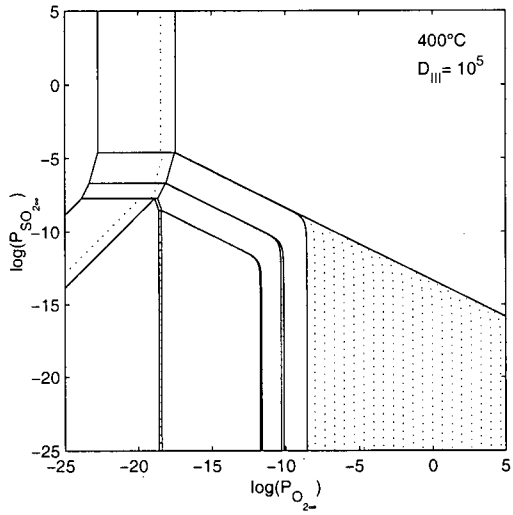
400°C
$D_{III}= 10^5$
$\log(P_{SO_{2-}})$
$\log(P_{O_{2-}})$

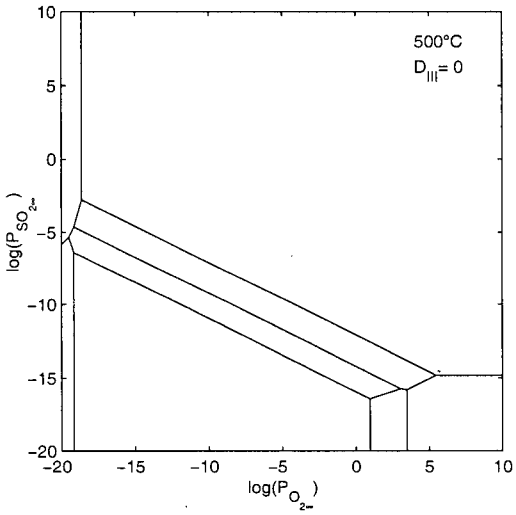
500°C
D_{III}= 0
$\log(P_{SO_{2-}})$
$\log(P_{O_{2-}})$

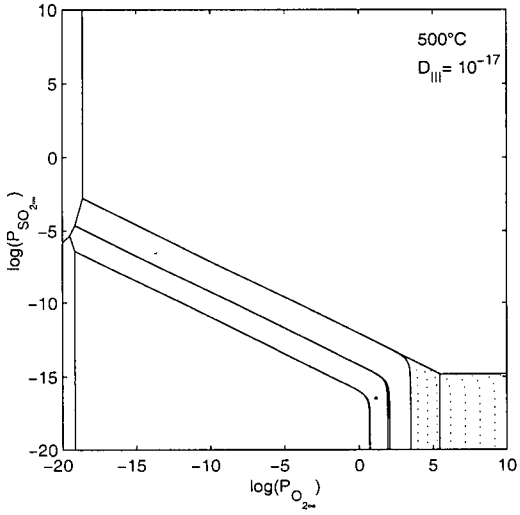
500°C
D_{III}= 10^{-17}
$\log(P_{SO_{2-}})$
$\log(P_{O_{2-}})$

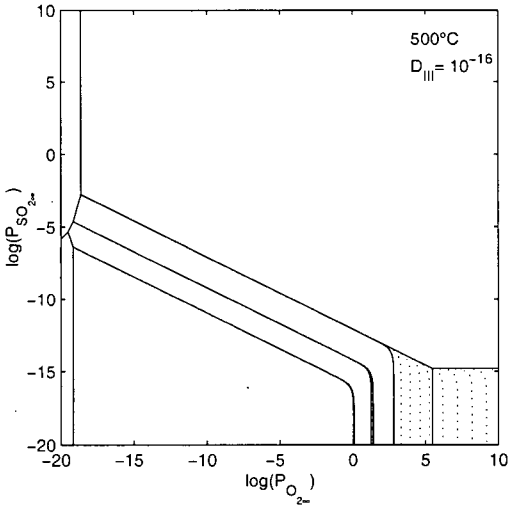
500°C
D_{III}= 10^{-16}
$\log(P_{SO_{2-}})$
$\log(P_{O_{2-}})$

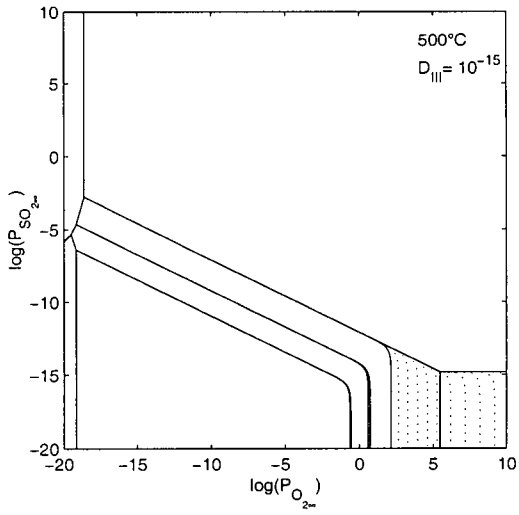
500°C
D_{III}= 10^{-15}
$\log(P_{SO_{2-}})$
$\log(P_{O_{2-}})$

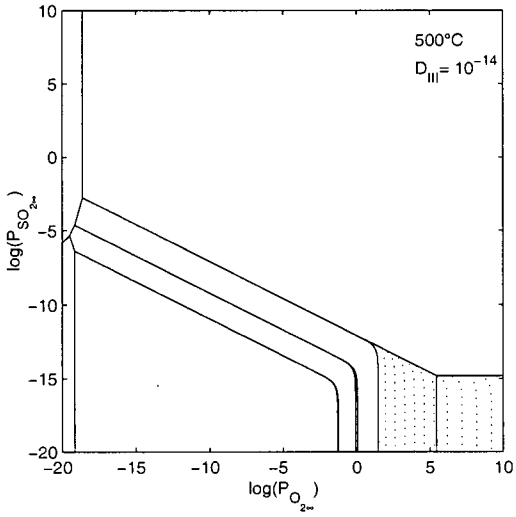
500°C
D_{III}= 10^{-14}
$\log(P_{SO_{2-}})$
$\log(P_{O_{2-}})$

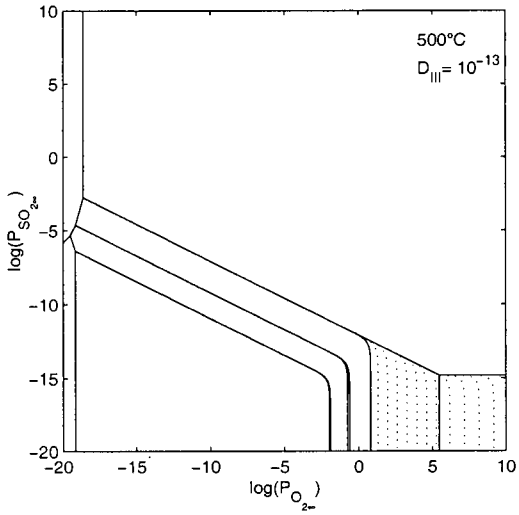
500°C
D_{III}= 10^{-13}
$\log(P_{SO_{2-}})$
$\log(P_{O_{2-}})$

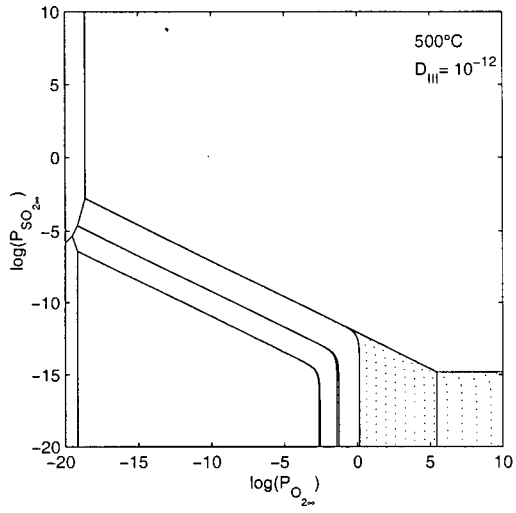
500°C
$D_{III}= 10^{-12}$
$\log(P_{SO_{2\infty}})$
$\log(P_{O_{2\infty}})$

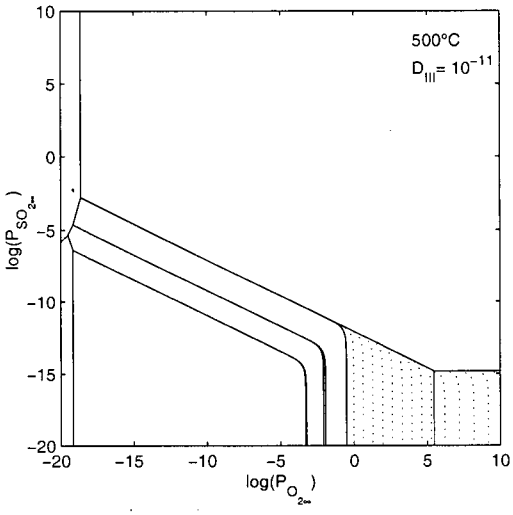
500°C
$D_{III}= 10^{-11}$
$\log(P_{SO_{2\infty}})$
$\log(P_{O_{2\infty}})$

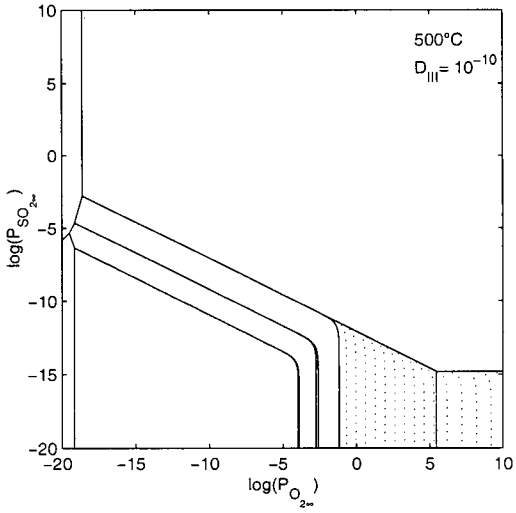
500°C
$D_{III}= 10^{-10}$
$\log(P_{SO_{2\infty}})$
$\log(P_{O_{2\infty}})$

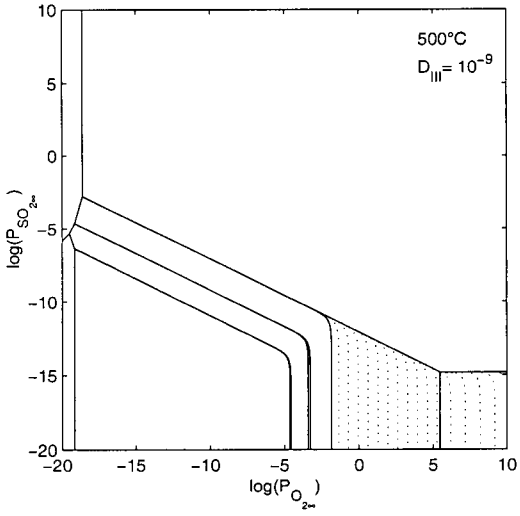
500°C
$D_{III}= 10^{-9}$
$\log(P_{SO_{2\infty}})$
$\log(P_{O_{2\infty}})$

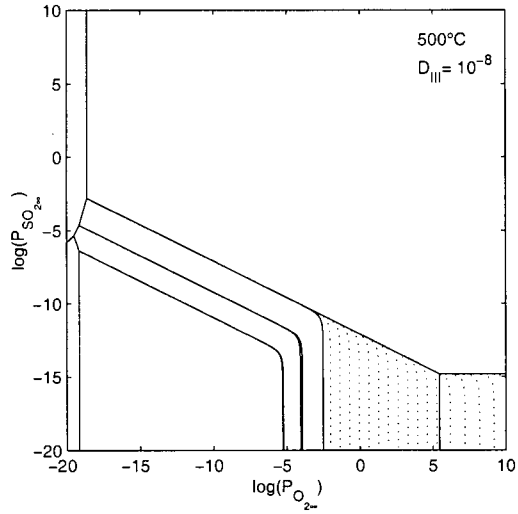
500°C
$D_{III}= 10^{-8}$
$\log(P_{SO_{2\infty}})$
$\log(P_{O_{2\infty}})$

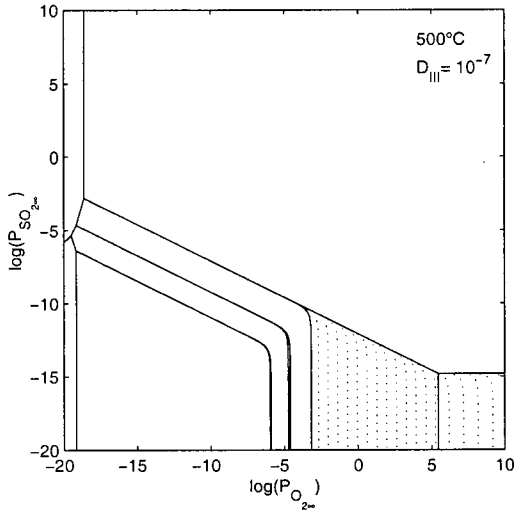
500°C
$D_{III}= 10^{-7}$
$\log(P_{SO_{2\infty}})$
$\log(P_{O_{2\infty}})$

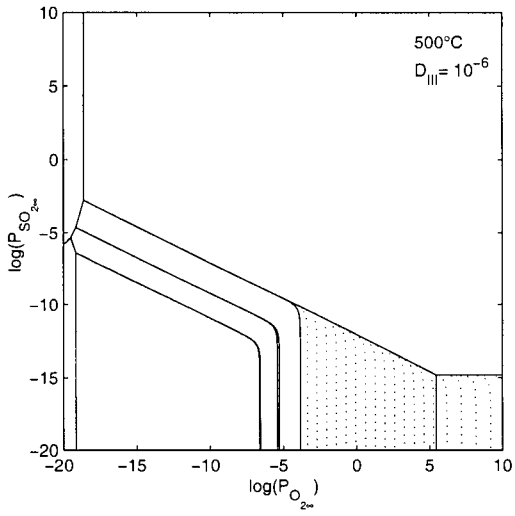
500°C
$D_{III}= 10^{-6}$
$\log(P_{SO_{2\infty}})$
$\log(P_{O_{2\infty}})$

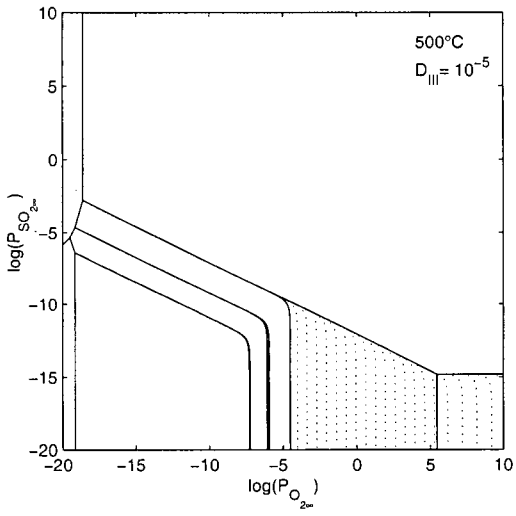
500°C
$D_{III}= 10^{-5}$
$\log(P_{SO_{2\infty}})$
$\log(P_{O_{2\infty}})$

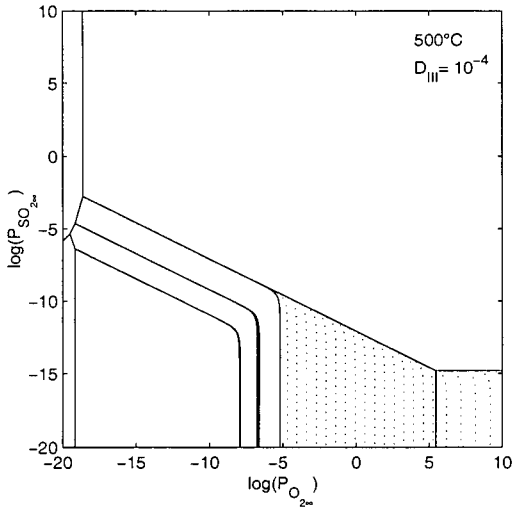
500°C
$D_{III}= 10^{-4}$
$\log(P_{SO_{2\infty}})$
$\log(P_{O_{2\infty}})$

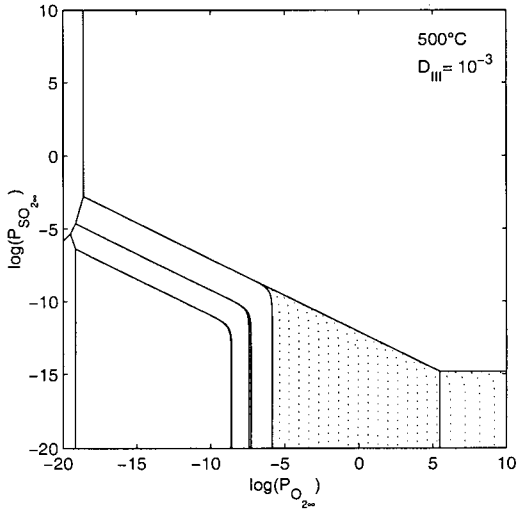
500°C
$D_{III}= 10^{-3}$
$\log(P_{SO_{2\infty}})$
$\log(P_{O_{2\infty}})$

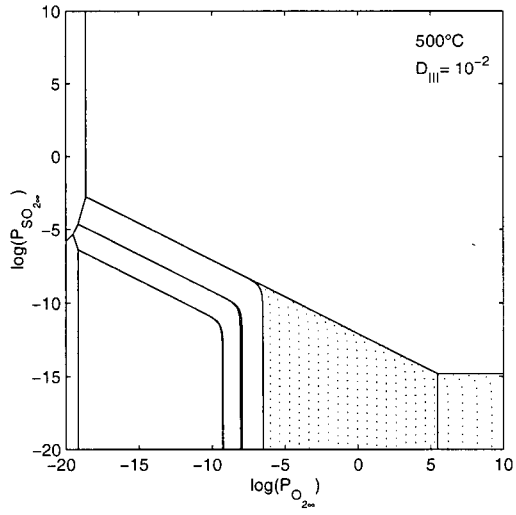
500°C
$D_{III}= 10^{-2}$
$\log(P_{SO_{2\infty}})$
$\log(P_{O_{2\infty}})$

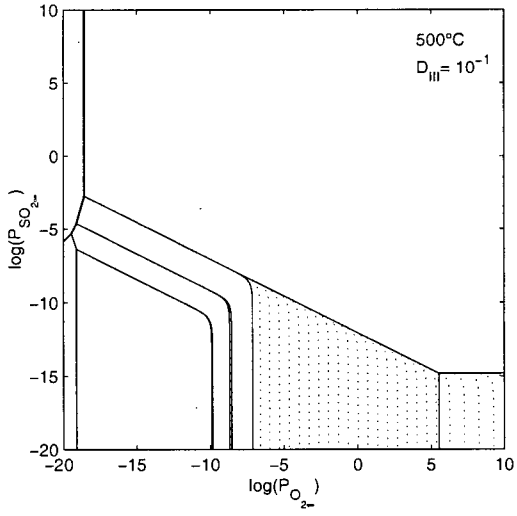
500°C
$D_{III}= 10^{-1}$
$\log(P_{SO_{2\infty}})$
$\log(P_{O_{2\infty}})$

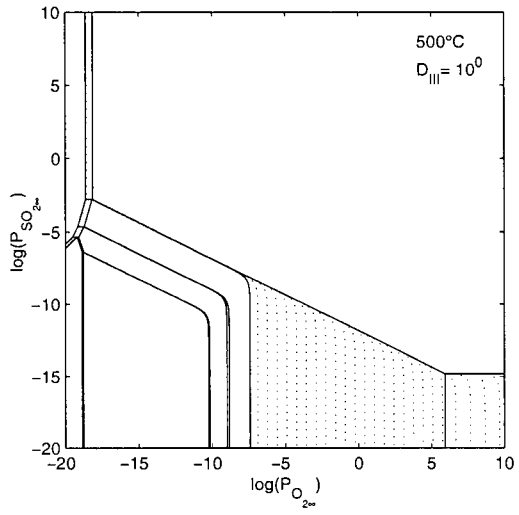
500°C
$D_{III}= 10^0$
$\log(P_{SO_{2\infty}})$
$\log(P_{O_{2\infty}})$

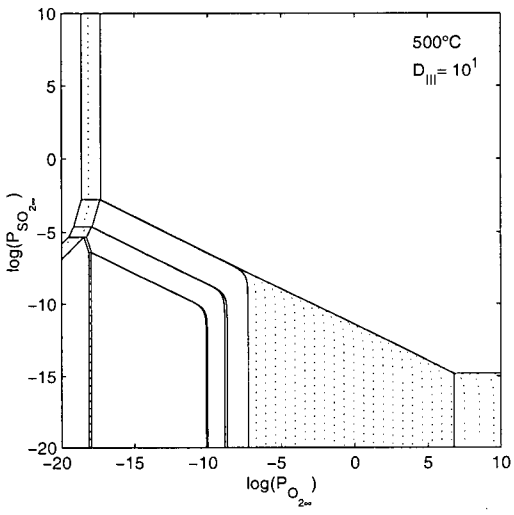
500°C
$D_{III}= 10^1$
$\log(P_{SO_{2\infty}})$
$\log(P_{O_{2\infty}})$

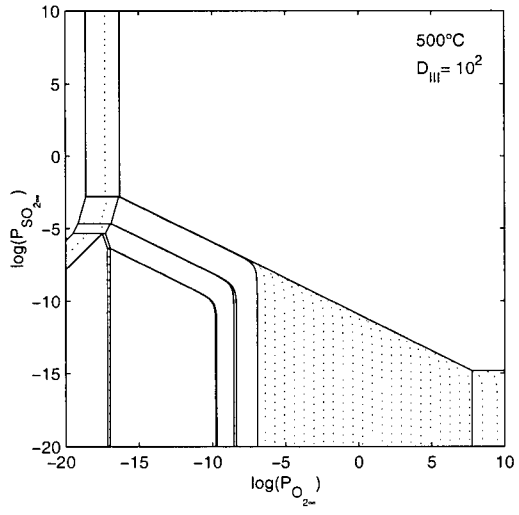
500°C
$D_{III}= 10^2$
$\log(P_{SO_{2\infty}})$
$\log(P_{O_{2\infty}})$

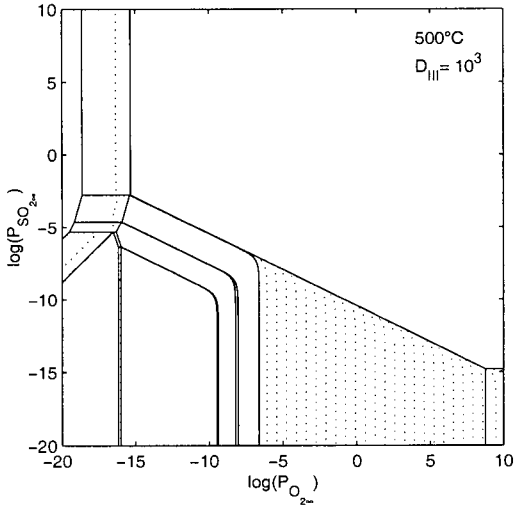
500°C
$D_{III}= 10^3$
$\log(P_{SO_{2\infty}})$
$\log(P_{O_{2\infty}})$

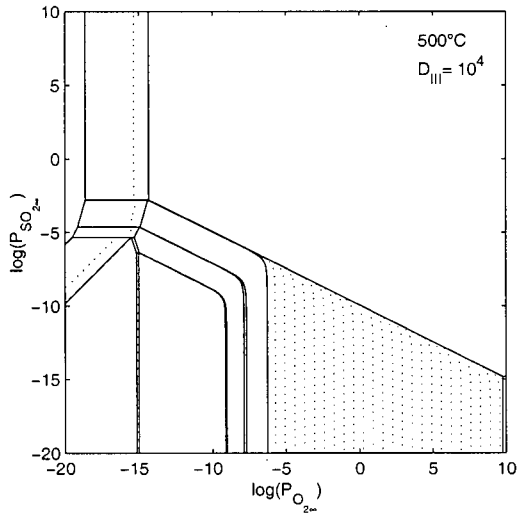
500°C
$D_{III}= 10^4$
$\log(P_{SO_{2\infty}})$
$\log(P_{O_{2\infty}})$

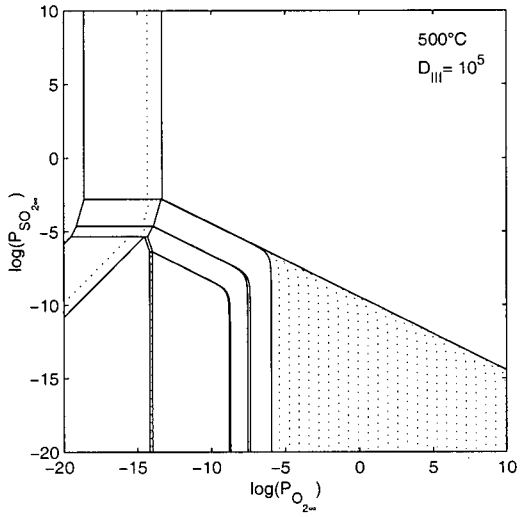
500°C
$D_{III}= 10^5$
$\log(P_{SO_{2\infty}})$
$\log(P_{O_{2\infty}})$

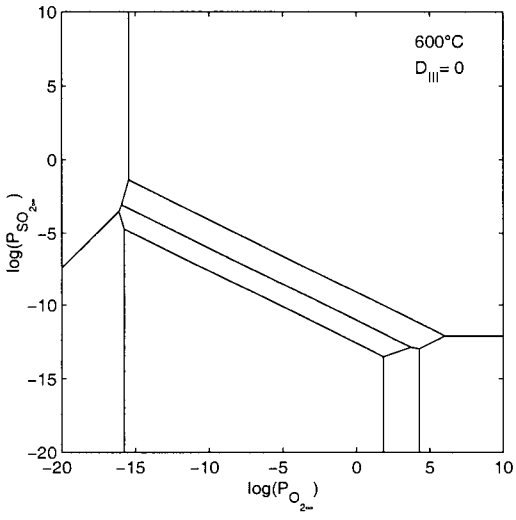
600°C
D_{III}= 0
$\log(P_{SO_{2\infty}})$
$\log(P_{O_{2\infty}})$

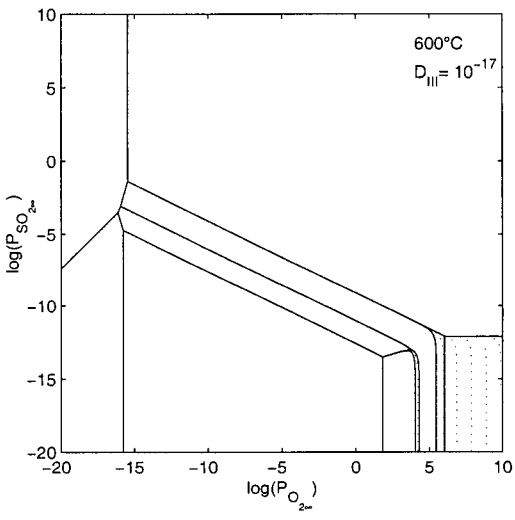
600°C
D_{III}= 10^{-17}
$\log(P_{SO_{2\infty}})$
$\log(P_{O_{2\infty}})$

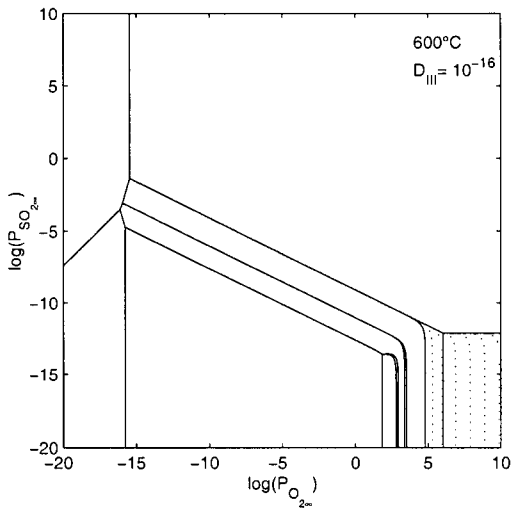
600°C
D_{III}= 10^{-16}
$\log(P_{SO_{2\infty}})$
$\log(P_{O_{2\infty}})$

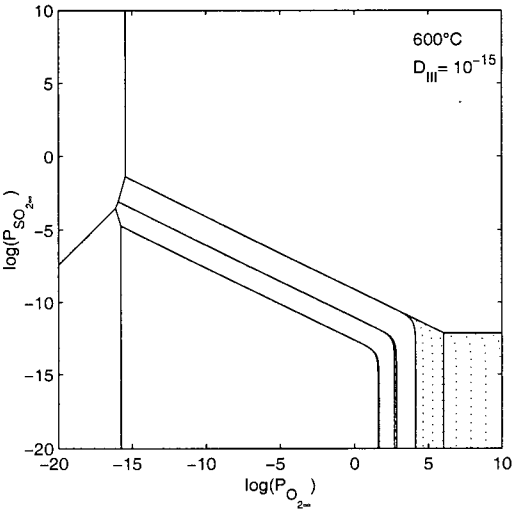
600°C
D_{III}= 10^{-15}
$\log(P_{SO_{2\infty}})$
$\log(P_{O_{2\infty}})$

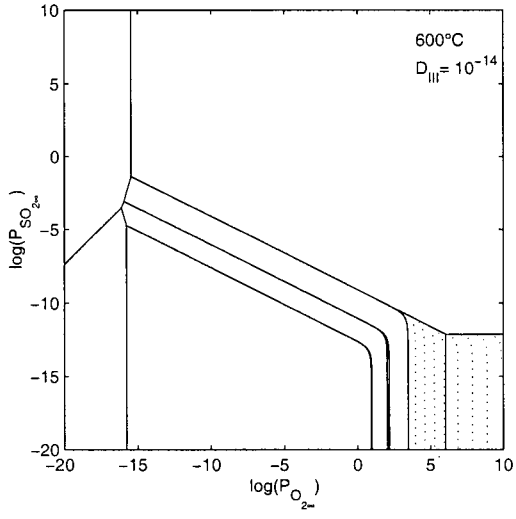
600°C
D_{III}= 10^{-14}
$\log(P_{SO_{2\infty}})$
$\log(P_{O_{2\infty}})$

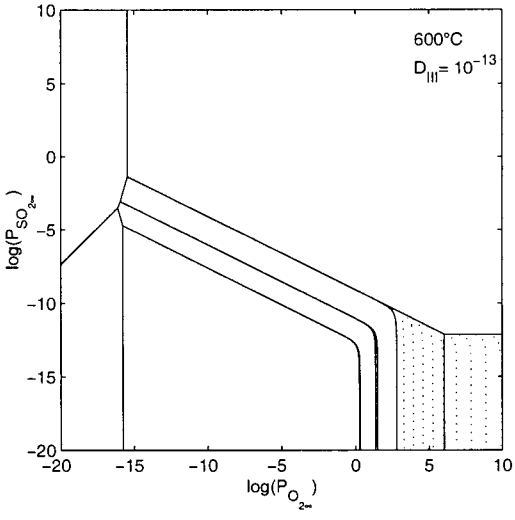
600°C
D_{III}= 10^{-13}
$\log(P_{SO_{2\infty}})$
$\log(P_{O_{2\infty}})$

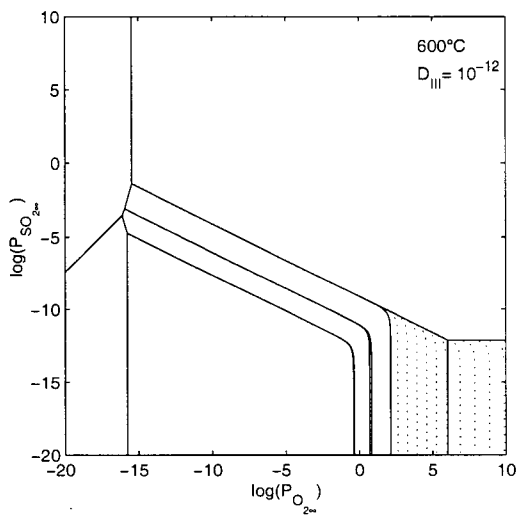
600°C
$D_{III}= 10^{-12}$
$\log(P_{SO_{2\infty}})$
$\log(P_{O_{2\infty}})$

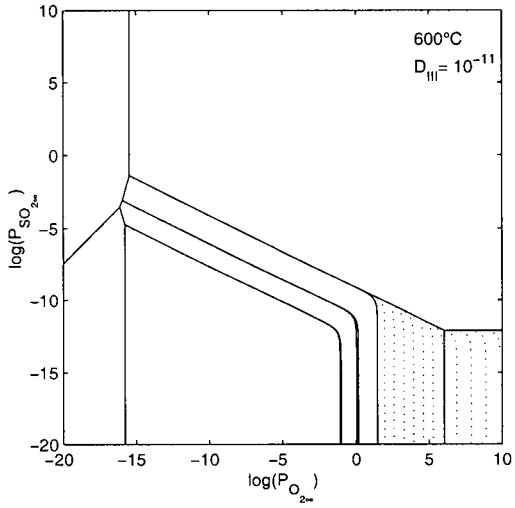
600°C
$D_{III}= 10^{-11}$
$\log(P_{SO_{2\infty}})$
$\log(P_{O_{2\infty}})$

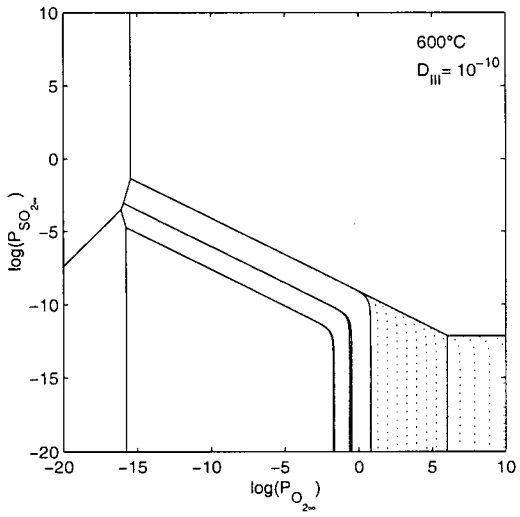
600°C
$D_{III}= 10^{-10}$
$\log(P_{SO_{2\infty}})$
$\log(P_{O_{2\infty}})$

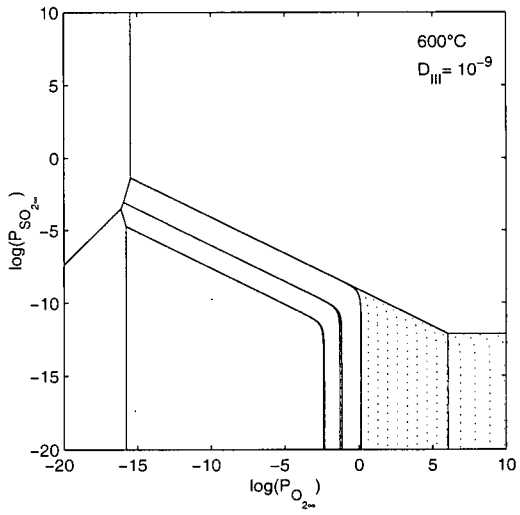
600°C
$D_{III}= 10^{-9}$
$\log(P_{SO_{2\infty}})$
$\log(P_{O_{2\infty}})$

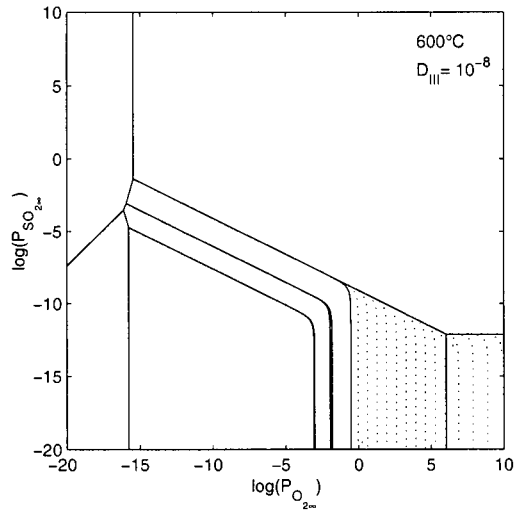
600°C
$D_{III}= 10^{-8}$
$\log(P_{SO_{2\infty}})$
$\log(P_{O_{2\infty}})$

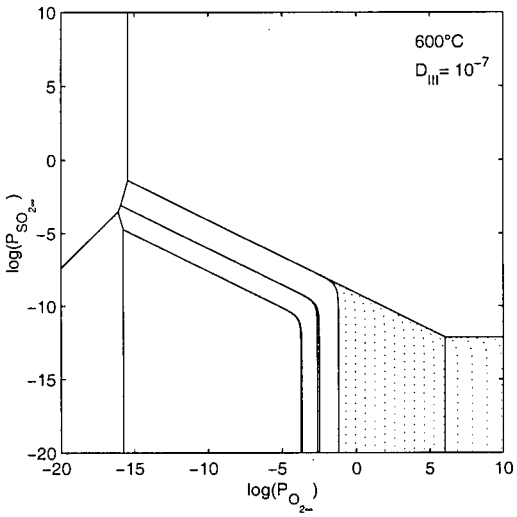
600°C
$D_{III}= 10^{-7}$
$\log(P_{SO_{2\infty}})$
$\log(P_{O_{2\infty}})$

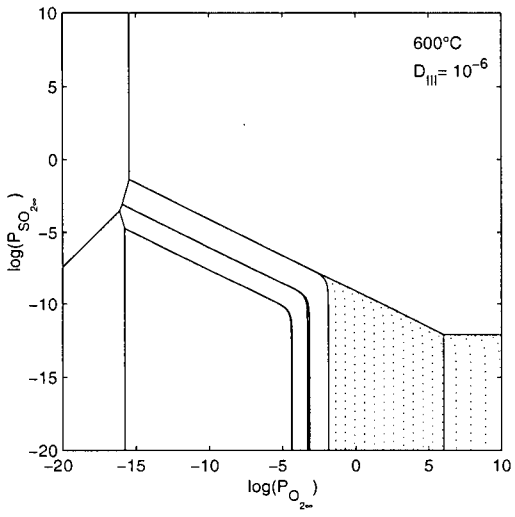
600°C
$D_{III}= 10^{-6}$
$\log(P_{SO_{2\infty}})$
$\log(P_{O_{2\infty}})$

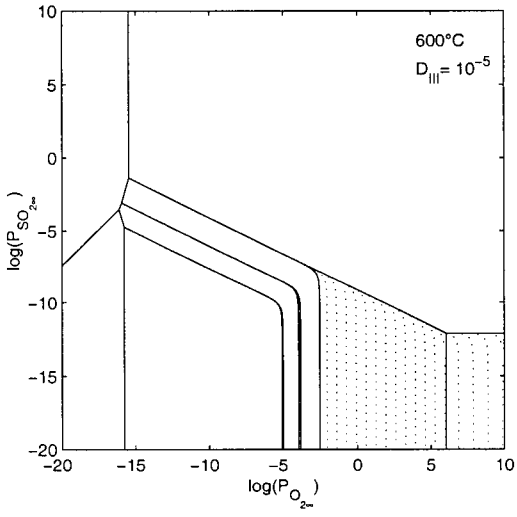
600°C
$D_{III}= 10^{-5}$
$\log(P_{SO_{2\infty}})$
$\log(P_{O_{2\infty}})$

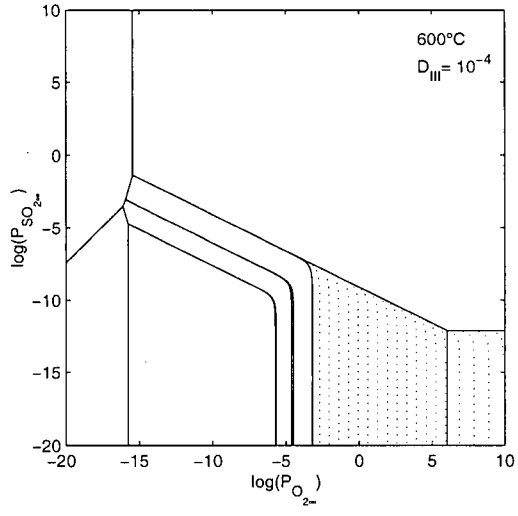
600°C
$D_{III}= 10^{-4}$
$\log(P_{SO_{2\infty}})$
$\log(P_{O_{2\infty}})$

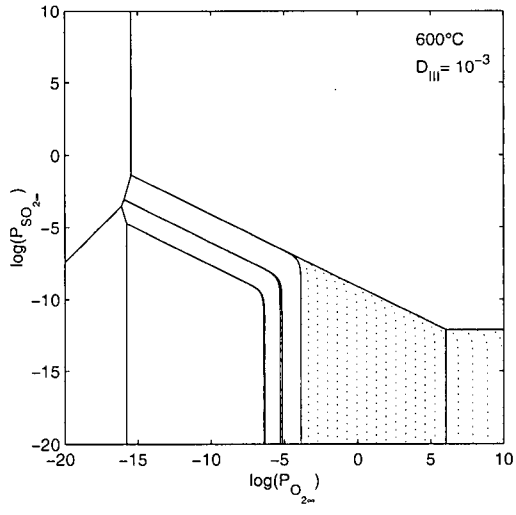
600°C
$D_{III}= 10^{-3}$
$\log(P_{SO_{2\infty}})$
$\log(P_{O_{2\infty}})$

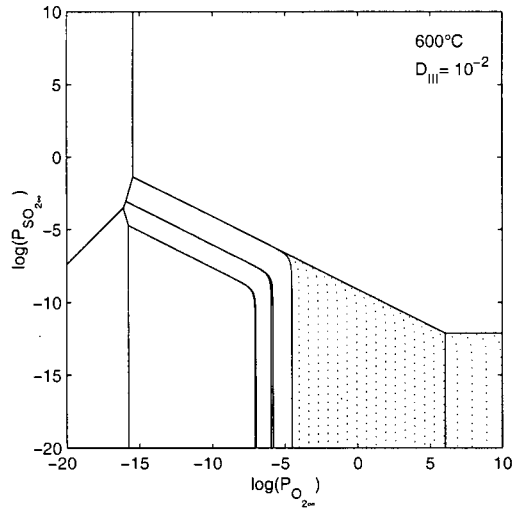
600°C
$D_{III}= 10^{-2}$
$\log(P_{SO_{2\infty}})$
$\log(P_{O_{2\infty}})$

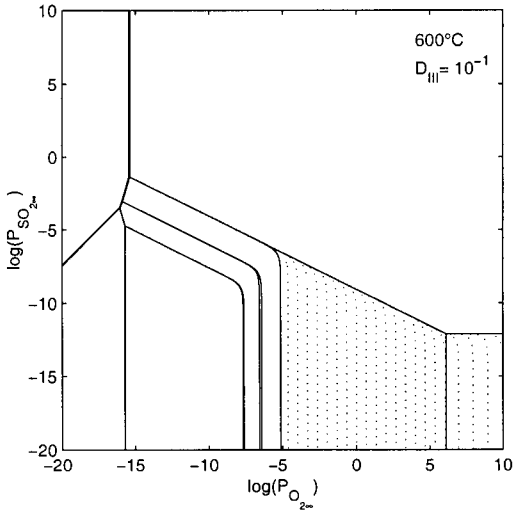
600°C
$D_{III}= 10^{-1}$
$\log(P_{SO_{2\infty}})$
$\log(P_{O_{2\infty}})$

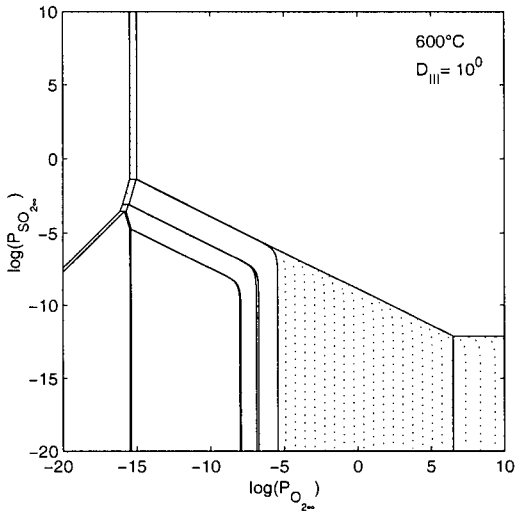
600°C
$D_{III}= 10^{0}$
$\log(P_{SO_{2\infty}})$
$\log(P_{O_{2\infty}})$

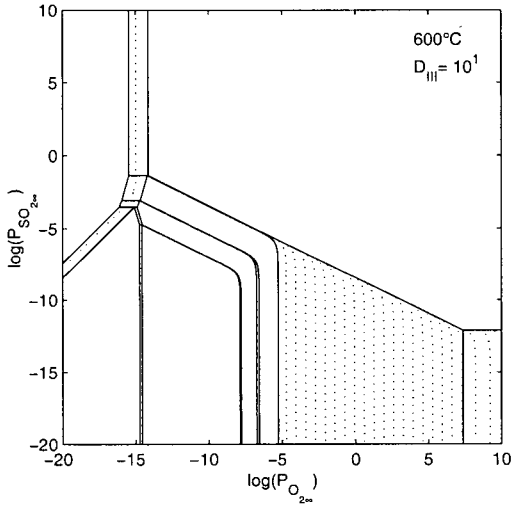
600°C
$D_{III}= 10^{1}$
$\log(P_{SO_{2\infty}})$
$\log(P_{O_{2\infty}})$

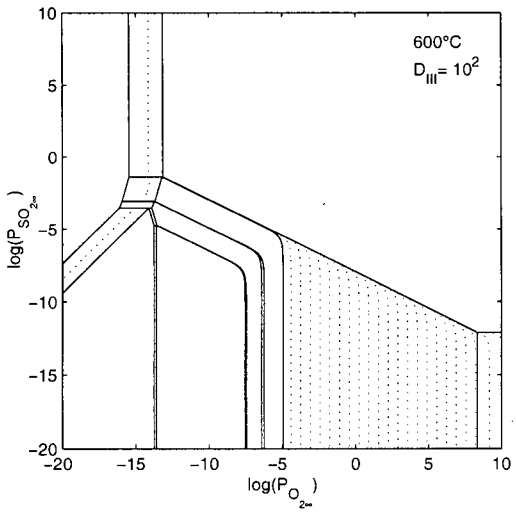
600°C
$D_{III}= 10^{2}$
$\log(P_{SO_{2\infty}})$
$\log(P_{O_{2\infty}})$

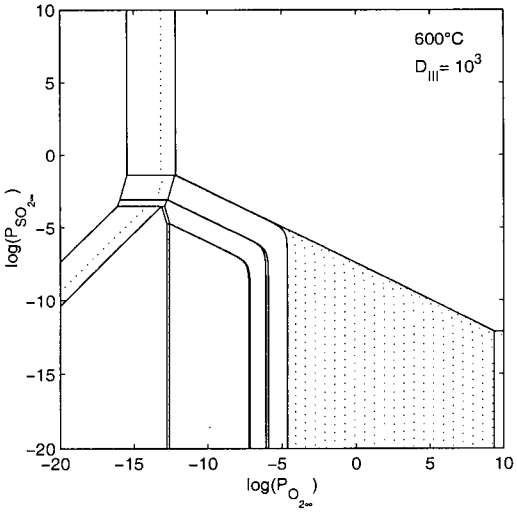
600°C
$D_{III}= 10^{3}$
$\log(P_{SO_{2\infty}})$
$\log(P_{O_{2\infty}})$

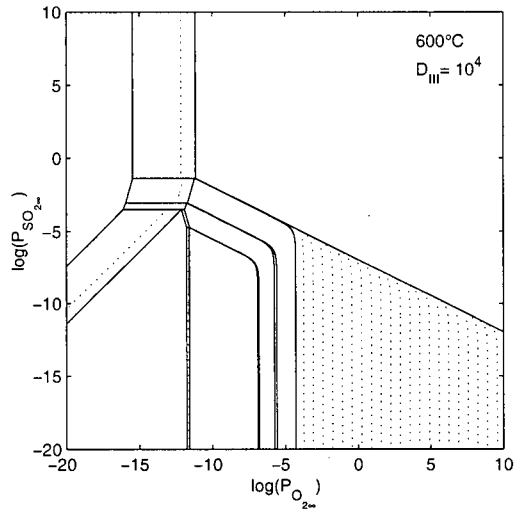
600°C
$D_{III}= 10^{4}$
$\log(P_{SO_{2\infty}})$
$\log(P_{O_{2\infty}})$

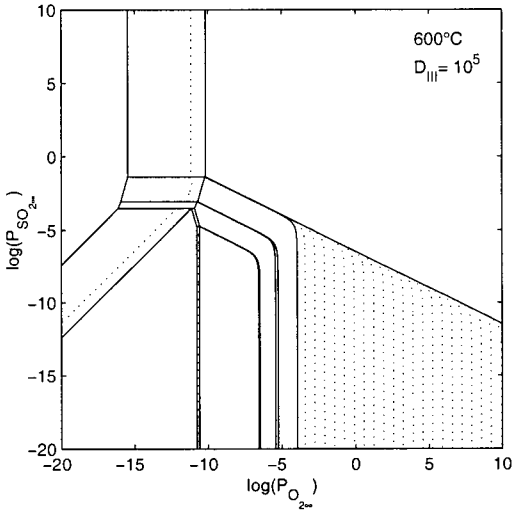
600°C
$D_{III}= 10^{5}$
$\log(P_{SO_{2\infty}})$
$\log(P_{O_{2\infty}})$

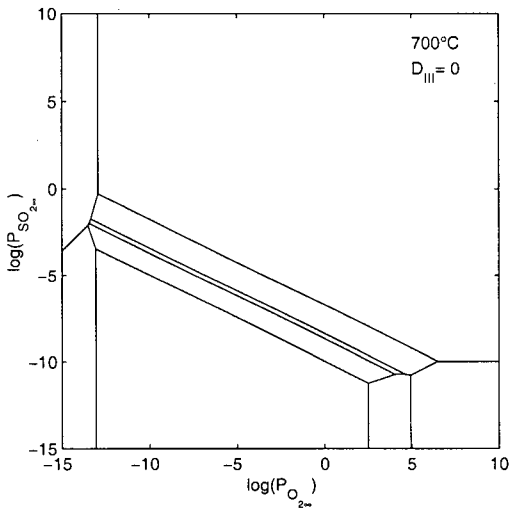
700°C
D_{III}= 0
$\log(P_{SO_{2-}})$
$\log(P_{O_{2-}})$

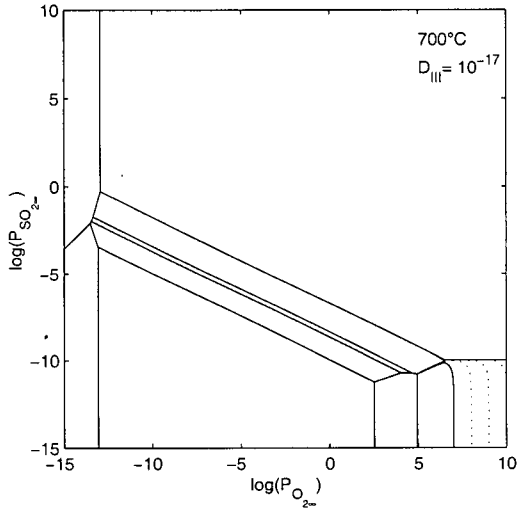
700°C
D_{III}= 10^{-17}
$\log(P_{SO_{2-}})$
$\log(P_{O_{2-}})$

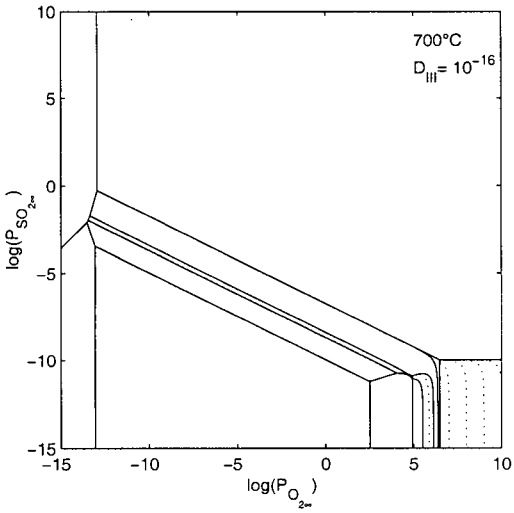
700°C
D_{III}= 10^{-16}
$\log(P_{SO_{2-}})$
$\log(P_{O_{2-}})$

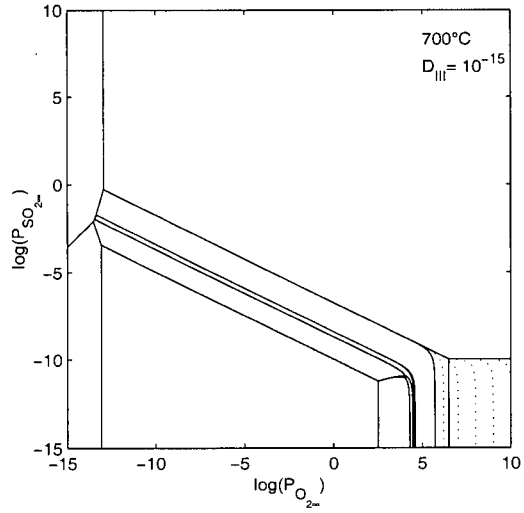
700°C
D_{III}= 10^{-15}
$\log(P_{SO_{2-}})$
$\log(P_{O_{2-}})$

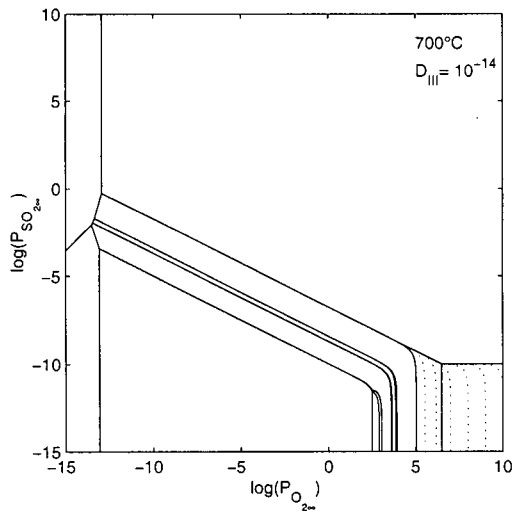
700°C
D_{III}= 10^{-14}
$\log(P_{SO_{2-}})$
$\log(P_{O_{2-}})$

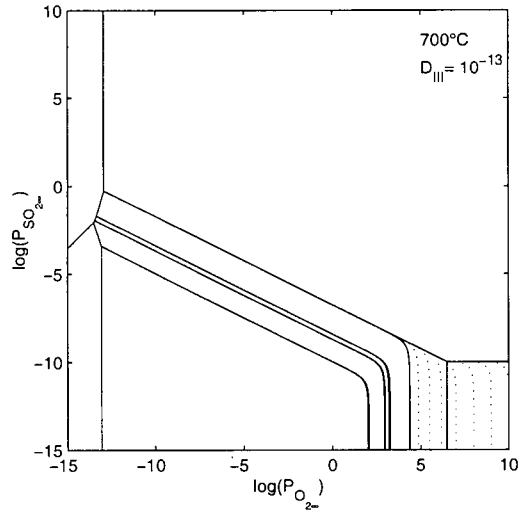
700°C
D_{III}= 10^{-13}
$\log(P_{SO_{2-}})$
$\log(P_{O_{2-}})$

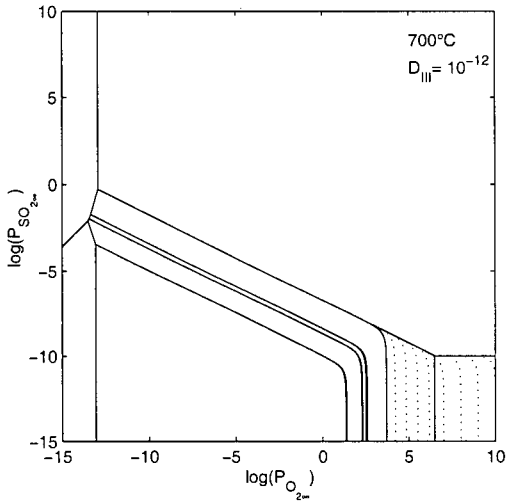
700°C
$D_{III}= 10^{-12}$
$\log(P_{SO_{2\infty}})$
$\log(P_{O_{2\infty}})$

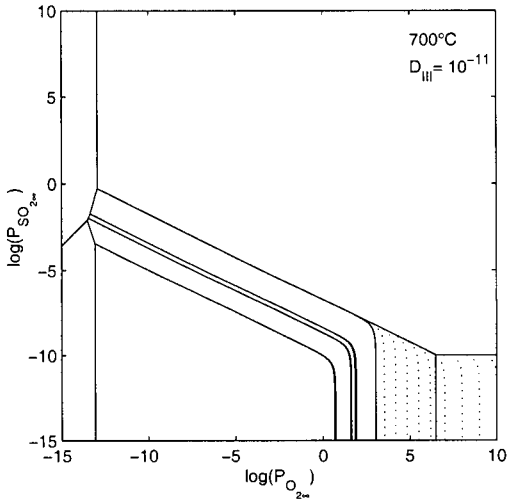
700°C
$D_{III}= 10^{-11}$
$\log(P_{SO_{2\infty}})$
$\log(P_{O_{2\infty}})$

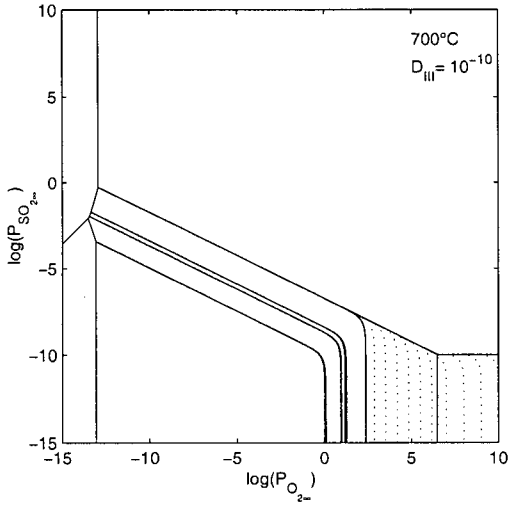
700°C
$D_{III}= 10^{-10}$
$\log(P_{SO_{2\infty}})$
$\log(P_{O_{2\infty}})$

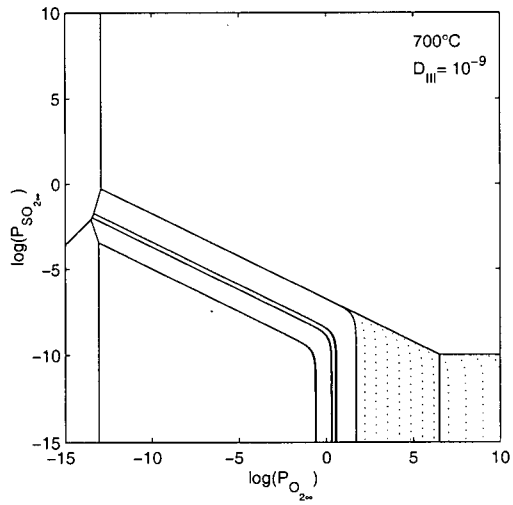
700°C
$D_{III}= 10^{-9}$
$\log(P_{SO_{2\infty}})$
$\log(P_{O_{2\infty}})$

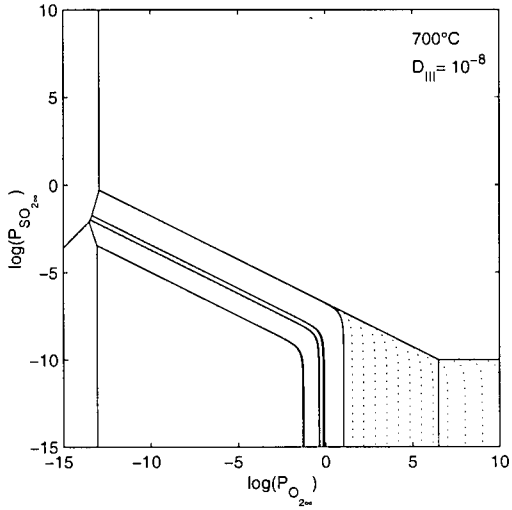
700°C
$D_{III}= 10^{-8}$
$\log(P_{SO_{2\infty}})$
$\log(P_{O_{2\infty}})$

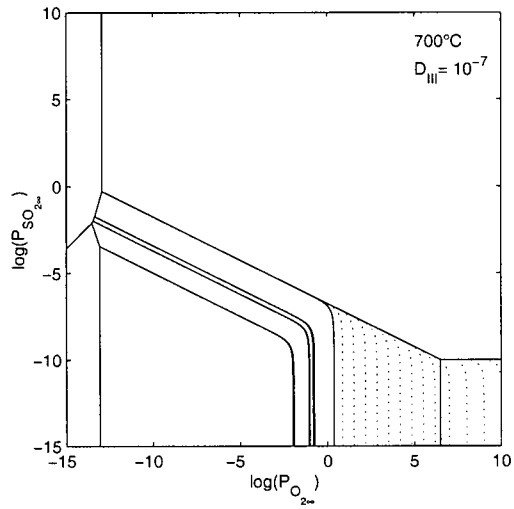
700°C
$D_{III}= 10^{-7}$
$\log(P_{SO_{2\infty}})$
$\log(P_{O_{2\infty}})$

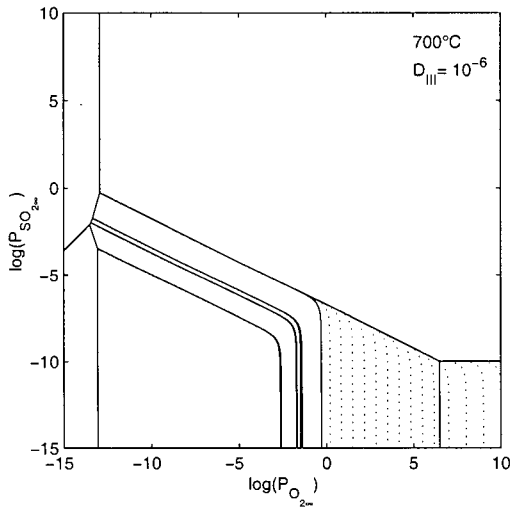
700°C
$D_{III}= 10^{-6}$
$\log(P_{SO_{2\infty}})$
$\log(P_{O_{2\infty}})$

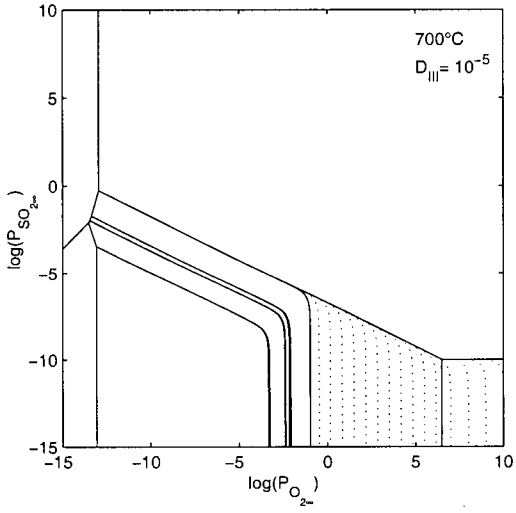
700°C
$D_{III}= 10^{-5}$
$\log(P_{SO_{2\infty}})$
$\log(P_{O_{2\infty}})$

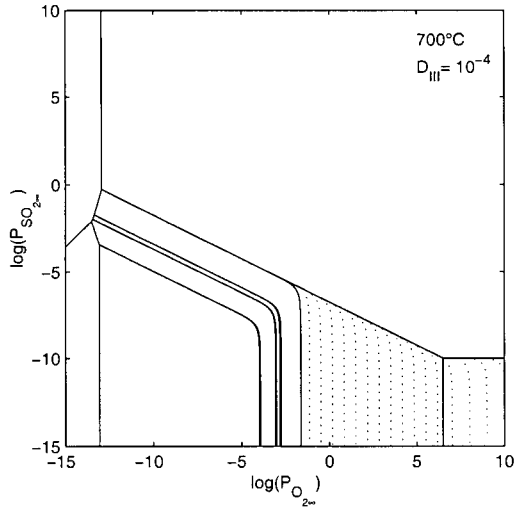
700°C
$D_{III}= 10^{-4}$
$\log(P_{SO_{2\infty}})$
$\log(P_{O_{2\infty}})$

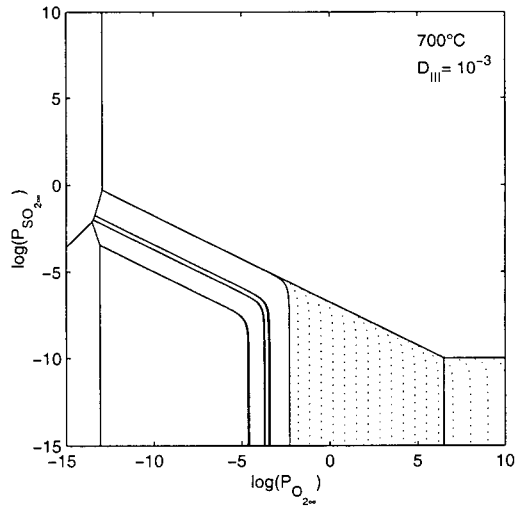
700°C
$D_{III}= 10^{-3}$
$\log(P_{SO_{2\infty}})$
$\log(P_{O_{2\infty}})$

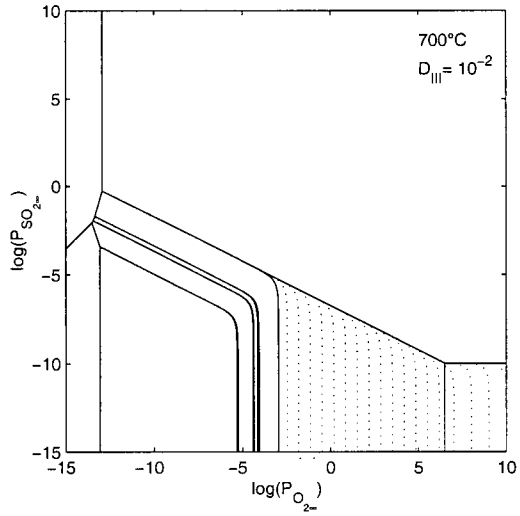
700°C
$D_{III}= 10^{-2}$
$\log(P_{SO_{2\infty}})$
$\log(P_{O_{2\infty}})$

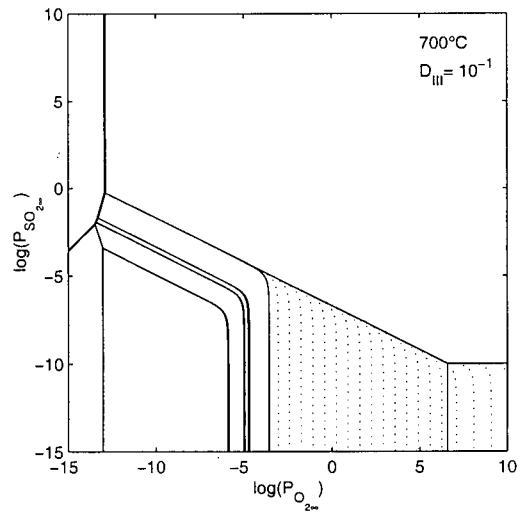
700°C
$D_{III}= 10^{-1}$
$\log(P_{SO_{2\infty}})$
$\log(P_{O_{2\infty}})$

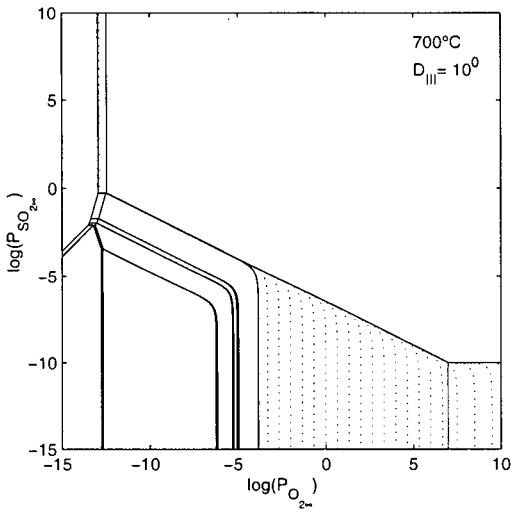
700°C
$D_{III}= 10^{0}$
$\log(P_{SO_{2\infty}})$
$\log(P_{O_{2\infty}})$

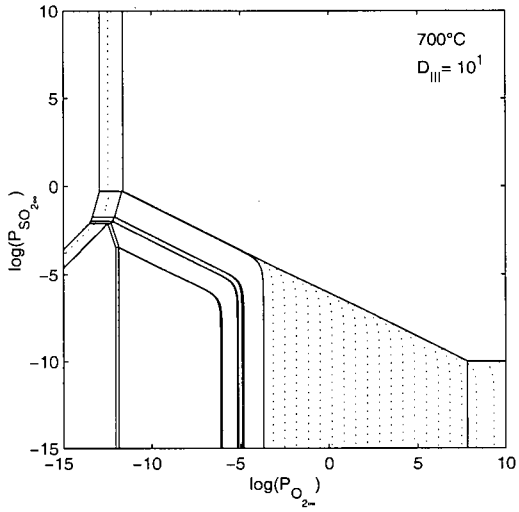
700°C
$D_{III}= 10^{1}$
$\log(P_{SO_{2\infty}})$
$\log(P_{O_{2\infty}})$

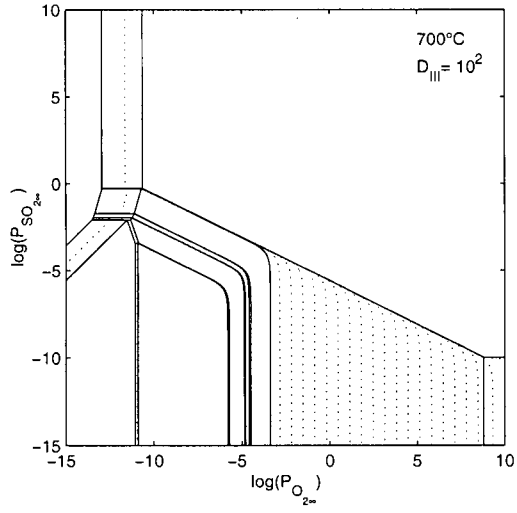
700°C
$D_{III}= 10^{2}$
$\log(P_{SO_{2\infty}})$
$\log(P_{O_{2\infty}})$

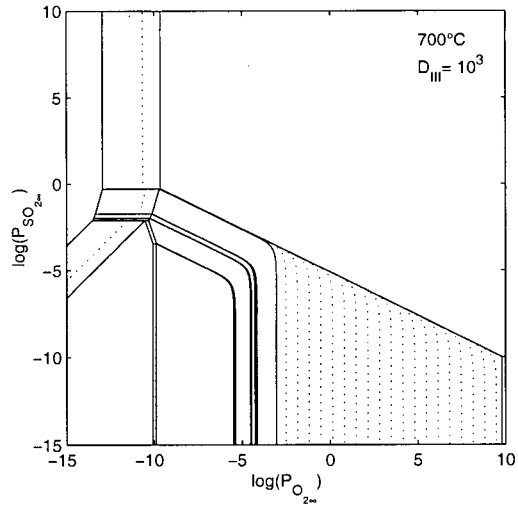
700°C
$D_{III}= 10^{3}$
$\log(P_{SO_{2\infty}})$
$\log(P_{O_{2\infty}})$

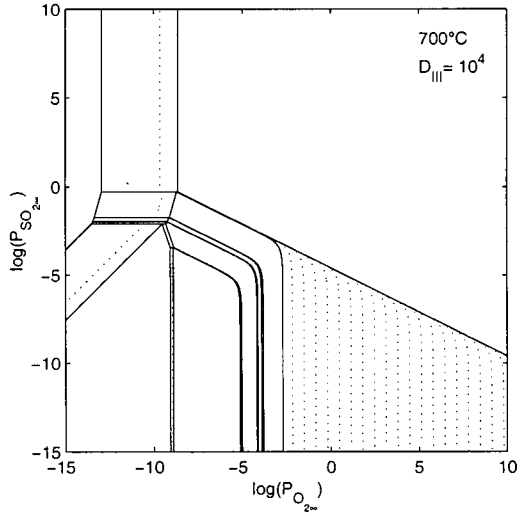
700°C
$D_{III}= 10^{4}$
$\log(P_{SO_{2\infty}})$
$\log(P_{O_{2\infty}})$

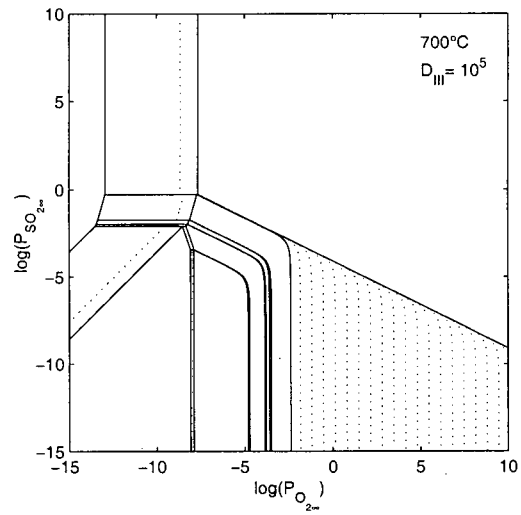
700°C
$D_{III}= 10^{5}$
$\log(P_{SO_{2\infty}})$
$\log(P_{O_{2\infty}})$

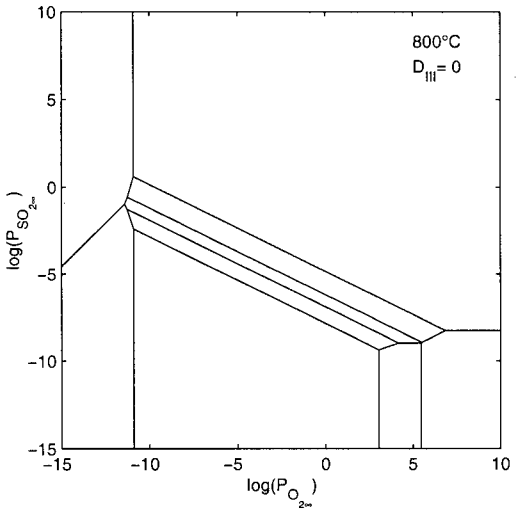
800°C
D_{III}= 0
$\log(P_{SO_{2\infty}})$
$\log(P_{O_{2\infty}})$

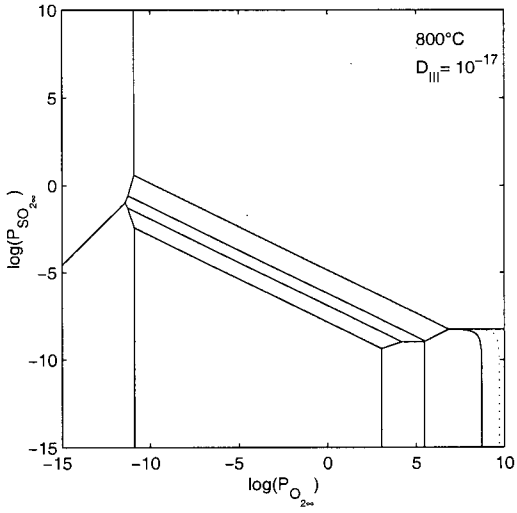
800°C
D_{III}= 10^{-17}
$\log(P_{SO_{2\infty}})$
$\log(P_{O_{2\infty}})$

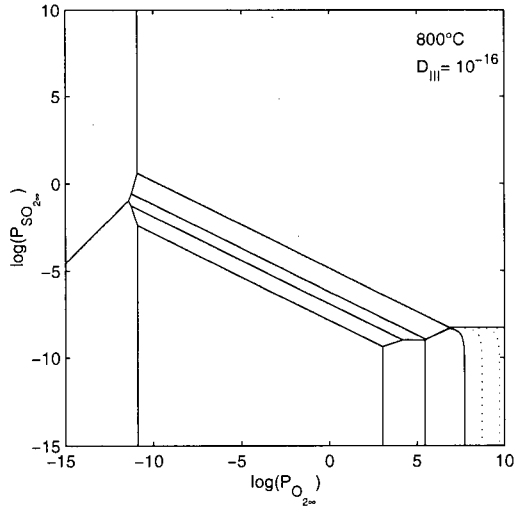
800°C
D_{III}= 10^{-16}
$\log(P_{SO_{2\infty}})$
$\log(P_{O_{2\infty}})$

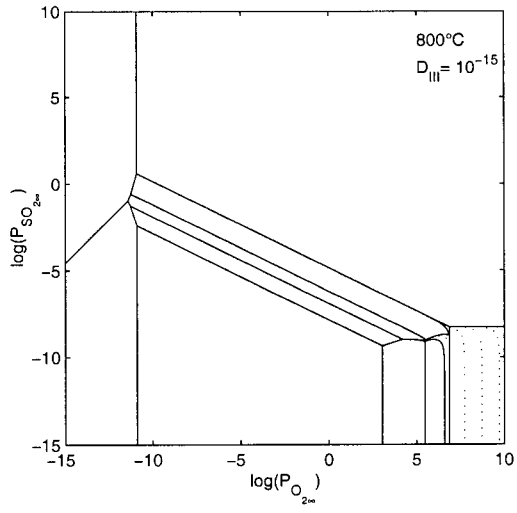
800°C
D_{III}= 10^{-15}
$\log(P_{SO_{2\infty}})$
$\log(P_{O_{2\infty}})$

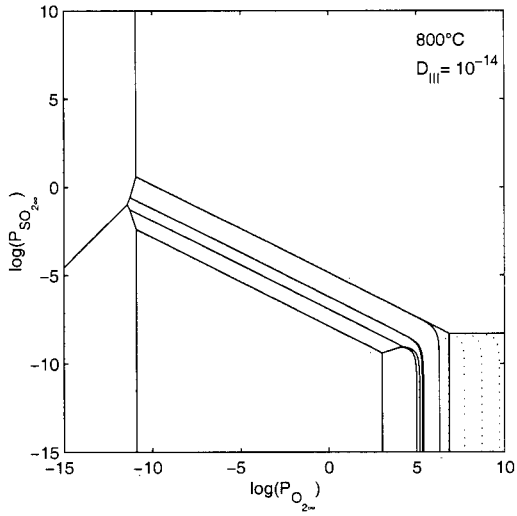
800°C
D_{III}= 10^{-14}
$\log(P_{SO_{2\infty}})$
$\log(P_{O_{2\infty}})$

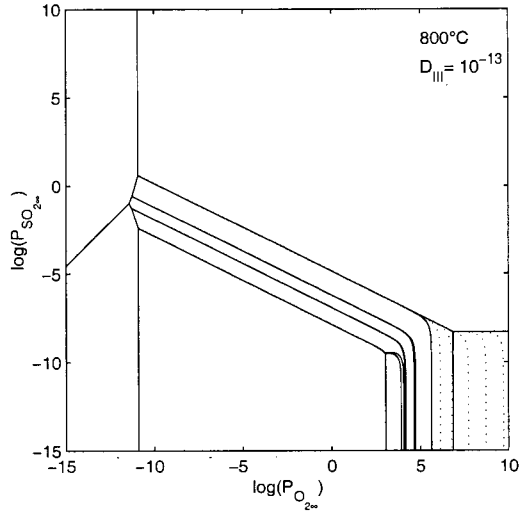
800°C
D_{III}= 10^{-13}
$\log(P_{SO_{2\infty}})$
$\log(P_{O_{2\infty}})$

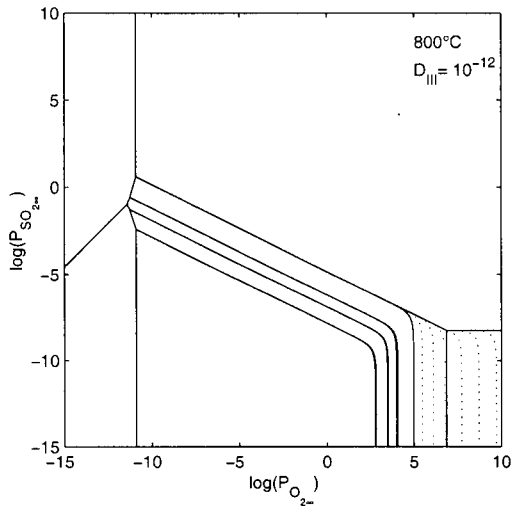
800°C
$D_{III}= 10^{-12}$
$\log(P_{SO_{2\infty}})$
$\log(P_{O_{2\infty}})$

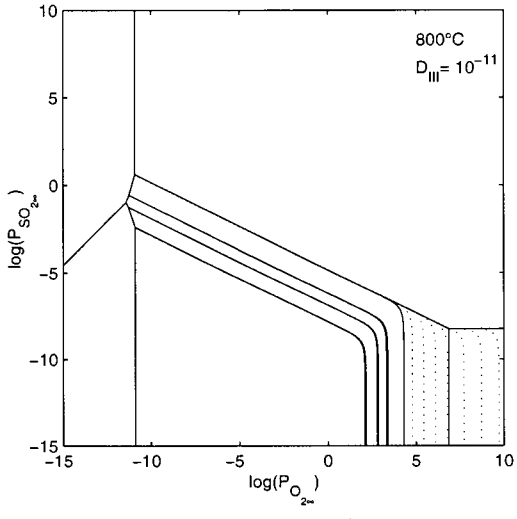
800°C
$D_{III}= 10^{-11}$
$\log(P_{SO_{2\infty}})$
$\log(P_{O_{2\infty}})$

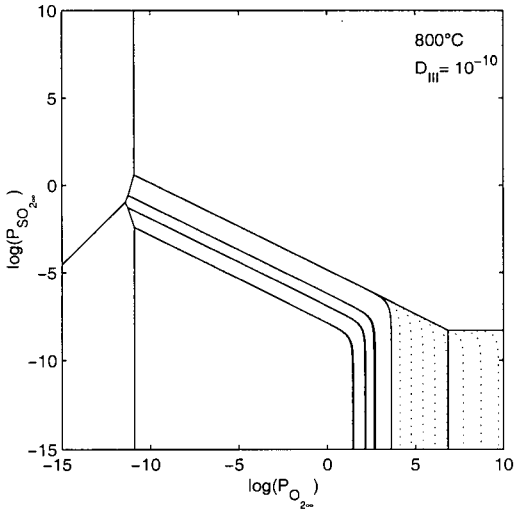
800°C
$D_{III}= 10^{-10}$
$\log(P_{SO_{2\infty}})$
$\log(P_{O_{2\infty}})$

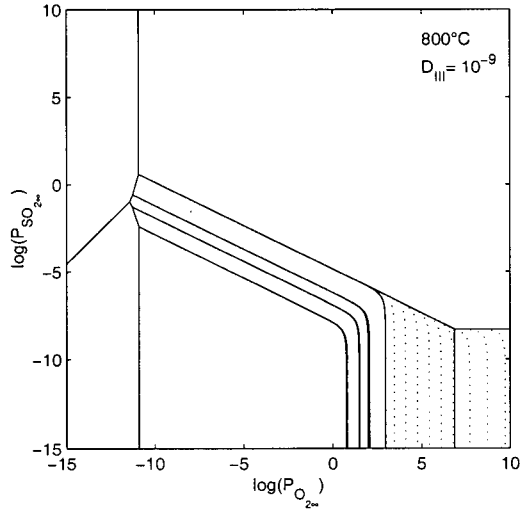
800°C
$D_{III}= 10^{-9}$
$\log(P_{SO_{2\infty}})$
$\log(P_{O_{2\infty}})$

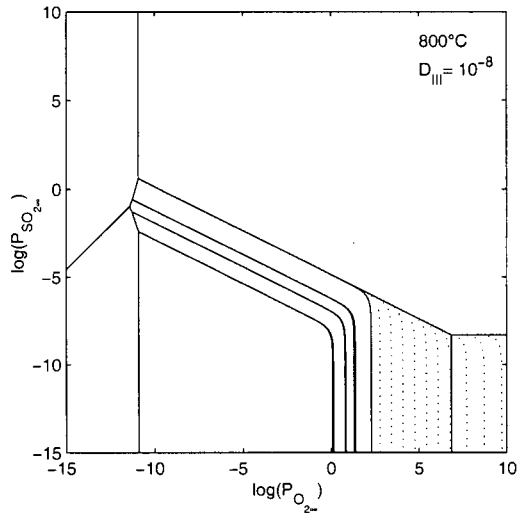
800°C
$D_{III}= 10^{-8}$
$\log(P_{SO_{2\infty}})$
$\log(P_{O_{2\infty}})$

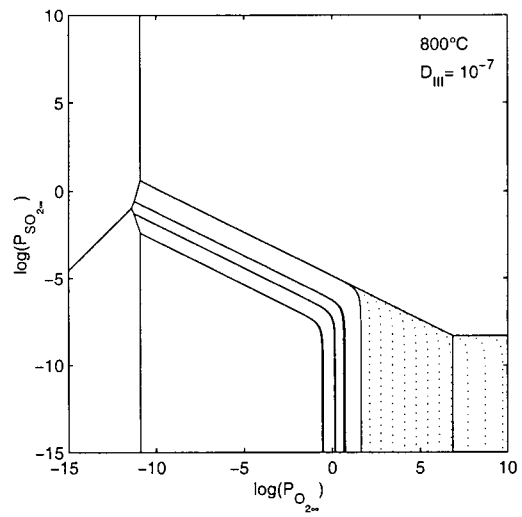
800°C
$D_{III}= 10^{-7}$
$\log(P_{SO_{2\infty}})$
$\log(P_{O_{2\infty}})$

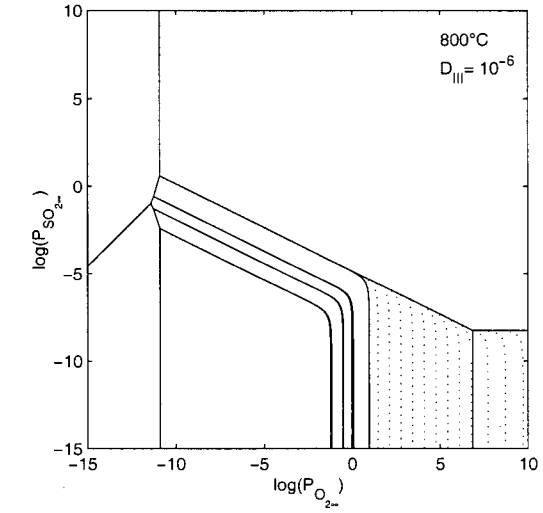
800°C
$D_{III}= 10^{-6}$
$\log(P_{SO_{2\infty}})$
$\log(P_{O_{2\infty}})$

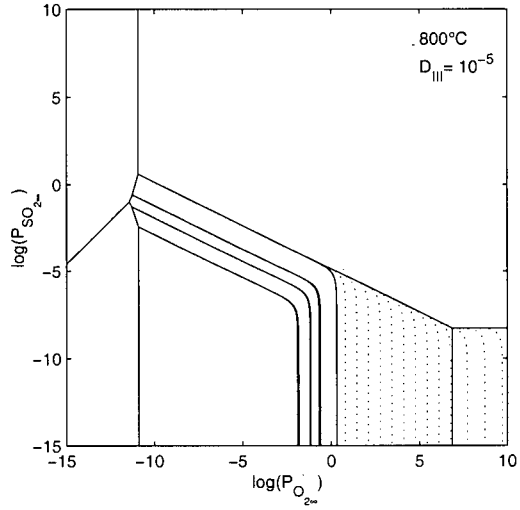
800°C
$D_{III}= 10^{-5}$
$\log(P_{SO_{2\infty}})$
$\log(P_{O_{2\infty}})$

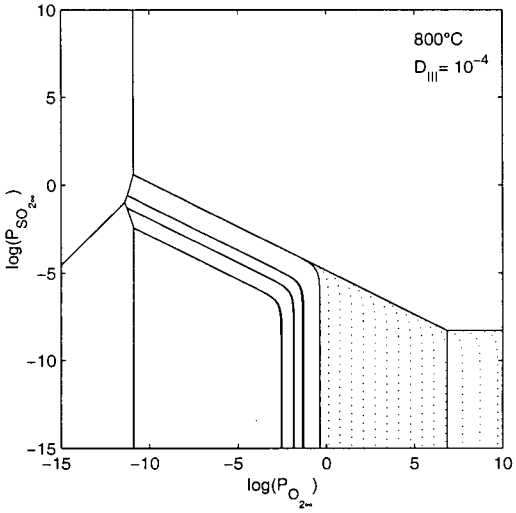
800°C
$D_{III}= 10^{-4}$
$\log(P_{SO_{2\infty}})$
$\log(P_{O_{2\infty}})$

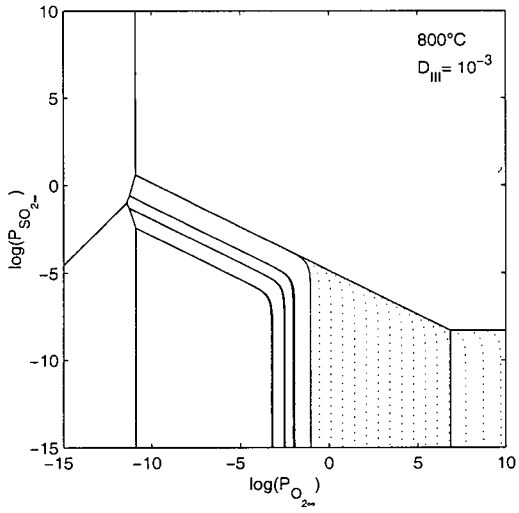
800°C
$D_{III}= 10^{-3}$
$\log(P_{SO_{2\infty}})$
$\log(P_{O_{2\infty}})$

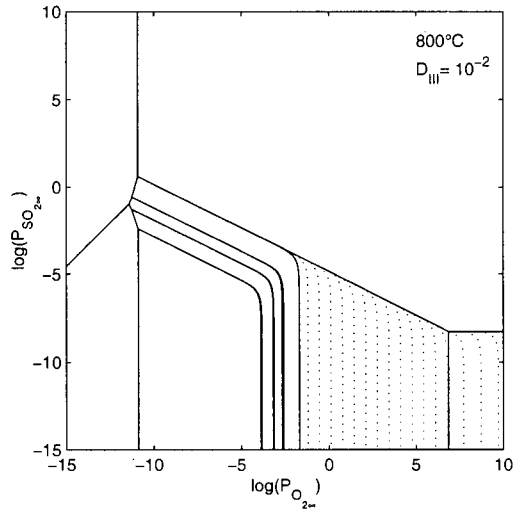
800°C
$D_{III}= 10^{-2}$
$\log(P_{SO_{2\infty}})$
$\log(P_{O_{2\infty}})$

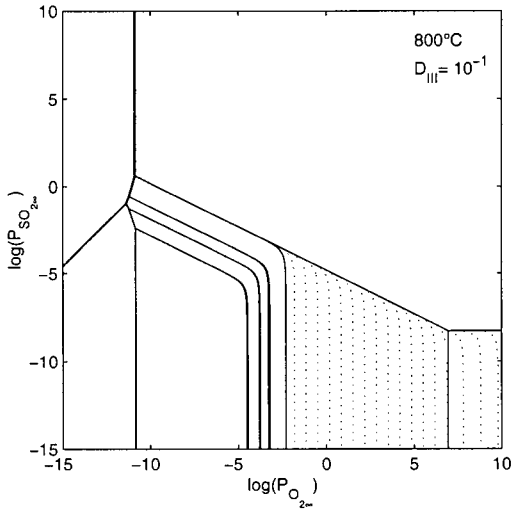
800°C
$D_{III}= 10^{-1}$
$\log(P_{SO_{2\infty}})$
$\log(P_{O_{2\infty}})$

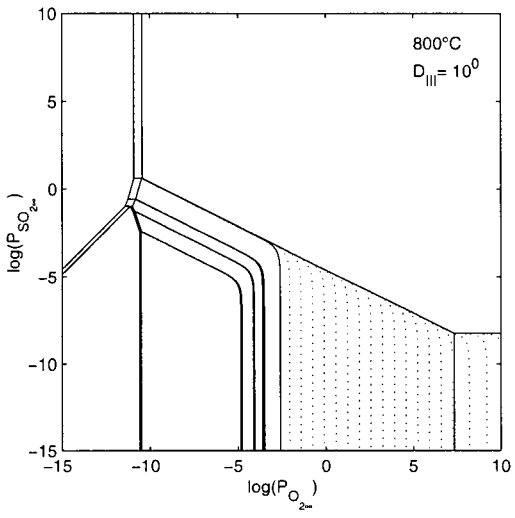
800°C
$D_{III}= 10^0$
$\log(P_{SO_{2\infty}})$
$\log(P_{O_{2\infty}})$

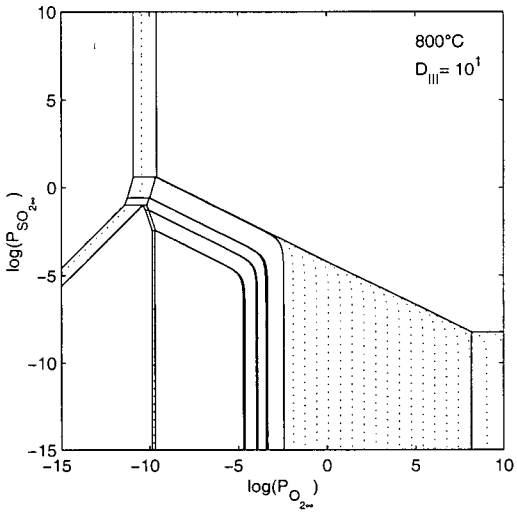
800°C
$D_{III}= 10^1$
$\log(P_{SO_{2\infty}})$
$\log(P_{O_{2\infty}})$

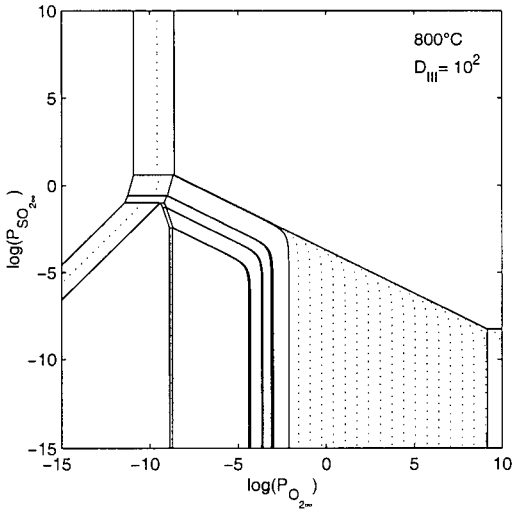
800°C
$D_{III}= 10^2$
$\log(P_{SO_{2\infty}})$
$\log(P_{O_{2\infty}})$

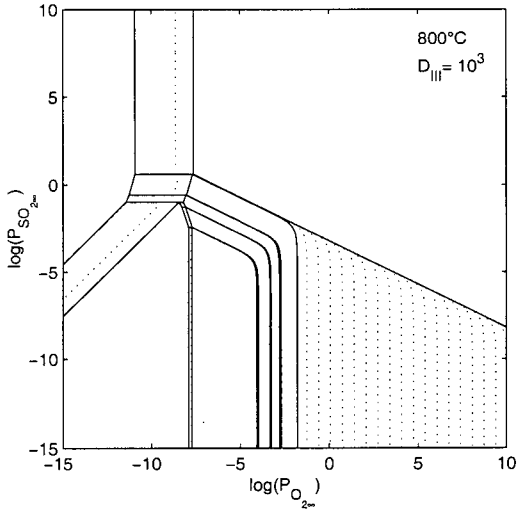
800°C
$D_{III}= 10^3$
$\log(P_{SO_{2\infty}})$
$\log(P_{O_{2\infty}})$

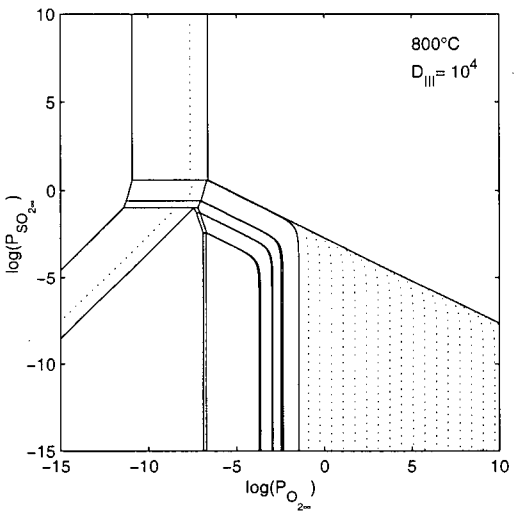
800°C
D_{III}= 10^4
$\log(P_{SO_{2\infty}})$
$\log(P_{O_{2\infty}})$
10
5
0
-5
-10
-15
-15
-10
-5
0
5
10

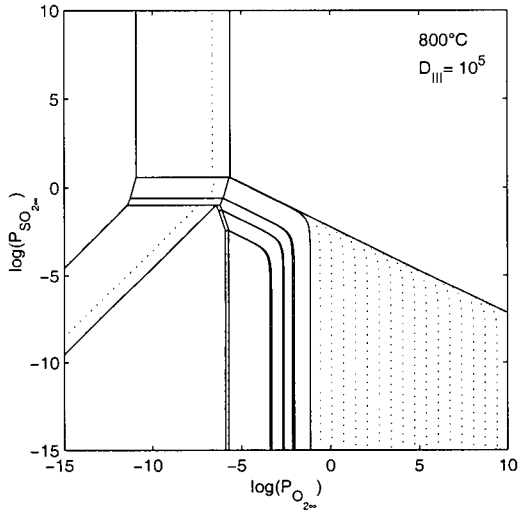
800°C
D_{III}= 10^5
$\log(P_{SO_{2\infty}})$
$\log(P_{O_{2\infty}})$
10
5
0
-5
-10
-15
-15
-10
-5
0
5
10

Appendix 6 : Furnace characterisation

Section 1: Residence time distribution

A residence time distribution analysis has been performed on the furnace used for the experimental work of this thesis.

Pulses of helium were introduced in an air flow by a three way valve. The pulses were detected by a thermal conductivity cell which has been described previously [65]. The cell forms a resistance bridge which is powered by a constant voltage and its output is measured by the 18-bit resolution data acquisition system. The system is assembled so that the gas entering the furnace is passing through the reference path of the cell and the output of the furnace is passing the cell by the sample path. This allows to characterize the pulse prior to and after entering the furnace.

Multiple experiments were performed by switching the three way valve for periods of less than one second thus creating helium pulses in a air stream. Between each pulse, a period of more than 15 minutes was waited to ensure that no helium was present from the previous pulse. The data acquired was normalized and integrated to yield a F-curve.

The F curve, presented in Figure A6.1, clearly shows a transient regime for about 60 seconds at room temperature and at a gas flow rate of 0.5 l/min. The F Curve of the original pulses show a transient regime of approximately 5 seconds in the same conditions. This transient measurement is probably influenced by the period of the pulse and the response time of the cell. Small differences in the curves are probably caused by different pulse length.

Using higher gas flow rates will reduce this transient period by the same factor as the flow rate is increased. Also, higher temperatures will also reduce the transient periods due to the lower gas density at higher temperatures for the same mass flow rates. In the experimental conditions, the transient can therefore be evaluated to less than 5 seconds.

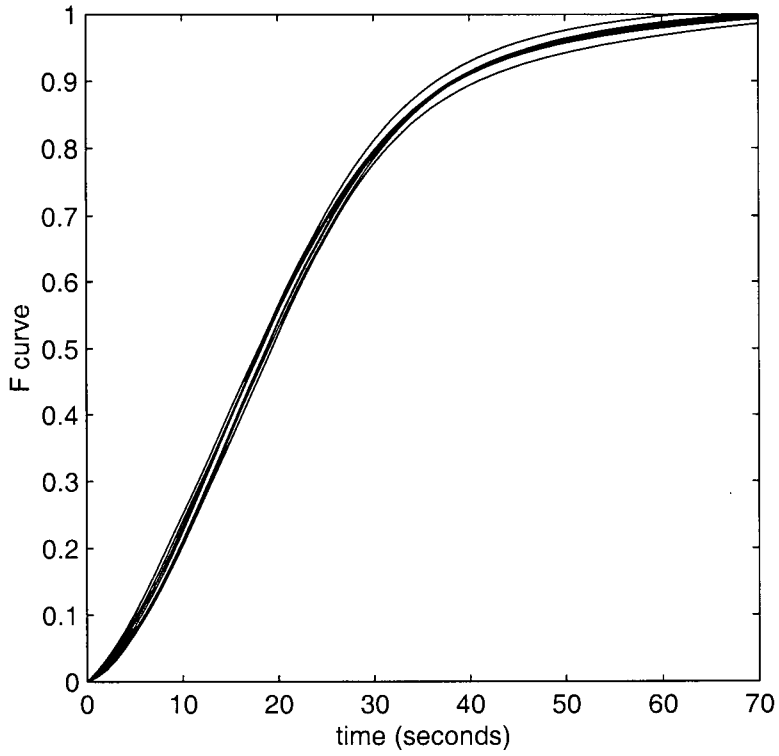

Figure A6.1: F curve determined experimentally for the furnace

Section 2: Temperature profile of the furnace

An axial temperature profile of the furnace was performed by taking measurements with a type K thermocouple. Measurements were taken every 10 mm from the position of the pellets in the direction of the gas flow. The pellets were positioned in the small isothermal region located near the pellets. The two pellets can therefore be assumed to be at the same temperature +/- 5°C.

Tableau A6.1: Temperature profile of the furnace

Position (mm)	Temperature (°C)
-20	506
-10	506
0	502
10	500
20	497
30	492
40	486
50	478
60	467
70	450
80	427
90	417
100	406